Processing of MgO-$MgAl_2O_4$ Ceramics and Study of its Microstructure, Strength and Thermal Shock resistance

A THESIS SUBMITTED TO
NATIONAL INSTITUTE OF TECHNOLOGY, ROURKELA
FOR THE AWARD OF DEGREE

OF

MASTER OF TECHNOLOGY (Research)

IN

CERAMIC ENGINEERING

BY

Deepak Mohapatra

UNDER THE GUIDANCE OF

Dr. D. Sarkar

DEPARTMENT OF CERAMIC ENGINEERING
NATIONAL INSTITUTE OF TECHNOLOGY
ROURKELA – 769 008, ORISSA (INDIA)

2006

Department of Ceramic Engineering
NATIONAL INSTITUTE OF TECHNOLOGY
ROURKELA – 769 008, Orissa (INDIA)

Dr.Debasish Sarkar
B.Sc.(Chem. Hons) & B.Tech. (Ceramics)
M.Tech.(IIT Kanpur) & Ph.D. (N.I.T, Rourkela)
Sr. Lecturer

C E R T I F I C A T E

*This is to certify that the thesis on "**Processing of MgO-$MgAl_2O_4$ Ceramics and Study of its Microstructure, Strength and Thermal Shock Resistance**" submitted by **Deepak Mohapatra** to the National Institute of Technology, Rourkela in partial fulfillment of the requirements for the award of the degree of **Master Of Technology (Research)** in **Ceramic Engineering** is a record of bonafide research work carried out by him under my supervision and guidance. His thesis, in my opinion, is worthy of consideration for the award of degree of **Master Of Technology (Research)** in accordance with the regulations of the institute.*

The results embodied in this thesis have not been submitted to any other university or institute for the award of a Degree or Diploma.

(D.Sarkar)

Tel: + 91 661 2462207 (O), 2463207 (R) Cell: 09437351756
Fax: + 91 661 247 2926/246 2999 Email: debasish_123@yahoo.com /dsarkar@nitrkl.ac.in

ACKNOWLEDGEMENT

At the onset, I would like to express my heartfelt thanks and deep sense of gratitude to my reverent teacher and honorable research supervisor Dr.D. Sarkar, for introducing me to this vast field of Spinel, for his constant encouragement, efficient planning, constructive criticism and valuable guidance during the entire course of my work. I thank you Sir for your help, inspiration and blessings.

I express my heartfelt thanks to Prof. S. K. Sarangi, Director, NIT Rourkela for providing the facilities to carry out this investigation. I would also express my sincere thanks to Prof. S. Bhattacharyya, Head, Department of Ceramic Engineering, N.I.T, Rourkela for his advice and constructive suggestion for the improvement of my work.

I would also take this opportunity to express my gratitude and sincere thanks to my honorable teachers Prof. S. Adak, Ex-Head, Department of Ceramic Engineering NIT, Rourkela, Dr. S. K. Pratihar and Dr. J. Bera for their invaluable advice, constant help, encouragement, inspiration and blessings.

Submitting this thesis would have been a Herculean job, without the constant help, encouragement, support and suggestions from my friends, especially R. P. Rana and Y. Nayak for their time to help. Although it will be difficult to record my appreciation to each and every one of them in this small space; I will feel guilty if I miss the opportunity to thank Debasish Mohapatra, D. K. Dash, Bandana Raut and others. I will relish your memories for years to come.

I would also express my sincere thanks to lab. members of Department of Ceramic Engineering, N.I.T., Rourkela, especially P. K. Mohanty for constant practical assistance and help whenever required.

My parents have always been a source of inspiration to me during the difficult times without which it would not have been possible to complete this work. I would like to thank Dr. S. J. Cho of Korea Research Institute of Science and Standards (KRISS), South Korea, for help in microstructure analysis.

Above all, I thank Almighty for giving me all these people to help and encourage me, and for the skills and opportunity to complete this thesis.

(**DEEPAK MOHAPATRA**)

P R E F A C E

Chapter – I introduces the topic and background of the existing field. **Chapter – II** deals with detailed literature review. Attempts have been made to systematically classify the available information under different sections. This chapter incorporates background information to assist in understanding the aims and results of this investigation, and also reviews recent reports by other investigators with which these results can be compared. The review finds unresolved questions in the literature that can't be answered by a single research work. The end of **Chapter – II** deals with the objectives of the present investigation. **Chapter – III** deals with the detailed experimental processes related to this research work. **Chapter – IV** deals with the results and discussion systematically with respect to powder processing, characterization, densification study and evaluation of mechanical properties. **Chapter – V** summarizes the conclusions, whereas, **Chapter – VI** illustrates the possibility of Future Works.

A complete list of references has been given towards the end of the thesis.

Table of Content

List of Figures

List of Tables

ABSTRACT

MgO rich spinel precursor containing Al_2O_3 : MgO in weight proportions of 1:1, 1:1.1, 1:1.2, 1:1.3, 1:1.4 is prepared by solid-state reaction route. The processed and calcined powders are characterized by Particle Size analysis, X-ray diffraction analysis and sintering behavior. The processed and calcined powder exhibits a bimodal distribution because of the presence of partially agglomerate and unagglomerated particle. However, the average particle size varies from 6.84μm to 3.48μm with increasing milling time. The optimized milling time and subsequent particle size are found 60h and 3.48μm respectively. In the calcined powder spinel phase evolution starts around 1000^oC and follows an increasing trend in crystallinity and spinelization with increasing temperature. The crystallite size is 19nm for lowest calcination temperature and lowest content of MgO and gradually increases with increasing temperature and maximum 33nm has been detected for powder with highest MgO content at 1300^oC for 2h. Initial calcination temperature and spinel seeds affect the densification as well as the extent of spinelization in the sintered bodies. The relative density after sintering at 1600^oC for 4h varies between 96-98% for Al_2O_3 : MgO=1:1, whereas composition with highest MgO content exhibits this variation within the range of 95-97%. Low spinel seeding calcined batches show better densification. Microstructure reveals presence of non-uniform grains and inter-granular pores at lower calcination temperature and substantial grain growth is observed in higher calcination temperature. Random grain orientation and increased inter-granular porosity is responsible to deteriorate the density of high content of MgO powder when sintered after calcination at 1300^oC. The mechanical properties of MgO rich spinel composites containing preformed spinel are more strongly influenced than the in-situ formed spinel composites by sintering temperature, volume fraction and particle size of spinel. The hardness of the MgO rich spinel composites is ~13.5GPa, which continuously decreases (13.7–12.1GPa) with the increase of spinel phase at sintered specimen. Higher amount of seed addition has an adverse affect on the hardness of the composites due to coarsening of the spinel grains and formation of subsequent porosity. The compressive strength (147-107MPa) is affected by the thermal expansion mismatch between spinel and

MgO and the partial bonding between MgO and spinel grains. The large amount of in-situ spinel seeding as a result of higher calcination temperature has a detrimental effect on strength values. The flexural strength of sintered specimens at room temperature as well as the retained strength of sintered specimens after 3cycles of thermal spalling has been measured. Both the tests have been carried out in 3-pt. loading system. The flexural strength is noted to be around ~137MPa for sintered specimen (with 70% spinel content) and has been found to decrease with increasing MgO content. The improved resistance (5-12% of original strength) to thermal shock in the ceramics is attributed to the the presence of higher amount of $MgAl_2O_4$ spinel at higher calcination temperature and microcrack network interlinking. The large thermal expansion coefficient difference between MgO and spinel, leads to extensive microcracking in ceramic materials with loss in strength values, when MgO content is higher.

CHAPTER 1

1.0. INTRODUCTION

Since the age of early civilization till today's space age, man's stages of development/evolution are associated with discovery, invention and development of new materials. Today's era boasts a storehouse of created means of improving the human condition that is at once thrilling and overwhelming. Yet like the fabled red shoes or the sorcerer's broom, discovery and invention will never stop. The arsenal still continues to grow. Today, thousands of new materials have come into use to revolutionize our lives. Development of new materials and their processing is helping the growth of novel technology in every field from Biology to Electronics to come into existence. In short it can be said that without materials there is no engineering. Ceramics today form the strategic materials base for development of new and advanced technology. Different spinel forms an interesting field in ceramics. The spinel is an exclusive category for different engineering applications. Mag-Al spinel is an important refractory material with its unique combination of desired properties.

Magnesium–Aluminum spinel (Mag–Al spinel) is an important advanced ceramic material possessing useful mechanical properties and wide range of applications even up to very high temperature. Magnesium aluminate spinel is an excellent refractory material for its high melting point, superior strength at ambient and elevated temperatures, excellent resistance against chemical attack and thermal spalling. These properties make it a superior refractory material for applications in side-walls and the bottom of steel teeming ladles, burning and transition zones of cement rotary kilns, etc.[1,2] For such applications spinel is used as a major component in an alumina rich or magnesia rich matrix, depending upon the environmental conditions prevailing in the application zone. Hence, magnesia rich or alumina rich spinel compositions are important from the application point of view.

The methods of fabrication of spinel refractory has been known since 1905[3] and the phase diagram of MgO-Al_2O_3 binary system has been well established since 1916 but still spinel did not get much of commercial success till mid eighties mainly due to complexity in process parameters. Spinel formation from its constituent oxides (Al_2O_3 and MgO) is associated with 5-7% volume expansion, which hinders the densification process and does not allow the material to

densify in the same firing schedule[4]. Hence a two-stage firing process was employed. The first step was to complete the spinel formation by getting the precursors calcined at an intermediate calcination temperature, and the second one to densify the formed spinel (1600^{o}-1800^{o}C). It is reported that the formation of spinel from magnesia and alumina does not produce dense product in a single stage firing, due to the volume expansion associated[5]. Hence the general practice is to complete the spinellisation process first and then crushing, milling, reshaping and sintering the spinel to achieve desired properties in the second-stage firing. Methods of preparing dense spinel products have improved considerably with progress of time. Various authors/ researchers have reported the preparation of spinel by different routes.

The limiting factors for spinel preparation are the requirements regarding purity of the raw materials, their reactivity, intermediate calcination temperature, higher sintering temperature etc. Earlier many synthesis routes for spinel preparation have been implemented such as co-precipitation[6], combustion synthesis[7], plasma spray decomposition of organo-metallic compounds in superficial fluids, freeze drying, hydrolysis of metal alkoxides etc. No doubt these methods have their advantages. These wet chemical routes reduce the formation/crystallization temperature of Mg-Al spinel to somewhat around 700^{0}C. Even they help producing nano-powders. And this high surface area to volume ratio of ceramic sol makes the powder sinteractive and hence high sinterability at lower temperatures is obtained. But the real challenge in synthesizing nano-structured powders using wet chemical routes is to control and engineer the physical properties of the starting materials as they affect the properties of the final products. To point out some disadvantages- in co-precipitation method usually Al/Mg- nitrate/ chloride salts are used. Repeated washing is required to remove the anions, which may alter the stoichiometric composition. Moreover, washing is a tedious and time consuming process. And regarding the combustion synthesis and sol-gel process- they involve chemicals that are sensitive to environment. Also, the reproducibility of the properties in the end products through these wet chemical routes is somewhat difficult to attain. However from industrial point of view, cost effective and less complicated techniques are required for large-scale application. In this context, solid-state reaction route is still the conventional and most feasible route in bulk production. However, the limitation is that it requires high calcination temperature and high sintering temperature. But to counter that there are mineralizers such as AlF_3, V_2O_5, Y_2O_3, NaCl, $MgCl_2$ etc. which promotes spinel formation at reduced calcination temperature and densification.

Many schools have been studying on processing parameters and characterization of spinel and its composites, both stoichiometric and non-stoichiometric[8]. Literature shows that

purer raw materials led to end products of better refractoriness and reactivity of starting materials largely influences both spinellisation reaction and densification of the spinel[9,10]. In another work, it has been reported that fineness of the precursors attained by milling also plays a significant role in reactivity of starting materials. Generally oxide ceramics by themselves do not exhibit properties suitable to be used in desirable application areas. However through multiphase ceramic materials there is a possibility of developing microstructure through which the properties can be tailor made to handle desirable service environment. Usually, MgO-rich spinel has been found to have better density and grain morphology than Al_2O_3 rich spinel. In earlier works, it has been reported that incorporation of spinel particles of specific amount and specific particle size into magnesia refractories has led to enhancement of mechanical properties of MgO-spinel refractories.

On the basis of the above findings and importance, the particular interest of this study was to develop spinel as end products that are rich in magnesia through solid state reaction. The purpose also was to develop such composites from the combination of sea water magnesia and commercially available α-Al_2O_3 powders by mix-milling them in weight proportion of Al_2O_3 : MgO (A : M = 1:1, 1:1.1, 1:1.2, 1:1.3, 1:1.4) through double-stage sintering process. By paying close attention to the earlier research work, it is well understood that the crystallization behavior and densification of MgO-rich spinel depend on the amount of initial MgO-phase content, amount of spinel seed and/or temperature. However, the effects of in-situ spinel seed content through solid-state reaction of MgO-rich $MgAl_2O_4$ spinel on crystallization and densification behavior are limited. In the present work, a wide range of MgO-rich spinel has been prepared from their constituent solid-oxides in weight proportion, through calcination at different temperatures. Phase analysis and densification has been carried out of the sintered specimens. The sintered MgO-rich spinels have been characterized and analyzed for the crystallization behavior, extent of spinel phase development and microstructure. Finally an attempt has been made to correlate the effect of spinel seed addition on the crystallization behavior, microstructure, hardness, compressive strength and flexural strength of sintered specimens. Additionally, the retained flexural strength of the thermally spalled samples has been carried out and correlated with microstructure.

CHAPTER 2

2.0. LITERATURE REVIEW

The literature review is divided into four major sections. Section 2.1 to 2.5 provide background information on the material, identify significance of the spinel group of minerals and specify the projected material with a discussion of relative advantages and disadvantages of the highlighted synthesis processes. Section 2.6 to 2.8 reviews the processing techniques and the corresponding results and properties observed by other investigators. This chapter incorporates background information to assist in understanding the aims and results of this investigation, and also reviews recent reports by other investigators with which these results can be compared.

2.1. Starting Materials

2.1.1. Alumina- Origin and Crystal Structure of α-Alumina:

Alumina is considered as a typical representative in the group of structural ceramics. These materials are usually intended to serve as structural parts subjected to mechanical loads at high temperatures. The common feature of structural ceramics is good mechanical behavior therefore, efforts in developing, fabricating, and optimizing these materials are concentrated towards high strength. Generally the objective of development of high strength ceramics is substitution of metallic materials in relevant regions. Certain examples of structural ceramics, in addition to alumina, are some pure oxide ceramics such as yttria (Y_2O_3), titania (TiO_2), zirconia (ZrO_2), magnesia (MgO); and alumina-magnesia spinel ($MgAl_2O_4$), as well as the two non-oxide ceramics which are extensively used in gas turbine applications, silicon nitride (Si_3N_4) and silicon carbide (SiC). Gitzen[11] in his work on aluminum oxide ceramic technology has traced the individual crystallographic phases of alumina. He has reported the presence of seven crystallographic phases of calcined, water free alumina had been found. The structural applications of aluminum oxides are limited almost entirely to the α–phase (α-Al_2O_3), also called corundum or, in its single-crystalline form, sapphire. Brag and Brag in 1915 were next to Gitzen, in determination of the crystallographic structure of corundum. In 1925 the first exact

attribution to the rhombohedral structure ("corundum structure") was made by Pauling and Hendricks. Further crystallographic studies were carried out by Winchell.[12]

The structure of aluminum oxide consists of close packed planes of the large oxygen ions stacked in the sequence A-B-A-B, thus forming a hexagonal close packed array of anions. The cations are placed on the octahedral sites of this basic array and form another type of close packed planes which are inserted between the oxygen layers. To maintain charge neutrality, only two thirds of the octahedral sites available are filled with cations. Fig. 2.1a illustrates the packing of Al and O in the basal plane. Since the vacant octahedral sites also form a regular hexagonal array, three different types of cation layers can be defined, depending on the position of the vacant cation site within layer, which may be named as a, b and c, and which are stacked in the sequence a-b-c-a-b-c. This gives the complete stacking sequence of anion and cation layers of the form A-a-B-b-A-c-B-a-A-b-B-c-A. It is only reproduced after the sixth oxygen layer or after the sequence a-b-c is repeated twice (Fig. 2.1b).

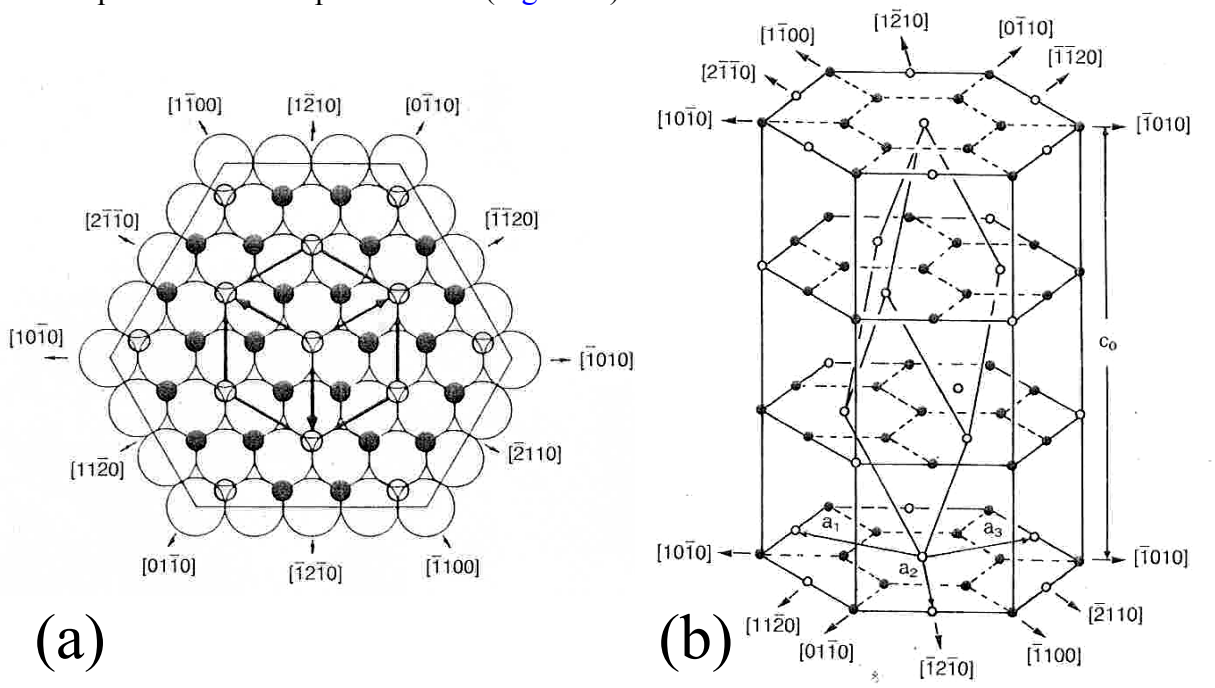

Fig.2.1. Basal plane of α-Al_2O_3 showing the hexagonal close packed anion sublattice (large open circles) and the cations occupying two-thirds of the octahedral interstices (small filled circles); small open circles are empty octahedral interstices (a).The cation sublattice in α-Al_2O_3 filled circles are Al, open circles are empty octahedral interstices (b) [13]

The unit cell of α-alumina defined in this way is called the crystallographic or structural unit cell, in contrast to the morphological unit cell, where the cation sequence is repeated only once and the height is half that of the structural cell. This important difference between the two cells, which has given rise to some confusion in the literature dealing with crystallographic

indices of sapphire, was pointed out clearly by Kronberg[14]. The structure of α-Al_2O_3 results in coordination number of 6 and 4 for the cation and the anion, respectively. The ionic radii for this coordination are 0.053nm for Al^{3+} and 0.138nm for O^{2-}. Lattice parameters a_0 and c_0 are 4.7589 and 12.991Å respectively.

2.1.2. Magnesia- Origin and Crystal Structure:

Magnesia or magnesium oxide is an alkaline earth metal oxide. Magnesium is the eighth most abundant element constituting about two per cent of the earth's crust and typically 0.12% of seawater. The majority of magnesium oxide produced today is obtained from the calcination of naturally occurring minerals, magnesite, $MgCO_3$, being the most common. Other important sources of magnesium oxide are seawater, underground deposits of brine and deep salt beds from which magnesium hydroxide [$Mg(OH)_2$] is processed. Both $MgCO_3$ and $Mg(OH)_2$ are converted to MgO by calcination. The thermal treatment of the calcination process affects the surface area and pore size and hence the reactivity of magnesium oxide formed. The source largely determines the level and nature of impurities present in the calcined material. Caustic calcined magnesia which is used in a wide range of industrial applications e.g. plastics, rubber, adhesives and acid neutralisation is formed by calcining in the range 700 – 1000^oC. By calcining in the range 1000 – 1500^oC the magnesium oxide is used where its lower chemical activity is required e.g. fertilizer and animal feed. Dead-burned magnesia, which is produced in shaft and rotary kilns at temperatures over 1500^oC, has reduced chemical reactivity therefore is more suited to refractory applications. Finally fused magnesia which is produced in an electric arc furnace from caustic calcined magnesia at temperatures in excess of 2650^oC is used for a variety of refractory and electrical applications.[15]

Magnesia has a wide range of refractory applications with good refractoriness and good corrosion resistance. Magnesia is widely used in the steel industry as a refractory brick often impregnated with carbon (tar, pitch, graphite) to give optimum properties for corrosion resistance in environments of basic slag, particularly in BOF furnaces or slag lines of treatment ladles. Recently Magnesia bricks often in combination with spinel or chrome are also used in ferroalloy, non-ferrous, glass and cement industries. Castables and sprayables based on magnesia are widely used for basic refractory linings for steel transfer applications. The lime to silica ratio present in the magnesia has a major influence on its properties. In the structure of

magnesia, the magnesium and oxygen ions (charged atoms) are arranged in a periodic lattice. Each positive ion is surrounded by negative ions, and vice- versa.

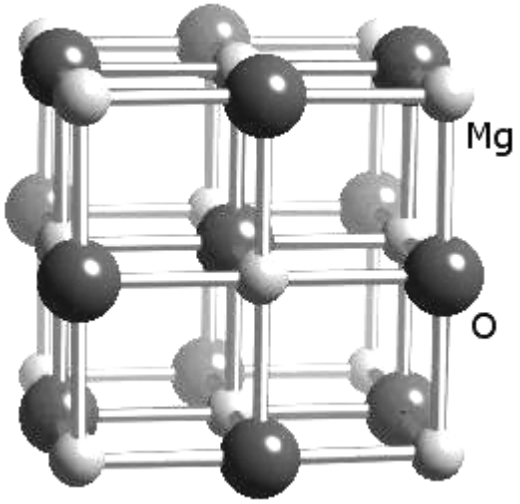

Fig.2.2 Crystal structure of Magnesia

Fig.2.3 shows a flow sheet of preparation of Seawater Magnesia[16]. Sea water is rich in MgO (2lb/100gal.) is reacted with an alkali source (normally CaO or dolime) to precipitate $Mg(OH)_2$. Generally, the limestone or dolomite quarried is crushed, washed, graded and calcined in rotary kilns at 1400-1500^oC to produce reaction lime or dolime. The lime is then slaked to a fine powder in pan hydrators. The hydrated product is then made into a slurry to facilitate handling and mixing with the sea water and is classified to remove impurities.

Sea water is first pretreated with small proportions of H_2SO_4 to remove the bicarbonates which would otherwise increase the CaO content of final MgO. H_2SO_4 reacts with calcium bicarbonate to give CO_2 which is dissolved in wooden desorption tower. This treated sea water is then pumped to agitated reaction vessels where it is mixed with the classified dolime/lime slurry and $Mg(OH)_2$ is precipitated as dilute solution.

The $Mg(OH)_2$ is allowed to settle in large diameter shallow tanks. The settled $Mg(OH)_2$ is washed and filtrated with seawater and fresh water. Then the resultant is calcined at 1600^oC to get sea water magnesite.

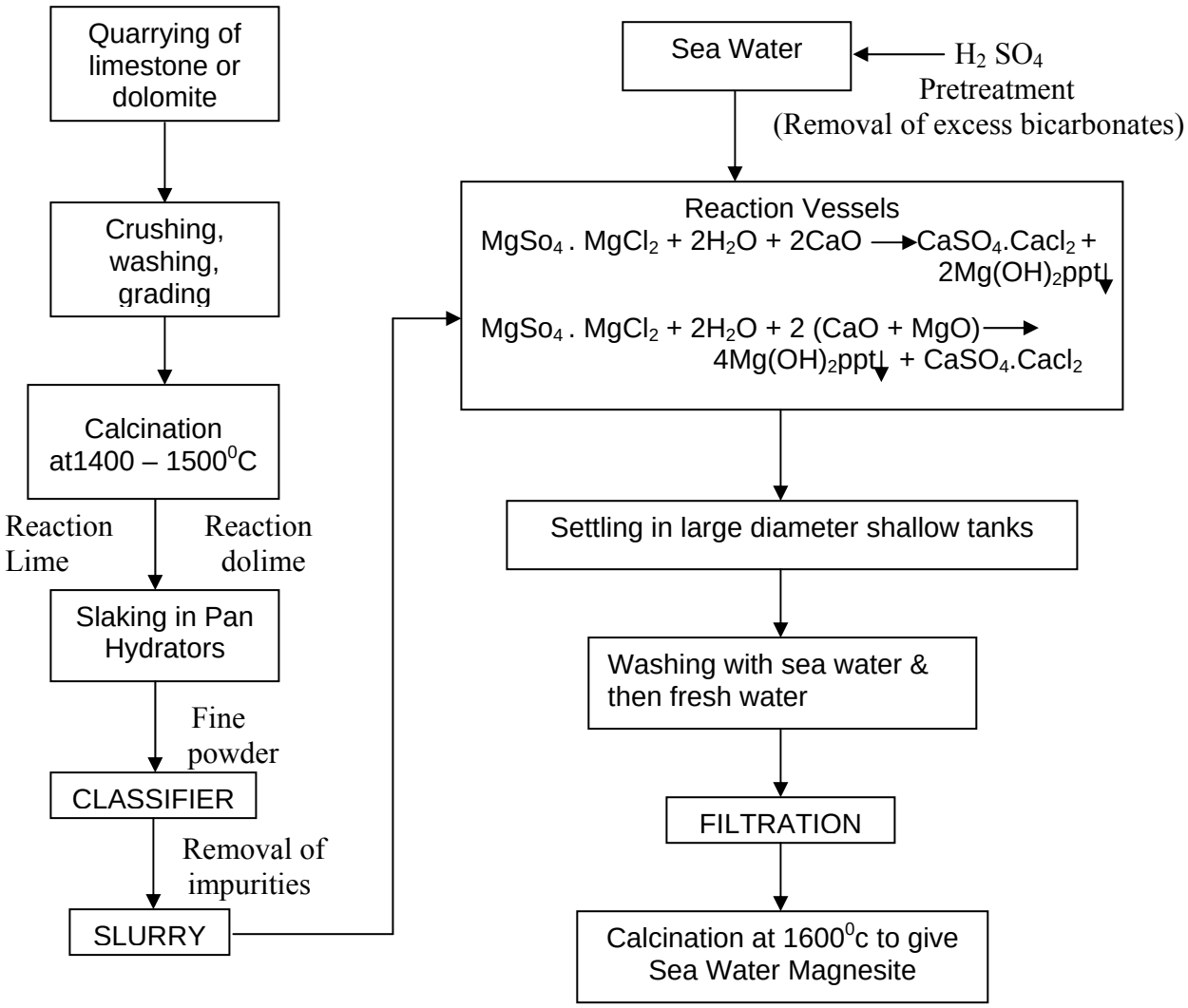

Fig.2.3 Methodology of Production of Seawater Magnesia[16]

2.2 A common feature of Refractory material

What sets Homo sapiens apart is the ability to imagine and create. This work addresses a small segment of that arsenal. Man's progress till date, has been marked by lots of invention and discovery. In an advanced society, virtually, every thing depends directly or indirectly, somewhere in its background, on manufacturing processes conducted at high temperatures. That goes for every thing we eat, drink, learn, use, wear, occupy or enjoy, for our work, our health and security, our mobility, our comfort and leisure. The positive impact of high-temperature processes on modern life is all pervasive. The hot manufacturing processes that comes into an ordinary man's mind, generally includes the making, shaping or treating of metals, ceramics including glasses and cements, electronic materials, fuels, a host of organic and inorganic chemical products, and more. Industrial refractories make these hot processes possible and economical when metal containment cannot compete. Refractories are thus *enablers* or *facilitators* of our productivity.[17]

Refractory means "hard to fuse". Refractories are class of materials, which can withstand high temperature, resist the action of corrosive environments and dust-laden currents of hot gases etc[18]. The refractory materials can be classified on the basis of composition and applications as follows:

A) Acid Refractories

These are the refractories that are attacked by basic slags and include:

(i) Alumino-Silicate Refractories

(ii) Silica Refractories

B) Basic Refractories

These are refractories that are attacked by acidic atmosphere and include:

(i) Magnesite Refractories

(ii) Dolomite Refractories

(iii) Chrome Magnesite and Magnesite-Chrome Refractories

C) Neutral Refractories

These are the materials that are attacked neither by acids nor by bases. Such materials are also used to replace basic refractories where the corrosive action is strong.

(i) Various forms of Carbon

(ii) Alumina

(iii) Artificial Refractories- eg. Zirconium carbide, Titanium Carbide and Silicon carbide etc.

(iv) Metals- eg. Iron, copper, nickel, molybdenum, platinum, tantalum, thorium, tungsten, vanadium, osmium and zirconium.

D) Special Refractories

These include expensive materials, which are used for the construction of crucibles and furnaces for experimental and other special purposes. eg. BeO, ThO_2, $ZrSiO_4$.

E) Insulating Refractories

These are the high porosity refractories having low thermal conductivity and high thermal insulation properties suitable for minimizing heat losses and maximizing heat conservation in the kilns and for furnaces.

F) Cermets

These are special refractories, which are a combination of a metal or an alloy and non-metal such as an oxide, carbide, nitride, or boride. They have high strength and resistance to high temperatures, which make them suitable for use in very special and more recent applications like those in space vehicles, missiles and nuclear energy plants etc.

2.3 Classification of Spinel

Spinel – A Mineral:

Spinel literally means a hard glassy mineral consisting of an oxide of magnesium and aluminium. It is a mixed/ternary oxide whose properties range between that of MgO and Al_2O_3. $MgAl_2O_4$ (Spinel) is the most stable compound of $MgO.Al_2O_3$ system[19].

Some common examples of minerals of spinel group are:-

Chromite – Iron Chromium oxide is the most important ore of chromium and is an important metal with a wide range of industrial uses. It is resistant to the altering affects of high temperatures and pressures and is used as a refractory component in the bricks and linings of blast furnace. It has isometric crystal system 4/m bar 3 2/m with opaque crystals. They exhibit a specific gravity of 4.5-4.8 and a hardness of 5.5.

Franklinite- Zinc Iron Manganese Oxide has metallic luster with an isometric crystal system; 4/m bar 3 2/m. It has a specific gravity of 5-5.2 and a hardness of 6. The crystals are opaque.

Gahnite- Zinc Aluminium oxide is one of the rarer members of this group. Gahnite produces crystals showing well-formed octahedrons which are generally translucent to almost opaque. The crystal system is isometric; 4/m bar 3 2/m and specific gravity is 4.55-4.6 and hardness is 7.5-8 Mohs respectively.

Magnetite- Fe_3O_4 is a member of the spinel group which has the standard formula $A(B)_2O_4$. The A and B represent usually different metal ions that occupy specific sites in the crystal structure. In the case of magnetite, Fe_3O_4, the A metal is Fe^{+2} and the B metal is Fe^{+3}; two different metal ions in two specific sites. The crystal system is isometric and has hardness of 5.5 - 6.5 in Moh's scale and specific gravity of 5.1.

Minium- Pb_3O_4 is actually composed of two different valence states (b^{+2} and Pb^{+4}. The two different valences of lead occupy different locations in the spinel type structure. Minium is a tetragonal (bar 4 2 m) mineral. The small sizes of the lead ions, no doubt, cause a distortion in the spinel structure. The specific gravity is 8.9 - 9.2 and hardness in moh's scale is 2.5 – 3.

2.3 (a) Spinel:

Natural spinels are common high temperature minerals in metamorphic rocks. Spinels might be also present as non-metallic inclusions in steel. Spinel is one of the end members of spinel group of minerals, which have general composition of AB_2O_4, where 'A' is a divalent atom such as Mg^{2+}, Fe^{2+}, Mn^{2+}, Zn^{2+}, and 'B' is a trivalent atom such as Al^{3+}, Fe^{3+}.

2.3 (b) Spinel Structure:

The spinel minerals have the generic formula AB_2O_4, where A is a cation with +2 charge and B is a cation with +3. The most common members include:

A	B	Formula	Mineral
Mg	Al	$MgAl_2O_4$	Spinel
Fe^{+2}	Fe^{+3}	$Fe^{+2}O.Fe^{+3}{}_2O_3=Fe_3O_4$	Magnetite
Fe^{+2}	Cr	$FeCr_2O_4$	Chromite

Spinels crystallize in the cubic space group Fd3m (2 2 7) with 8 tetrahedral 'a' sites and 16 octahedral 'd' sites[20]. The usual anions are oxygen and are located in the 32 'e' sites arranged in

cubic closed packed layers. The cubic closed packed layers of anions alternate with cation layers. The unit cell contains 8 molecules of AB_2O_4. The physical and chemical properties of spinel is decided by 'A' and 'B' as well as by the distribution of these cations in the different crystallographic sites[21,22,23].

In the "normal spinel" structure, all the divalent cations are located on tetrahedral 'a' sites, while all trivalent cations are exclusively on octahedral 'd' sites. If we represent tetrahedral sites by ( ) and octahedral sites by [ ] then "normal spinel" can be said to have a formula of $(A)[B]_2O_4$. In the "inverse spinel" structure, half of the trivalent [24] ions are on the tetrahedral 'a' sites and the divalent cations occupy together with the remaining half of the trivalent ions octahedral 'd' sites. The formula for inverse spinel as represented in above would be $(B)[AB]O_4$. Further it can be said that the structures with intermediate cation distribution exists between these two limiting cases. The formula of these structures with intermediate cation distribution can be $(A_{1-x}B_x)\ [B_{2-x}A_x]O_4$; where x is inversion parameter and $0 \leq x \leq 1$.

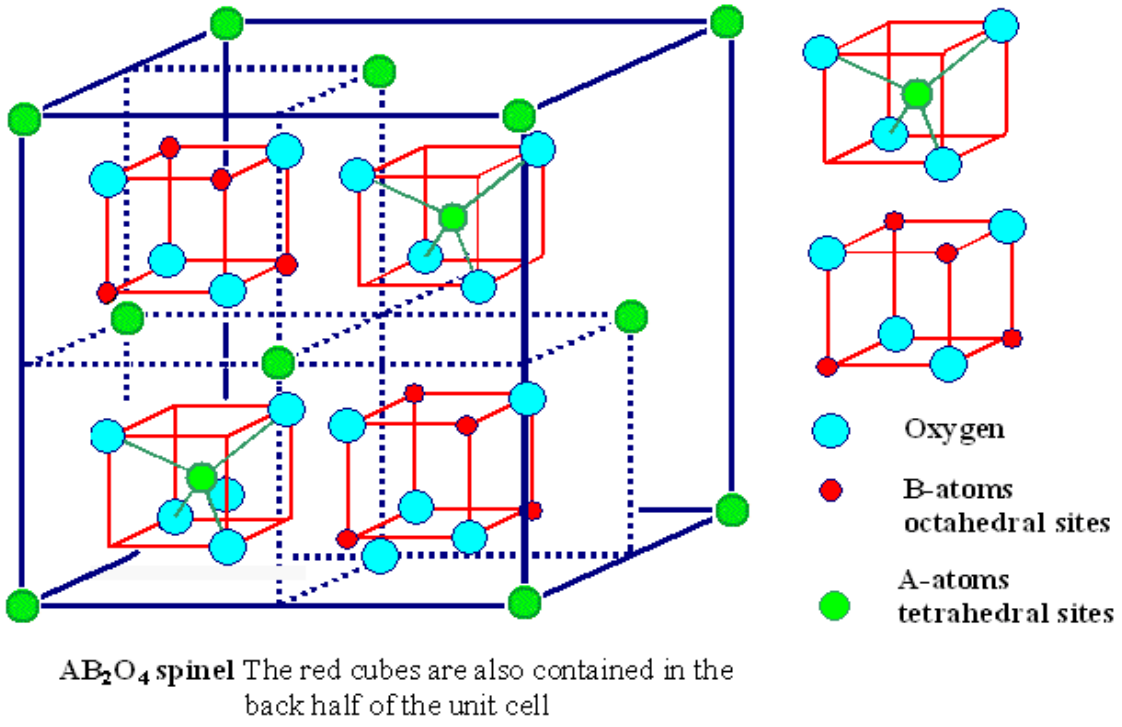

AB_2O_4 spinel The red cubes are also contained in the back half of the unit cell

Fig.2.4 Structure of $MgAl_2O_4$ Spinel

2.3(c) Normal and Inverse Spinels:

Since there are twice as many filled octahedra as tetrahedra, and the formula for spinel is AB_2O_4, it is possible to fill all the octahedra with B (trivalent) atoms and the tetrahedra with A (divalent) atoms. We can't reverse the roles of A and B and fill all the sites. If we were to try, we could only fill half the octahedra with A, and the tetrahedra would only take up half the B atoms. The remainder would fill the still-vacant octahedra. Such a structure is called an *inverse spinel*. Spinel and chromite are normal spinels, magnetite is an inverse spinel[25]. In reality, most spinels are somewhere between the two end states. In the "normal spinel" structure, all the divalent cations are located on tetrahedral 'a' sites, while all trivalent cations are exclusively on octahedral 'd' sites. If we represent tetrahedral sites by ( ) and octahedral sites by [ ] then "normal spinel" can be said to have a formula of $(A)[B]_2O_4$. In the "inverse spinel" structure, half of the trivalent ions are on the tetrahedral 'a' sites and the divalent cations occupy together with the remaining half of the trivalent ions octahedral 'd' sites. The formula for inverse spinel as represented in above would be $(B)[AB]O_4$[26,27]. Further it can be said that the structures with intermediate cation distribution exists between these two limiting cases. The formula of these structures with intermediate cation distribution can be $(A_{1-x}B_x)\ [B_{2-x}A_x]O_4$; where x is inversion parameter and $0 \leq x \leq 1$.

2.3 (d) Importance of Magnesium Aluminate Spinel:

Magnesium Aluminate ($MgAl_2O_4$) spinel ceramic is of significant technological interest for refractory and structural applications at elevated temperature due to its high melting point, good mechanical strength and excellent chemical resistance. It is the only stable compound present in $MgO.Al_2O_3$ system. Owing to its chemical compatibility with alumina, zirconia and mullite spinel is an attractive matrix for ceramic matrix composites[28]. The major application areas of spinel refractory are transition and burning zones of cement rotary kilns, sidewalls and bottom of steel teeming ladles and checker work of glass tank furnace generators because they are resistant to corrosion by slag. For such applications spinel is used as a major component in an alumina rich or magnesia rich matrix, depending upon the environmental condition prevailing in the application zone. Hence, magnesia rich or alumina rich spinel (non-stoichiometric) compositions are important from the application point of view.

Spinel type compounds are used in electrochemical devices and batteries as energy sources for portable telecommunication devices. Together with their application as transparent

semiconductors in solar cells and displays, and even in the field of biology in dentistry spinels are very promising research objects in materials science.

2.4 Phase diagram of MgO-Al_2O_3

The concerned phase diagram is MgO-Al_2O_3 binary system. Here the end components are MgO and Al_2O_3 having high melting temperature 2800°C and 2020°C.

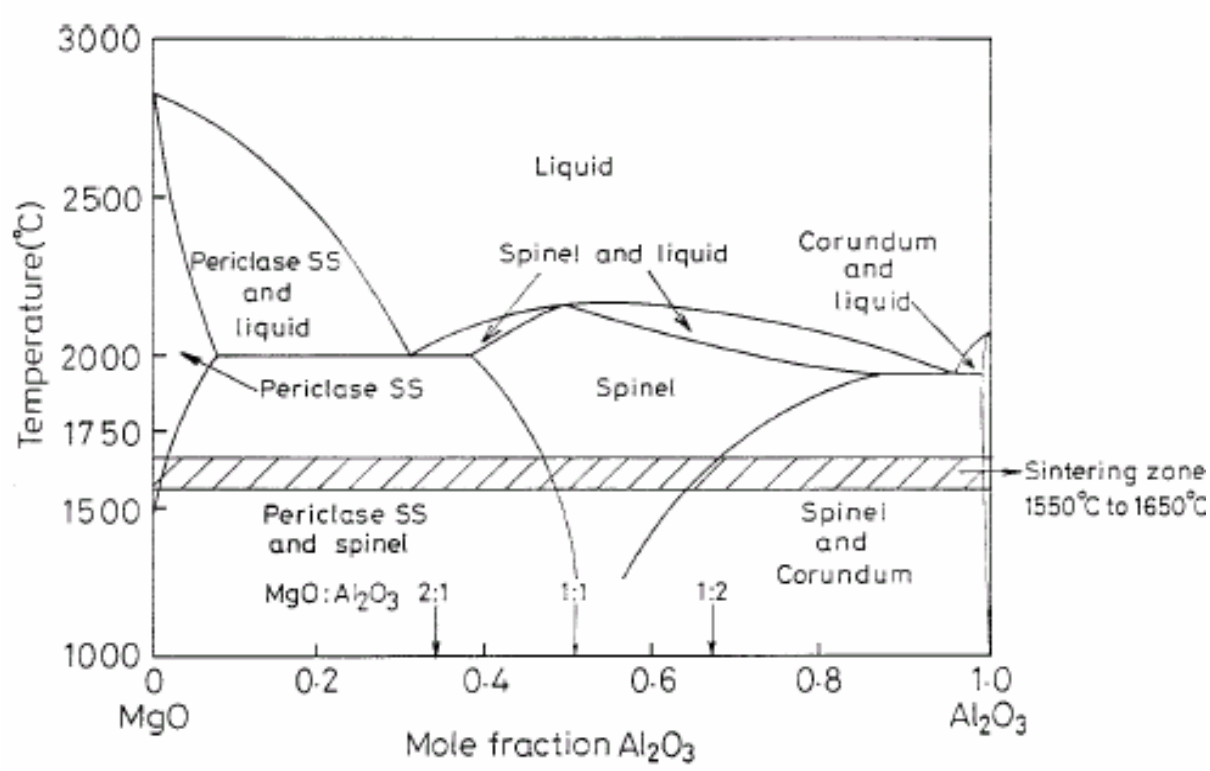

Fig. 2.5 Phase diagram of $MgAl_2O_4$ spinel[29]

MgO and Al_2O_3 form spinel at equimolar proportion i.e. 50:50 molar composition. The spinel hence formed is a eutectic compound showing congruent melting nature. Spinel has got high melting point around 2135°C. The spinel divides the whole system into two independent eutectic systems those are MgO-$MgAl_2O_4$ and $MgAl_2O_4$-Al_2O_3 as shown in the diagram. So if a stoichiometric proportion of MgO and Al_2O_3 is taken, heated and cooled down slowly then at eutectic point, it gets converted to pure spinel.

The MgO.Al_2O_3 system is of considerable interest to the refractories technologist because: -

- Firstly, because spinel MgO.Al_2O_3 is a refractory in its own right
- Second because it shows that no liquid is formed with any mixture of pure magnesia and alumina at temperature below 1900°C

Chesters and Parmelee showed that the reaction between equimolecular amounts of magnesia and alumina results in a substantial reaction-expansion[15]. This composition or one higher in magnesia composition can be made to produce steel-tight basic linings.

2.5 Reaction Mechanism in Spinel Formation

Formation of spinel from its constituent oxides is a counter diffusion process of Mg^{+2} and Al^{+3} ions[30] and this solid-state reaction depends on large number of parameters. Solid-state reaction between MgO and Al_2O_3 to form spinel occurs at the Al_2O_3-$MgAl_2O_4$ and the MgO-$MgAl_2O_4$ interfaces. The reaction between these phases is governed by counter diffusion of the Al^{3+} and Mg^{2+} ions through the rigid oxygen lattice or the spinel phase. Three Mg^{2+} ions diffuse for every two Al^{3+} ions, which diffuse in the opposite direction. Three moles of spinel are formed at the Al_2O_3-$MgAl_2O_4$ interface for every mole formed at the MgO-$MgAl_2O_4$ interface because of ionic charges and stoichiometry[31,32]. This is illustrated by the following schematic section through a growing $MgAl_2O_4$ layer, which is called as Jander solid-state reaction geometry.

2.6 Properties of $MgAl_2O_4$

Spinel exhibits following properties[33]

1) High melting point ~ 2135^{o}C
2) Hardness of ~ 8 Mohs / 14GPa
3) Density ~ 3.58 g/cc
4) Young's modulus ~190 GPa
5) Resistance to chemical attack
6) Low electrical loss
7) Chemical compatibility with Al_2O_3, ZrO_2, Mullite
8) Thermal Conductivity ~ 15W/m^{o}K
9) Nonmagnetic
10) Luster is Vitreous
11) Thermal Expansion Coefficient of ~7.6x10^{-6}/ ^{0}C

2.7 Application Areas

Certain application areas in which spinel finds technical importance are[34]:

(i) Refractory Applications-Transition and burning zones of cement rotary kilns. Sidewalls and bottom of steel teeming ladles and checker work of glass tank furnace.

(ii) Electronic Applications-Humidity and Infrared Sensors.

(iii) Optical Devices-Transparent material for arc enclosing envelopes and windows for pressure vessels and bullet-proof vehicles, furnace sight glass. Substrate of luminous faceplate of CRT, polarimeter for LED, Watch crystals, Safety goggles, as components in optical computer and high-speed printer, High-pressure arc lamp and lens, pressure vessel sight glass, furnace sight glass.

(iv) Armour materials-Missile domes, submarine port & covering for a tank port

(v) Alkali metal vapour discharge devices

(vi) Ceramic ultra filtration membranes

(vii) Insulating material for fusion reactor core- Container for nuclear waste

(viii) Ceramics in dentistry

(ix) A valve flap, valve seat, a water-jet cutting flow-shaper, a nozzle for process fluids.

(x) Tribological applications

2.8 Synthesis and Properties of Spinel Composites

Methods of fabrication of spinel have been known since 1905 and phase diagram has been known since 1916 but it took time to gain commercial success till 1980s due to its complexity in process parameters: mainly the volume expansion of ~5-7% which occurs during $MgAl_2O_4$ spinel formation from its constituents. Spinel formation from its constituent oxides is associated with 5-7% volume expansion which hinders the densification process to take place in the same firing[4]. Various workers studied the effect of raw materials reactivity on spinel formation and densification. Formation of spinel from magnesia and alumina does not allow the material to densify in a single stage firing. Hence the general practice is to complete the spinellisation process first and then crushing, milling, reshaping and sintering the spinel to achieve desired properties in the second firing. Therefore two-stage sintering process and a number of relevant processing parameters have greatly influenced the cost of production. The limiting factors for spinel preparation are the requirements regarding purity of the raw materials, their reactivity, intermediate calcinations temperature, higher sintering temperature etc.

Many authors/researchers have employed various experimental methods to produce spinel. Many authors achieved spinel formation at a temperature as low as 600°C. This section describes various methods implemented by various authors to produce spinel.

Kainarskii et.al[35] studied the stability of sintered spinel, spinel-corundum, and corundum refractories with certain oxides, salts, alkalis and alkaline metals at 1500-1700°C. They found that magnesia-spinel and spinel were least reactive while corundum was the most affected. Spinel sintered refractory was best in corrosive atmosphere. Antonov et.al[36] studied refractoriness of periclase-spinel refractories prepared from pure (seawater) and ordinary sources. They found refractories produced from pure sources better in refractoriness than those from ordinary sources. They studied the effect of impurities on the refractoriness of the products. Microstructure of the pure source product was compared with that of ordinary source products. In another work of their's Antonov et.al[8] have emphasized on solid phase reaction for bulk production. They have tried to determine the technological parameters of synthesis of magnesia-alumina spinel from periclase and bauxite. A temperature of 1500°C was reported to be optimum for spinel synthesis from the starting materials. Microstructure study showed that excess magnesia retarded grain growth. The authors also studied the effect of additives on density, degree of crystallization, coloration and refractive index of magnesia rich spinel. Kostic et.al[10] studied densification of partially synthesized spinel mixtures with and without addition of CaO/SiO_2 mixture. The degree of densification was found to be proportional to the initial amount of spinel phase in the mixture. CaO/SiO_2 mixture enhances grain growth in each spinel composition and also helps enhance the densification. Pasquier et.al[37] studied the effect of isostructural and non-isostructural spinel seeding on synthesis of $MgAl_2O_4$ through different methods. TEM micrographs confirmed that spinel seeding led to difference in morphology of powders among the various routes. They observed that isostructural spinel seeding led to a decrease in crystallization temperature of $MgAl_2O_4$ due to nucleation and epitaxial growth mechanism. Gusmano et.al[38] studied mechanism of $MgAl_2O_4$ spinel formation from thermal decomposition of Co-precipitated hydroxides of alumina and magnesia in different molar ratios. They observed crystallization of spinel phase at a temperature as low as 400°C due to reaction between $\eta-Al_2O_3$ and $Mg(OH)_2$. Ko and Chan[39] observed that the spinel content had a positive effect on the Hot Strength of alumina castables in the temperature range of 1000-1500°C. The hot modulus of rupture of selected material increased with increasing content of spinel. Sarkar et.al[40] studied effect of compositional variation and fineness of precursors on the densification of

MgO-Al_2O_3 compacts. Densification was observed to be easier and better for magnesia rich composition with 4h attritor milling; but difficult for alumina rich composition. They found that MgO rich and Al_2O_3 rich spinel had periclase and corundum as secondary phase respectively. Microstructure revealed well developed compacted structure for stoichiometric and MgO rich composition. Wantae Kim et.al[41] carried out planetary ball milling of amorphous $Mg(OH)_2$ and gibbsite for 120min. crystallization of spinel phase was observed at 780°C after 15mins of grinding. The authors claim that grinding promotes aggregation which deflocculated into fine particles after calcination. R. Sarkar et.al[42] observed that TiO_2 improved density of stoichiometric and Al_2O_3 rich spinels sintered at 1550°C; but higher amount of additive had a deteriorating effect due to grain growth, which is supported by the micrographs. The roundedness in grain structure affected the strength properties. The authors reported that TiO_2 addition did not had much effect on MgO rich spinels. Laurence et.al[25] studied influence of synthesis routes on $MgAl_2O_4$ spinel properties. They observed higher crystallinity, higher incorporation of Al^{3+} in tetrahedral sites and better electrical properties in samples synthesized from sulfate precursors than from calcination of oxide mixtures. The better properties was explained by better homogeneity of sulfate mixture than oxides due to presence of liquid phase between 160-650°C. Ganesh et.al[43] prepared stoichiometric $MgAl_2O_4$ spinel with $AlCl_3$ as additive by conventional double-stage firing process. The authors reported that $MgAl_2O_4$ spinel when incorporated into high alumina and chrome refractories improved their resistance to slag penetration and thereby erosion. In their work, L. B. Kong et.al[44] implemented high-energy ball milling process to attain $MgAl_2O_4$ spinel phase.

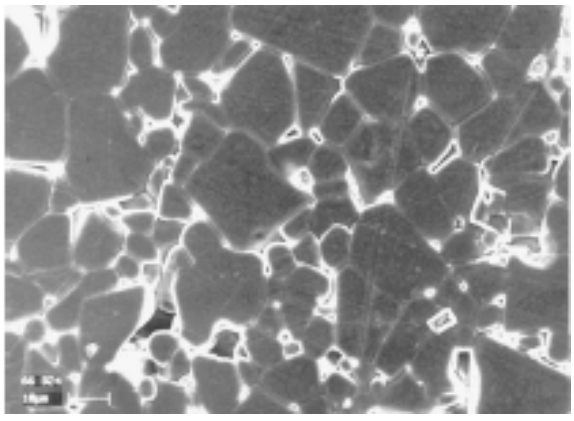

Fig.2.6 SEM photomicrograph of MgO-rich spinel[45]

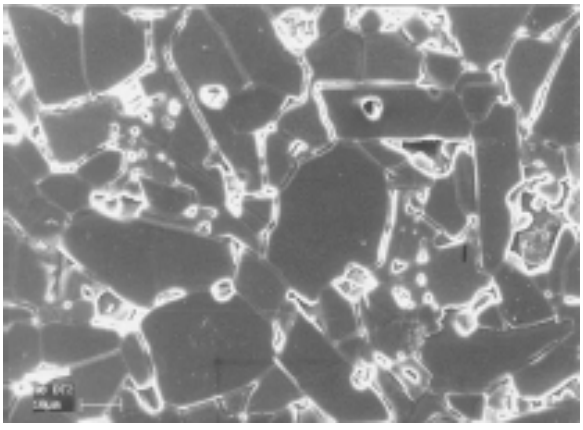

Fig.2.7 SEM photomicrograph of Al_2O_3-rich spinel[45]

The sintering of milled-mixed MgO and Al_2O_3 powders led to spinel formation at 900°C/2h. The density as well as the crystallinity of spinel phase was observed to increase with

higher sintering temperatures. Microstructure also revealed better density with temperature due to high reactivity of the starting materials due to intensive grinding. Ritwik Sarkar et.al[45] varied the reactivity of alumina by calcination between 800-1600^{o}C and studied its effect on the densification of non-stoichiometric spinels.

With increase in calcination as well as sintering temperature, the authors observed a beneficial effect on densification of alumina rich spinels but not for the magnesia rich spinels due to coarsening effect. They observed higher grain size in micrographs of high alumina content samples. In another work, Sarkar et.al[46] studied densification behavior of MgO rich spinels on the basis of alumina reactivity.

The increase in calcination temperature of alumina caused inertness and increased the expansion behavior of the composition. The authors observed least/no effect of calcination of alumina in sintered density due to reduced sinterability/inertness. Calcination of alumina and variation in sintering temperature of spinel did not influence the phase content of sintered products. At higher calcination as well as sintering temperature the authors reported a reduced hot strength due to coarsening effect. Sarkar et.al[47] also studied effect of various additive oxides on the densification of presynthesized and reaction sintered spinels. They reported better density in reaction sintered products. TiO_2 and Cr_2O_3 showed beneficial effect on densification while V_2O_5 and B_2O_3 had detrimental effects. Tripathi et.al[48] reported in their seminal work that solid oxide reaction sintering of spinel developed from sintered magnesia-alumina (SMA) had better densification (89%RD) than when developed from caustic magnesia-alumina (CMA). The higher surface area and lower crystallite size leads to higher densification ratio and thus higher expansion and exaggerated grain growth retards the densification process.

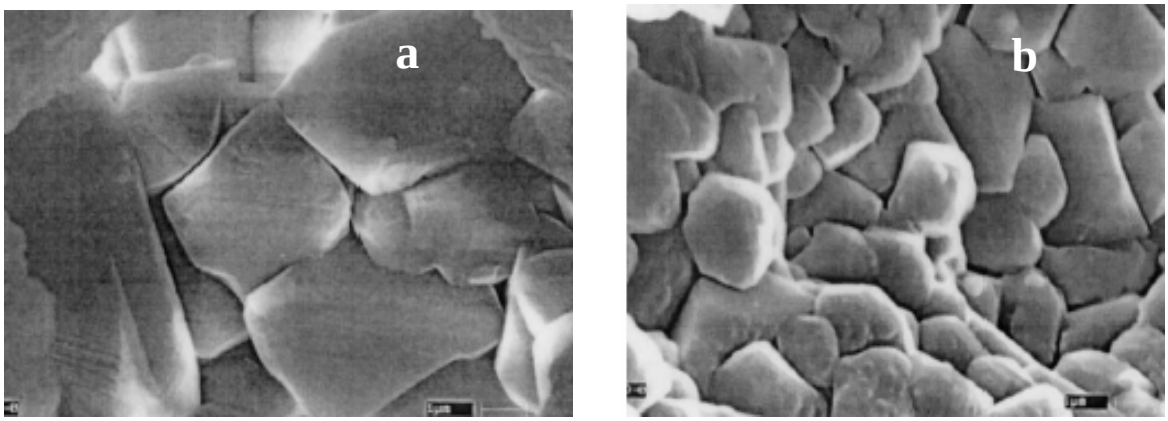

Fig.2.8 SEM micrographs of sintered spinels[48]: a) Caustic magnesia alumin b) Sintered magnesia alumina

S.K Behera et.al[7] synthesized spinel by autoignition process using citric acid as fuel and metal nitrates as oxidizers. The authors have reported crystallization of spinel around 650°C and attained theoretical density at 1150°C/30min. The authors calculated activation energy required for densification of their system and reported vacancy diffusion influences densification. In an extension to this work Barpanda et.al[49] reported disorderness of spinel phase at lower calcination temperature which became obsolete at higher temperature. A combined effect of chemical composition and associated exothermicity of the reaction has been studied. The disorderness-orderness is confirmed by XRD and Raman spectroscopy analysis.

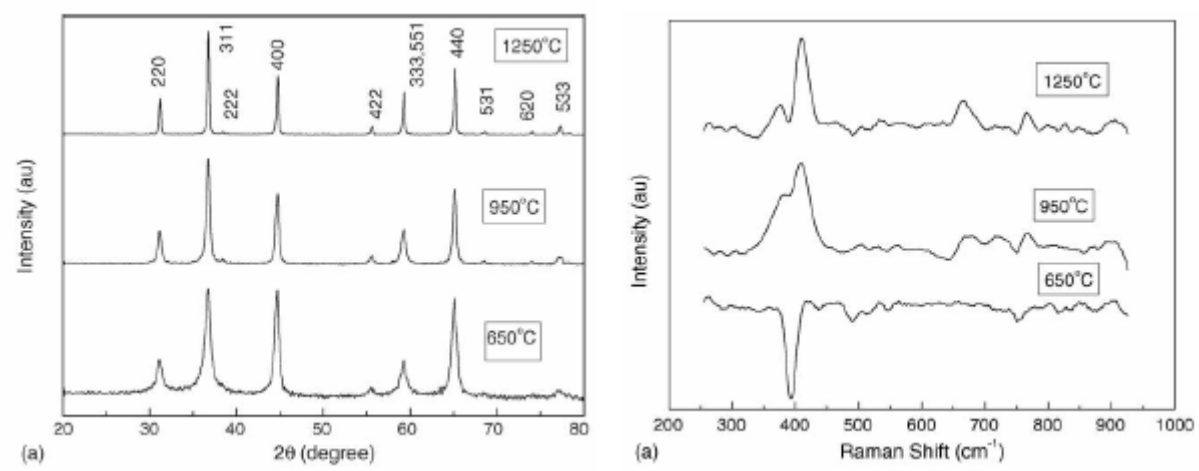

Fig.2.9 a) XRD and (b) Raman spectroscopy exhibiting disorderness and orderness[49].

Jia Xiaolin et.al[50,51] studied the effect of amount and size of spinel crystal seeds on the sol-gel synthesis of $MgAl_2O_4$ spinel. In their work they worked on factors influencing the $MgAl_2O_4$ synthesis and recommended 1% crystal seeds. Initial crystallization temperature was ~ 600°C and fully crystallized spinel phase was reported at 700°C. In his work on stoichiometric and non-stoichiometric spinels from co-melting method Zawrah[52] reported well crystalline spinel phase at 1000°C. The author reported that the crystallinity decreased with higher alumina content due to the decrease of lattice parameter and grain sizes. The author observed greater than 98%TD in stoichiometric spinel upon use of Fe_2O_3 as sintering aid.

Ghosh et.al[53] studied the effect of spinel addition in MgO refractories. $MgAl_2O_4$ spinel synthesized from solid-oxide reaction route was incorporated into magnesia refractory. A gradual decrease in thermal expansion behavior was observed with increasing spinel content. This is due to lower thermal expansion of spinel than magnesia. This work shows; incorporation of spinel greatly improves the refractoriness under load, retained strength after thermal shock and

hot modulus of rupture characteristics for the periclase body. The authors optimized 20wt.% spinel addition for better properties with 670kg/cm^2 of Hot MOR at 1200^{o}C, RUL of ~1680^{o}C and ~380kg/cm^2 of retained strength after 5 cycles. Recently, Aksel et.al[54-56] illustrated the influence of varying the amounts of spinel with a similar median particle size, with different distribution, on the mechanical properties and thermal shock performance of MgO–spinel composites. Mechanical properties of composites decreased significantly with increasing spinel content due to the thermal expansion mismatch that the bending strength of MgO-spinel composite is ~160MPa, which had been prepared with the addition of 5wt% of spinel powder and sintered at 1650^{o}C through hot pressing method. The author also found that the 3-pt bending strength (233±7 - 61±4 MPa) as well as the Young's Modulus (268±30 - 80±5 GPa) decreased uniformly with increasing additions of spinel, and with increasing spinel particle size. They observed that microcracks and grain boundary separation at MgO-spinel interface and concluded these defects caused failure on loading. The authors have studied in details about the crack mechanism involved in enhancement of strength at room temperature and after thermal shock. They observed that loss of strength and modulus was greater for larger spinel particles because of the increased extent of local tensile stress field. The authors have also studied the thermal shock parameters, fracture behavior before and after thermal shock and work of fracture and fracture surface energy.

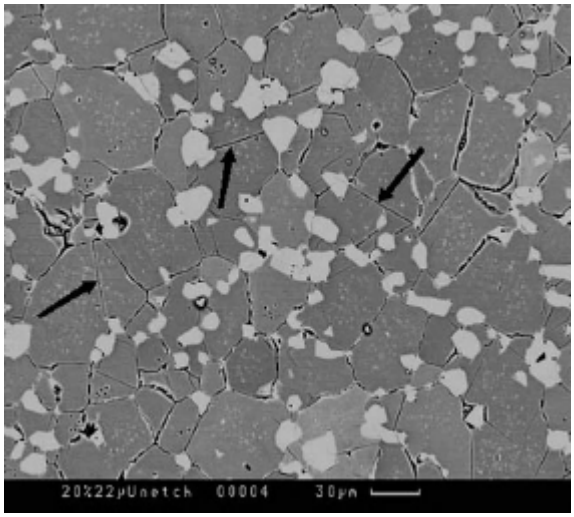

Fig.2.10 SEM micrograph[54] of a 20% 22 µm spinel A composite, showing crack length and linked microcracks between the spinel particles (dark grey: MgO, light grey: spinel)

However, Simonov[57] in his work observed the compressive strength of the preiclase and MgO-spinel materials varied within the range of 25-80MPa with an open porosity of 12.6-18.3%. Cunbing et.al[58] carried out hardness test on transparent $MgO.nAl_2O_3$ spinel ceramics (n=1, 1.3,

1.5, 1.8) under load of 200 and 1000g and observed an increasing trend of hardness (9-12GPa) for transparent spinel ceramics with increasing alumina content. But they observed a discontinuous trend of flexural strength measurement for 1700°C hot pressed specimens with highest strength of ~220MPa at n=1.3.

2.9 Processing parameters and Properties at a glance

The Table 2.1 below shows different processes implemented by various authors under various processing conditions and the results they concluded upon after their research work

Table 2.1: Properties attained with implementation of various processing routes

Methods	Raw Materials	Processing Conditions	Properties
[6]Combined Gelation-Precipitation	$Al_2(SO_4)_3.16H_2O$ $MgSO_4.7H_2O$ 0.5 mol/l solution mixed to give 1:1 molar ratio of Al_2O_3 : MgO. Gelation carried out by NH_4OH addition	Dried gel calcined at 300-1200^{0}C/1h. Uniaxially pressed samples were heated @ 10^{0}C/min up to 1100-1475^{0}C/3h	Average particle size of calcined sample 0.2μm. Surface area of 8.5m^2/g Phase development starts from 600^{0}C. Crystalline phase at 1000^{0}C. 95% of densification.
[7]Autoignition of citrate-nitrate gel	$Al(NO_3)_3.9H_2O$, $Mg(NO_3)_2.6H_2O$, and citric acid. Citrate–Nitrate ratio of 1:1. Self-ignition of the gel-like mass yielded a black mass.	Black Ash calcined at 650-1100^{0}C/9h. & at 1600^{0}C for 4h. Granulated powders were uniaxially compacted at 300MPa into cylindrical pellets (12mm ϕ, 3mm high). Sintering carried out in range of 650-1300°C 30 mins & 2h.	Phase development starts from 650^{0}C. Crystalline-ordered phase at 1100^{0}C above. Crystallite size ranged between 12nm-32nm. ~ TD achieved. Activation energy for densification calculated to 16.4 kcal/mol. Lattice constant 8.08A
[52]Co-Melting Method	$Al(NO_3)_3.9H_2O$ [A], and $Mg(NO_3)_2.6H_2O$ [M]	Mixing of precursors to give A/M=1,1.1, 1.2, 1.3, 1.4. Mixtures heated on hot plate at 250^{0}C till melting; then air quenched. Resulting solids heated for 2h at 500^{0}C Calcination done at 1000^{0}C.Fe_2O_3 used as sintering aids in different proportion	Crystalline Mg-Al peak obtained at 1000^{0}C. TG shows 20% wt.loss. Crystallinity decreased with higher Alumina % Crystal size obtained was between 12-59nm. Particle size obtained was between 10-60nm. Infrared spectroscopy showed bands of AlO_6 groups building up

Methods	Raw Materials	Processing Conditions	Properties
		Uniaxially pressed samples @ 60MPa sintered between 1450-1650^{0}C at 10^{o}C/min.Infrared spectroscopy was done. Plastic hardness [PH] and [EM] Elastic modulus tests done for mechanical property study	MgAl formation. >98% TD achievable Fe_2O_3 presence led to increase of sinterability after 1650^{0}C and improved mechanical properties;EM~280GPa and PH~15 GPa
[44]Mechanochemical Processing	Commercially available MgO and Al_2O_3.	Planetary ball milling at room temperature for 12h. in WC vial & WC balls as grinding media at 200 rpm Uniaxially pressed compacts @ 50MPa Sintered between 900-1500^{0}C/2h at 10^{0}C/min	Milled mixture yields a grain size ~ 100-300nm Beyond sintering temp. of 1100^{0}C grain size increases to 0.5-1.5µm. ~96% TD achieved. ~98%TD with grain size of 2-5µm obtained at 1550^{0}C/2h
[41]Mechanochemical Processing Dry grinding	$Al(OH)_3$ having mean particle size of 25.8µm and $Mg(OH)_2$ of mean particle size 2.9µm	Stoichiometric composition was mixed using an agate mortar with pestle in acetone. Planetary ball milling at 790rpm was employed for grinding from 5 to 240 min. Calcination of ground mixture was done at 600-1200^{o}C for 1h.	Crystalline Mg-Al phase from ground mixture was detected at 780^{0}C after 15 min of grinding. Prolonged grinding promotes the aggregation of ground fine particles, but the aggregates deflocculate after calcination.
[59]Mechanochemical Processing	$Mg(OH)_2$ [M] and $Al(OH)_3$ [A]	M & A calcined jointly [R] (for spinel presynthesisation) as well as separately named [C]. M & A mixed in 1:1 molar ratio. Calcination @4^{0}C/min at 1400 and 1600^{0}C.Mixing of R & C done in Attritor mill for2,4,6h. Isostatic pressing of	Milling improves densification for both batches R and C. ~99.5% TD achieved for both batches after milling for 6h and sintering at 1650^{0}C. Higher calcination temperature and longer milling produces better densification. Deleterious effect of

Methods	Raw Materials	Processing Conditions	Properties
		milled powders done at 175MPa. Sintering @1^{0}C/min at 1550,1600,1650^{0}C/2h	spinellisation (due to expansion) has been avoided in the single stage firing process
[60]Microwave assisted Solid - State Reaction	Caustic MgO and $Al(OH)_3$	Starting materials were mixed with Carbon black in 10-50wt.% Carbon containing raw mix was compacted to cylindrical rods (Φ25mm, 90mm high) @ 7.1MPa. Rods exposed to micro waves of 2.45GHz for 30-100 min.	Powder with >80% spinel content were produced in presence of 20wt.% C and >93% spinel content with 50wt.% C after 100min The process saves power and processing time, with good sintering characteristics in Properties terms of BD, AP etc.
[40]Solid State Reaction	Al_2O_3 and MgO	Oxides mixed in molar ratio of MgO: Al_2O_3= 2:1, 1:1 and 1:2 were Attritor milled for 2, 4 and 6 hrs. Compaction by CIP @ 175 MPa (Φ25mm) Sintering @1^{0}C/min at 1550,1600, 1650^{0}C for 2h	High density was achievable in all three batches due to milling. MgO rich batch show ease of sintering. Al_2O_3 rich batch shows less sinterability but milling helps positively Attritor milling/4h is effective & economic. Spinel was major phase in sintered Al_2O_3 rich and stoichiometric batch implying solubility of excess Al_2O_3.

In present work effect of increasing variation of MgO is seen- in the resulting spinel formation, crystallite size, densification behavior, and mechanical strength (Brazilian Disk Test), flexural strength and thermal spalling; through Solid-State reaction method.

2.10 Objective of the thesis

The extensive literature survey reveals that the synthesis of spinel powders through various routes has been attempted by number of researchers. Simultaneously, attempts to decrease the crystallization temperature of spinel phase, increase the densification by additives, developing a better microstructure have been made. The thermo-mechanical properties of MgO-spinel composites have been studied by spinel incorporation into MgO have been studied by different researchers. However, the thermo-mechanical properties of spinel composites developed from Al_2O_3 : xMgO (where x =1, 1.1, 1.2, 1.3, 1.4) in different weight proportions through solid state reaction route has not yet been reported according to best my knowledge. The intent of this work is to create substantial experimental database on the preparation, processing, characterization and mechanical properties of the developed specimens- to observe the effect of increasing variation of MgO in the resulting spinel formation, densification behavior, and mechanical strength (Brazilian Disk Test) through solid-state reaction method. Subsequently, the flexural strength at room temperature and the retained strength of thermally spalled specimens were also carried out. The project was implemented in two stages. The first-stage involved the powder processing and characterization. In the second-stage, the mechanical and thermo-mechanical characterization by Brazilian Disk Test and three-point loading system.

Hence, objectives of the present investigation can be summarized as follows:

The objectives of this work include:

- To prepare spinel from different composition (i.e. with variation in Al_2O_3 : MgO) through Solid state route.
- To analyze the phase formation with increasing calcination temperature by XRD technique.
- To obtain dense $MgAl_2O_4$ by cold pressing and subsequent sintering at desired temperature (1600^0C) in ambient atmosphere.
- To analyze the effect of initial calcination temperatures and subsequent spinel content on densification of final products.
- To characterize the resultant material by XRD and SEM.
- To study different mechanical properties like: hardness, compressive strength, flexural strength and retained strength after thermal spalling and correlate with microstructure as well as spinel content in sintered specimens.

CHAPTER 3

3.0. EXPERIMENTAL PROCEDURE

3.1 Experimental Apparatus

During this research work, several equipments and engineering appliances were used. The purpose and list of the equipments are listed in Table 3.1

Table 3.1 Summary of machineries and their use in this research

Equipment	Purpose
Agate Mortar & Pestle	For PVA mixing to calcined samples. Grinding and mixing of samples manually.
Automatic Grinding & Polishing Unit Buehler, Ecomet 3-Automet 3	For smooth and fast polishing of sintered specimen
Ball Mill	For wet mixing of MgO and Al_2O_3 powders
Crucibles	For powder calcination
Dilatometer (0-1600^{0}C) NETZSCH DL 402C	To study densification and expansion behavior of pressed samples at different temperature
Dryer	To dry out acetone from wet mixed powder
Electrical Resistance Muffle Furnace (1700^{0}C) BYSAKH & CO.	Calcination of milled samples and Sintering of pressed pellets
Electronic Balance *Adair Dutt & Co.*	Powder material, density were measured accurately
Glass Apparatus Conical flasks, glass rod, beaker, burette, pippete, funnels	For Chemical Analysis of starting materials by Acid-dissolution method
Hydraulic Press 10 T, SoilLab Testing Instruments	Pressing/forming of powdered samples into desired shapes
Instron Flexure Tester Model-Hounsfield H10KS, U.K	Mechanical strength testing-Diametrical Compressive strength, Three-point Flexural Strength
Particle Size Analyser Malvern Mastersizer/E, UK	Agglomerate size distribution analysis of milled samples
Scanning Electron Microscope JEOL JSM 840	Microstructural analysis of polished samples
Ultrasonic Bath Teksonics	Surface cleaning of specimens
Universal Diamond Cutting Tool Buehler, Isomet, Germany	To cut away a sample accurately at desired position
X-Ray Diffraction Phillips PW 1830, Holland	Quantitative and qualitative Phase Analysis

3.2 Chemical Analysis of Raw Materials

The starting raw materials were taken for chemical analysis by acid dissolution method to determine the composition of constituents present in the as received powders.

(a) Sea water Magnesia

3.2.1. Determination of Silica:

In a pre-weighed platinum crucible 0.5 grams of properly ground fine MgO powder was taken. To this 10 grams of Na_2CO_3 and few beads of NaOH were added. This mass was mixed properly and was fused at 1000^oC for 1 hour. The cooled fused mass was then dissolved in acid. The fused mass was treated with 100 cc of 1:1 HCl acid in a beaker. The solution was then baked overnight on a hot plate at a temperature of 40-50^oC. Then 50 cc of 1:1 HCl was added to the baked mass. The mass was then warmed and cooled. The resultant was then filtered through Whatman 40 filter paper with simultaneous hot water washing. The filtrate was then collected in a 250-ml. volumetric flask. This filtrate was marked as Filtrate 1. The residue was then taken in a pre-weighed platinum crucible and fired at 1000^oC for 1 hour. The residual after firing was reported as Silica content in the sample taken.

The equation 1 was used to determine the Silica content in the sample: -

Taking weight of MgO sample as W_s

Final weight of crucible after firing the first filtration residue at 1000^0C/1h = F_w and

Initial weight of crucible without the filtration residue = I_w

$$\text{Silica (in \%)} = \left[\frac{Fw - Iw}{Ws}\right] \times 100 \qquad \text{---------- (1)}$$

3.2.2 Determination of Mixed oxide (Fe_2O_3 and Al_2O_3):

The volume of Filtrate 1 was made up to the mark. Then 50 cc of the made up volume of the Filtrate1 was taken in a conical flask. A few drops of methyl red indicator was added to it which turned the solution red. This was followed up by addition of AAC buffer till the color turned yellowish. The resultant solution was then warmed. Then filtration was carried out using Whatman 42 filter paper. The filtrate was collected in another 250-ml volumetric flask and named as Filtrate2. The residual was then fired at 1150^oC for 1 hour. The fired residue was reported as mixed oxide.

The equation 2 was used to determine the mixed oxide content in the sample: -

Taking the weight of the MgO sample as W_s

Final weight of crucible after firing the first filtration residue at 1150^oC/1h = F_w and

Initial weight of crucible without the filtration residue = I_w

$$\text{Mixed oxide (in \%)} = \left[\frac{Fw - Iw}{Ws}\right] \times 5 \times 100 \quad \text{---------- (2)}$$

To determine the **Fe_2O_3 content** -10 cc of the Filtrate 2 was taken in a conical flask. 10 cc of NH_4CN (Ammonium Thiocyanate) was added to it. This turned the solution blood red in color. This resultant solution was then titrated against standard Mercurous nitrate solution with vigorous shaking till colorless end point was attained. The amount of $Hg(NO_3)$ consumed gave the iron oxide content present in the sample. The difference from mixed oxide was reported to be Al_2O_3 content present in the sample.

Taking the weight of the MgO sample as W_s

Considering amount of $Hg(NO_3)$ consumed to be *x*

1ml. of 0.0015 M $Hg(NO_3)$ solution ≡ 1.197704 x 10^{-4} grams of Fe_2O_3

Fe_2O_3 content present in the sample was determined by the equation 3.

$$Fe_2O_3 \text{ (in \%)} = \left(\frac{x \times 1.197704 \times 10^{-4}}{W_s}\right) \times 25 \times 100 \quad \text{----------(3)}$$

Al_2O_3 (in %) = Mixed oxide content - Fe_2O_3 content

3.2.3 Determination of MgO:

In a conical flask 10 ml aliquot of Filtrate 2 was taken and to it 10 ml of AAC buffer was added. A pinch of Erichrome Black-T indicator was added to the solution, which resulted in wine red color of the solution. This solution was then titrated against standard EDTA (Ethylene d-ammine tetra acetate) solution (0.01M) till sky blue end point was attained. The volume of EDTA consumed gives us the magnesia content of the sample.

1ml of 0.01 EDTA solution ≡ 4.031 x 10^{-4} grams of MgO

Taking amount of EDTA solution consumed to be *y*

And weight of the sample taken as W_s

The Magnesia content in the sample was determined by the given equation

$$\text{MgO (in \%)} = \left(\frac{y \times 4.031 \times 10^{-4}}{W_s} \right) \times 5 \times 25 \times 100 \quad \text{---------- (4)}$$

3.2.4 Determination of CaO:

The volume of the Filtrate 2 was made up in the volumetric flask. In a conical flask 10 ml of Filtrate 2 was taken and to it 10 ml of NaOH (20%) was added. Then a pinch of P & R indicator was added to the above solution, which resulted in a light violet color of the solution. The resultant solution was then titrated against standard (0.01M) EDTA (Ethylene Di-Amine Tetra Acetate) solution till a colorless end point reached. The amount of EDTA consumed gave the CaO content in the sample.

1ml of 0.01 EDTA solution ≡ 5.608 x 10^{-4} grams of CaO

Taking amount of EDTA solution consumed to be z

And weight of the sample taken as W_s

The Calcium oxide content in the sample was determined by the under given equation

$$\text{CaO (in \%)} = \left(\frac{z \times 5.608 \times 10^{-4}}{W_s} \right) \times 5 \times 25 \times 100 \quad \text{---------- (5)}$$

(b) Commercially available Alumina

The same methodology as mentioned in the case of Sea water magnesia was employed to determine various constituents present in taken amount of Alumina powder.

The chemical properties of the starting raw materials are given in Table 4.1 in Chapter 4.

3.3 Processing of Precursor

3.3.1. Milling:

Seawater Magnesia and commercially available Alumina were used as starting materials. The starting materials were mixed according to weight proportions of (Al_2O_3 : xMgO where x is 1, 1.1, 1.2, 1.3, 1.4). The starting raw materials i.e. Magnesia and Alumina were taken in different containers according to required weight proportion. The containers were numbered according to the weight proportion, from 1 to 5 for distinction. Thus five different batches were

prepared. The weighed powders for each batch were mixed with acetone, and to each container certain numbers of high dense ZrO_2 balls were added to act as grinding media. The powder was mixed with acetone as grinding aid to reduce the excess heat generation during grinding. The ZrO_2 balls were filled to the slurry up to $3/4^{th}$ volume of the container. The powders were then ball milled for 60 hours in presence of acetone with high dense ZrO_2 balls as grinding media. Fig. 3.1 represents the procedure followed for powder processing.

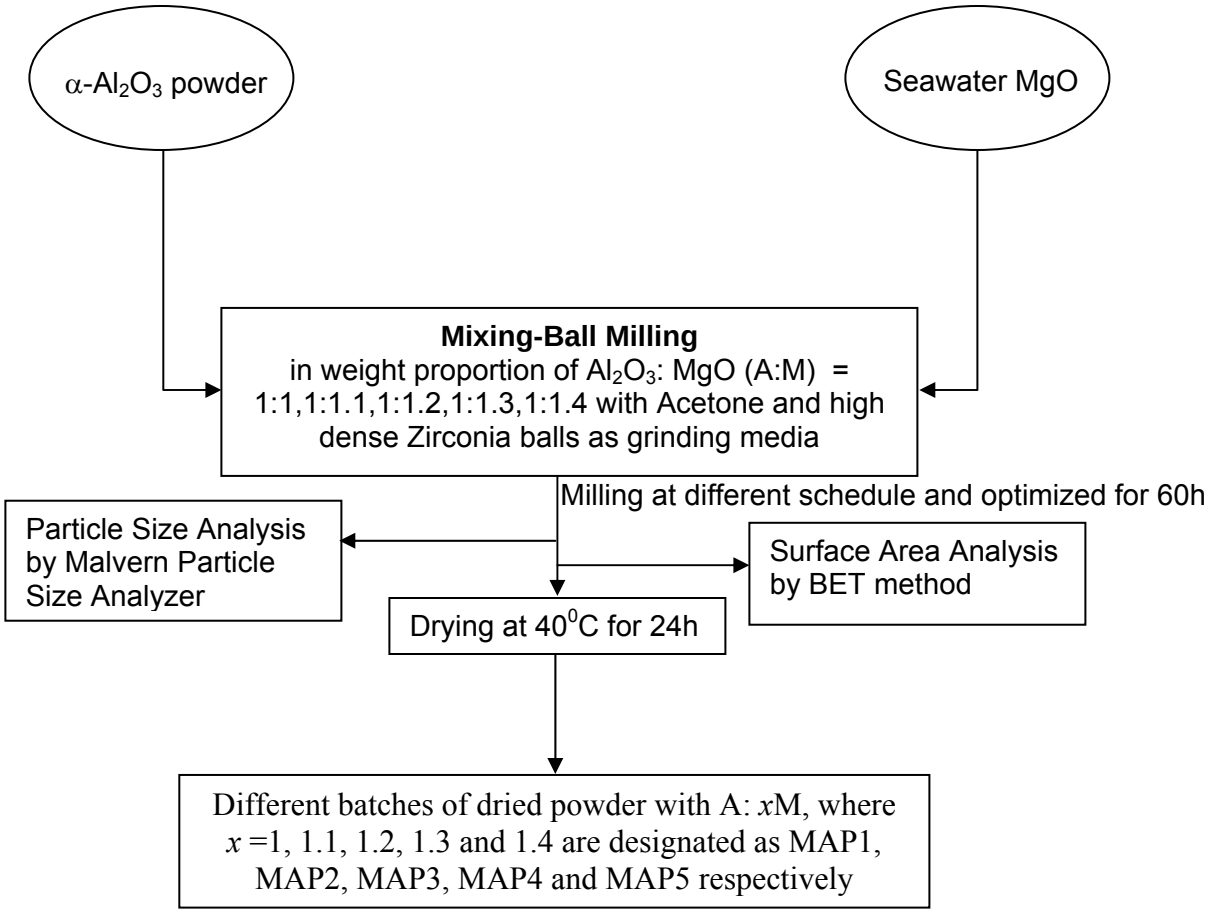

Fig.3.1: Flow sheet of $MgAl_2O_4$ powder processing from starting materials.

3.3.2. Drying:

After the milling process, each container was cleared of the milled contents. The contents of each container were poured onto different clean petridish. Each petridish was marked according to the number of the container to distinguish each sample composition. The milled samples were subsequently dried in air for 24 hours to get rid of the acetone.

3.4 Particle Size Analysis

A laser diffraction method with a multiple scattering technique has been used to determine the particle size distribution of the milled powder. To measure the particle size through laser scattering method, the instrument detects the correlation between the intensity and the angle of light scattered from a particle, and then calculates the particle size based on the Mie-scattering theory. In order to capture scattered light signals over this range of angles, the equipment utilizes a number of high-angle and back-scatter detectors, together with a short wavelength blue LED laser. As the particle size becomes smaller, the scattered light signal shifts to the side and rear with respect to the light source. Shorter wavelength detects the smaller particle size. The scattered light can be measured by a series of photo detectors placed at different angles. This is known as the diffraction pattern for the sample. As the instrument measures clouds of particles rather than individual ones, it is known as an "ensemble" technique, with the advantage that at smaller sizes (e.g. 1microns) the system is measuring literally millions of particles which gives some statistical significance to the measured results. The particles size distribution (volume percent) of the suspension was carried out in computer-controlled particle size analyzer (Malvern, Mastersizer 2000, UK) via a software program. The powders must not be agglomerated and completely dispersed in the liquid so that they are separated into discrete unattached particles. Powdered samples used to be well dispersed in a liquid medium of known density and viscosity. The milled samples were taken for particle size analysis after 20, 40 and 60 hours. Fig. 4.1 shows the particle size analysis of samples.

3.5 Surface Area Analysis

Specific surface area of ultrafine submicron ceramic powder is an important objective to predict the green compaction and sintering characteristics. This can be measured by a common BET method. The BET method (Brunauer, Emmet, Teller after the developers of the basic calculations) involves adsorbing a monolayer of liquid nitrogen onto the surface of a mass of particles, then measuring the amount of nitrogen that is released when that monolayer is vaporized.

Specific surface area of milled as well as calcined powders was determined by BET surface area analyzer (Quantachrome Instruments, U.S.A.). Surface area was determined as per BET method. About 2-3gm sample was taken in the sample cell and degassed at 100^{o}C in vacuum up to a maximum of 3mbar. The sample holder mouth was closed by a stopcock. Sample

was cooled and the cell was placed in liquid nitrogen bath. Pure nitrogen (N_2) gas was passed over the sample and adsorption of the gas on the surface of the sample took place at liquid nitrogen temperature. The equipment measured the amount of gas adsorbed on the surface of the sample and calculated the specific surface area. Based on this nitrogen quantity, the surface area of the sample can be calculated from the BET equation[61]:

$$\frac{1}{V}\left(\frac{x}{1-x}\right) = \frac{c-1}{cVm}x + \frac{1}{cVm} \quad \ldots\ldots\ldots\ldots (6)$$

V = volume of gas adsorbed, V_m = volume of gas adsorbed at monolayer coverage, X = P/Po, P= Ambient Pressure, Po = total pressure, c= exp((e-ev)/kT), A plot of (1/V)(x/(1-x)) versus x gives a straight line with slope = m= (c-1)/(cV_m), Intercept = b= 1/cV_m, Solve to get V_m and c where, V_m = 1/(slope + intercept). This is normalized by the mass of particles tested to give a specific surface area, in m^2/gm.

Fig.3.2 shows the methodology implemented in carrying out the densification and characterization of processed powders.

3.6 Calcination of Processed Powders

Spinel formation from its constituent oxides is associated with 5-7% volume expansion, which hinders the densification process to take place in the same firing. Hence the general practice is to complete the spinellisation process first and then crushing, milling, reshaping and sintering the spinel to achieve desired properties in the second firing. The processed powders (as discussed in Section 3.3) were then taken in alumina crucibles for calcination at various temperatures ranging from 1000^{o}C to 1300^{o}C at an interval of 100^{o}C with 2 hours of soaking time at peak temperature. The calcinations were carried out in oxidizing atmosphere in a programmable muffle furnace. Generally a heating rate of 4^{o}C/ minute was employed for calcination process. Calcination of the powders were done for the determination of phase with respect to different composition and temperature.

Calcination process leads to: -

- Spinel phase development
- Reactivity of the powder changes with calcinations at various temperature

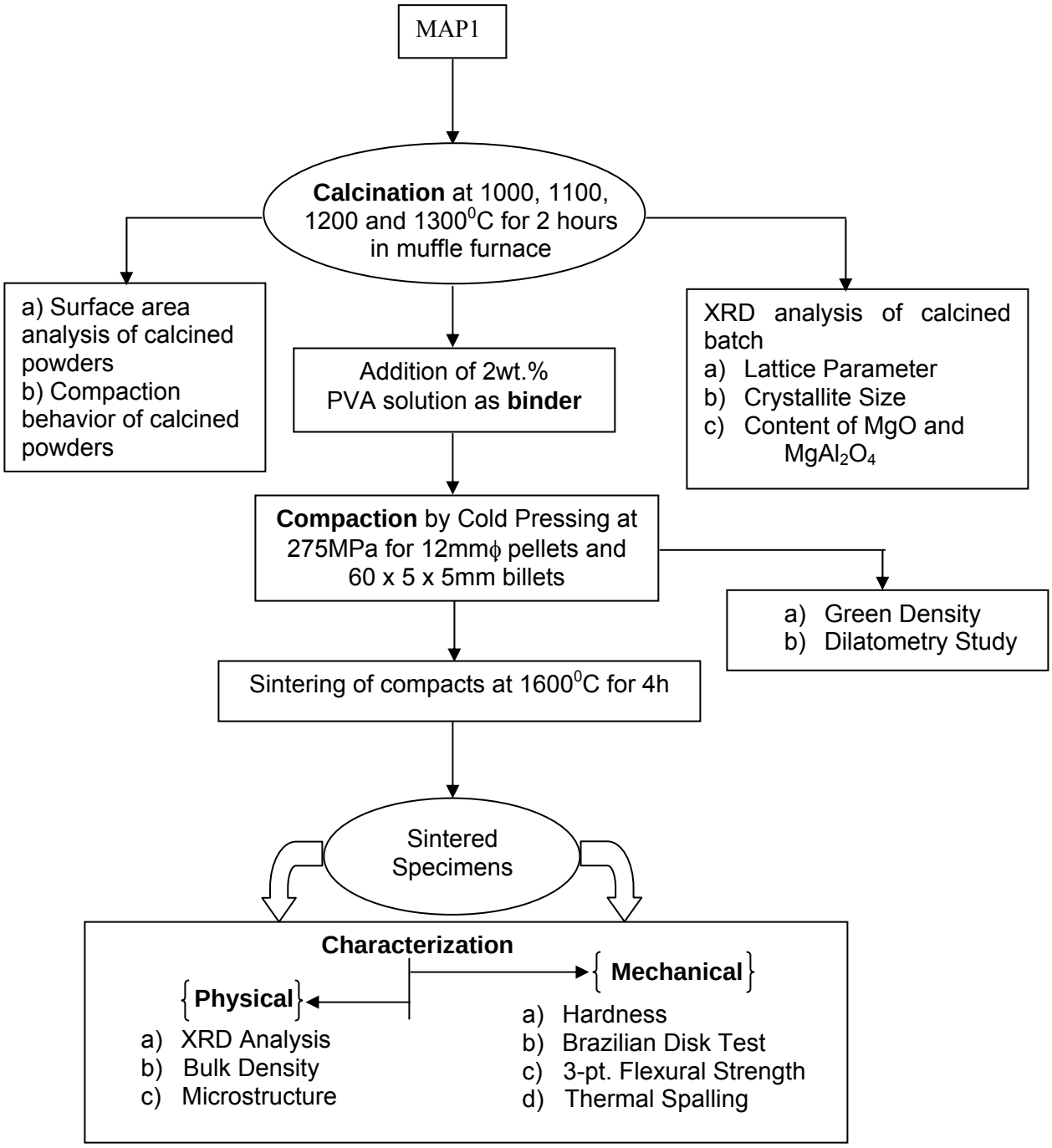

Fig.3.2: Flow sheet of Densification and Mechanical property characterization.

The same process was carried out for other 4 batches (MAP2, MAP3, MAP4, and MAP5)

3.7 Phase Analysis of calcined powders

Prior to synthesis of spinel powder the starting oxide materials were characterized using XRD technique. In a powder, thousands of grains have random orientations. With random orientations we might expect most of the different atomic planes to lie parallel to the surface in

some of the grains. Thus, by scanning through an angle θ of incident x-ray beams from 0 to 90^o, we would expect to find all angles where diffraction has occurred, and each of these angles would be associated with a different atomic spacing. The instrument used to do this is an X-Ray powder diffractometer.

A powdered mineral sample is packed on a sample holder so that it can be irradiated by the X-ray tube, which is capable of producing a beam of monochromatic X-ray. To detect the diffracted X-rays, an electronic detector is placed on the other side of the sample from the X-ray tube, and allowed to rotate to produce angles from 0 to 90^o. The instrument used to rotate both the X-ray tube and the detector is called a goniometer. The goniometer keeps track of the angle θ, and the detector records the rate of X-rays coming out of the other side of the sample (in units of counts/sec) and sends this information to the computer. The identification of different phases was carried out by powder X-ray diffraction study. For phase analysis of the starting raw materials' powder, X-ray data were collected using a fully automated Philips X-pert system (PHILIPS PW1830, The Netherlands) with Cu-K_α radiation, with a λ value of 1.54056Å. The voltage and current was set at 35 kV and 30mA respectively with the copper target, with a step size of 0.02^o (2θ) and a count time of 1s per step.

Fine powdered form of calcined batch of MAP1 (Al_2O_3 : MgO=1:1)and was placed on the sample holder using the help of glass slide and was subjected to X-Ray irradiation from angle of 20^0 to 80^0. In the same way the alumina was also grounded and as in case of magnesia was subjected to X-Ray diffraction to detect the phases present. After the scan of the samples the X-ray intensity (counts/sec) was be plotted against the angle θ to produce a plot. The angle 2θ for each diffraction peak can then be converted to d-spacing, using the Bragg's equation. The crystal structure of each of the diffraction peaks with a different atomic plane in terms of the Miller Index (h k l) for that plane was determined through standard APD software.

Calcination process as mentioned in the above section was meant for spinel phase development, prior to sintering stage. It was also meant to reduce the chances of volume expansion and poor densification. Thus after calcinations process the calcined samples of various batches were taken for phase analysis by X-ray diffraction method. The arrangement was same as discussed in Section 3.3. The phase analysis study of various calcined samples is explained in Section 4.13 with respect to the Fig.4.3.

3.7.1 Determination of Crystallite Size:

The crystallite size of the calcined powders was determined from X-ray line broadening using the Scherer's equation[62] as follows:

$$D = \frac{0.9\lambda}{B\cos\theta} \quad \text{----------} \ [62](7)$$

where D is the crystallite size,

λ is the wavelength of the radiation,

θ is the Bragg's angle and

B is the full width at half maximum

Line broadening due to the equipment was subtracted from the peak width before calculating the crystallite size using the following formula[62]:

$$B^2 = B^2_{meas.} - B^2_{equip.} \quad \text{----------} \ (8)$$

Where, B_{meas}= Observed full width at half maximum from peak values using APD $B_{equip.}$ = Instrumental/equipmental broadening. The value of B_{equip} is 0.09.

The crystallite size of various calcined samples was measured using the formula mentioned in equation 7 and 8. The graph plotted between the observed crystallite size of various batches with respect to various calcinations temperature is shown in Fig.4.4

3.7.2 Lattice Parameter Calculation:

The lattice parameter is the length of the unit cell, which is defined to be the smallest repeat unit that satisfies the symmetry of the crystal. From the X-Ray diffraction data of the calcined samples of various compositions the lattice parameter value was calculated.

Usually we have wavelength λ and the d-spacing is related as the following

$$\lambda = 2d \sin\theta \quad \text{----------}[62](9)$$

But also $$d = \frac{a}{\sqrt{(h^2 + k^2 + l^2)}} \quad \text{----------}[62](10)$$

So we get, $$a = \frac{\lambda}{2 \sin \theta} \sqrt{\left(h^2 + k^2 + l^2\right)}$$ ----------(11)

The lattice parameter for a cubic system is calculated from equation 10 where

a = Lattice parameter

λ = wavelength of radiation

θ = Half of the 2θ in degrees

h, k, l are the Miller indices.

3.7.3. Determination of $MgAl_2O_4$ formation:

The phase analysis after calcinations was also aimed to calculate the extent of spinellisation in each batch. From the height counts of the 100% intensity of the major phases present in each sample (calcined powder), the extent of spinellisation was calculated. The major peaks observed were that of Al_2O_3, $MgAl_2O_4$ and MgO. Usually these peaks were observed around a 2θ value of 35.15, 36.866 and 43 respectively. The height counts of the peaks present in these corresponding 2θ values were noted. Using the undergiven formula the spinellisation in each batch composition was measured

$$Vol.\%MgAl_2O_4 = \frac{Heightcounts of MgAl_2O_{4(311)}}{\sum Heightcounts\left(MgAl_2O_{4(311)} + MgO_{200} + Al_2O_{3(104)}\right)}$$ ----------[63](12)

3.8 Densification

3.8.1 Binder Addition:

Binder was added to give calcined powder green strength. Here 2wt.% PVA (Poly Vinyl Alcohol) solution was used as binder. The calcined powder was taken in a mortar and as per the weight of the powder 2wt.% PVA solution was added to it. Then it was mixed thoroughly with the help of pestle to get proper mixing. After mixing, it was dried for removal of water content of the binder solution. After that the binder added spinel powder (dried) was grounded with the help of agate-mortar to fine powdered form.

3.8.2. Pressing of Green Specimens:

The binder mixed powder was compacted to give a desired shape for further characterization. About 0.85grams of PVA added calcined spinel powders were taken for making each pellet. The weighing was done in an electronic balance. The powders were pressed uniaxially in a steel die into cylindrical pellets (12 mmΦ, 3mm high). The steel die was cleaned using acetone and cotton. It was lubricated using 3wt.% Stearic acid. The powder was added slowly into the die with bottom punch. Then it was tapped slowly to allow uniform leveling of the powder and better filled density. Then the top punch was applied slowly. The pressing was done uniaxially at 275MPa. A holding time of 60seconds was given for pressing of each sample. The pressure was released to get the green pellet. The pressure was decreased slowly to avoid pressing defects in the samples. In this manner a number of pellets were prepared. The steel die was cleaned up and lubricated after each pellet pressing.

Similarly, briquettes of dimensions 60mm x 5.3mm x 5.7mm were pressed in a rectangular die of the given dimensions. As mentioned the die was cleaned up with acetone and was lubricated with 3wt.% Stearic acid. To get the specified dimensions specific amount of PVA mixed fine powder was put into the die slowly. The sample was then pressed uniaxially at 275MPa. The holding time at peak load was 90seconds. The green dimension of every specimen was noted using a Slide Calliper.

3.8.3. Dilatometry study of Pressed Specimens:

The final step of production is sintering. Sintering should be done at a specific temperature, which provides the optimum and maximum densification. Dilatometry study helps to determine the temperature optimum to get better densification and densification behavior. Sintering at lower temperature may not provide better densification. As like, sintering at still higher temperature may lead to fall in density, due to coarsening effect because of grain growth. Thus the sintering behavior study with the help of dilatometer helps determine the sintering temperature zone. The green pellets here were taken for Dilatometry study. The equipment used was NETZSCH DL 402C Dilatometer with an operating range of 25-1600^{o}C. The dimension of green compacts to be put under Dilatometry study was measured. The green compact was then put under test at a temperature range starting from room temperature to 1600^{o}C. The heating rate employed here was 5^{o}C per minute. The behavior was studied with alumina reference.

Fig.3.3. High Temperature Dilatometer DIL 402C (NETZSCH)

Fig.4.6 shows the sintering behavior of samples. The dilatometry study of green compact is discussed in details in Section 4.2.1 of Chapter 4.

3.8.4. Sintering of Specimen:

Sintering is the term used to describe the consolidation of the product during firing to give the consolidated product higher strength. During this process the pores are eliminated and densification of particles takes place. The specimens were sintered at 1600^0C with 4hours soaking time at the peak temperature. The detail of the heating schedule for sintering of various samples is illustrated in Fig.3.4.

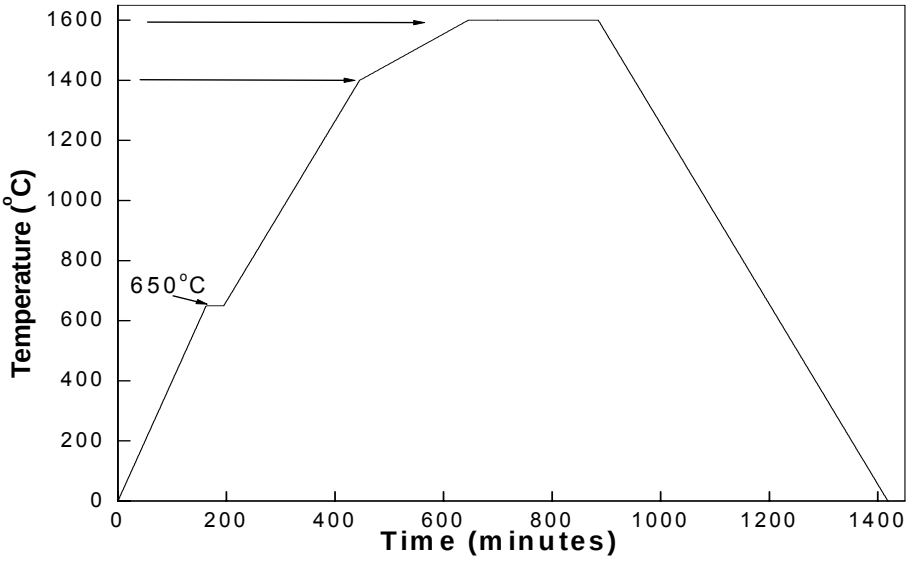

Fig.3.4: Temperature Profile during Sintering

As shown in Fig.3.4, a heating rate of nearly 4^0C/ minute was employed till point 'A' i.e. 650^0C. Then a heating rate of 3^0C/ minute was employed till point C i.e.1400^0C. Then at 1^0C/ minute the sintering temperature was reached after 10 hours. After the soaking period of 4 hours,

the furnace was cooled to room temperature. All the calcinations and sintering of samples was carried out in a micro-controller based Electrical resistance muffle furnace.

1 The soaking for 30 minutes at 650^0C is given for binder burnout.

2 The soaking at final temperature is for densification and grain growth. Sintering leads to voids and pore elimination.

The sintered products were then characterized in terms of densification, phase analysis, microstructure, and mechanical property studies.

3.9 Study of Bulk Density and Apparent Porosity

The sintered specimens were used to characterize the physical properties such as bulk density, apparent porosity, phase analysis, microstructure, mechanical and thermo-mechanical properties as mentioned in Fig.3.2.

The bulk density and apparent porosity of the sintered specimen were measured by Archimedes' Principle. Here the immersing agent used was kerosene. The dry weight of the sintered specimens was taken. Then the specimens were immersed in kerosene in a beaker. The beaker with samples immersed in it was then put under vacuum in a desiccator so that kerosene fills up the entire open pores present in the sintered specimen.

Then the suspended and soaked weights of the specimens were taken. From these the bulk density and the apparent porosity were calculated.

Dry weight of the sample = W_d

Suspended weight of the sample = W_{Su}

Soaked weight of the sample = W_{Skd}

$$BulkDensity = \left(\frac{W_d \times DensityOfKerosene}{W_{Skd} - W_{Su}} \right) \times 100 \text{ ---------- (13)}$$

$$ApparentPorosity = \left(\frac{W_{Skd} - W_d}{W_{Skd} - W_{Su}} \right) \times 100 \text{ ---------- (14)}$$

3.10 Phase Analysis of Sintered Specimens: -

After the density and porosity study the sintered specimens were taken for phase analysis using X-Ray diffractometer. As mentioned in Section 3.3, same technique was used for phase analysis present in sintered specimens. The pellets were placed on sample holder using an

adhesive like substance. The extent of spinel content in sintered specimens was estimated using the equation 12.

3.11 Sample preparation for Microscopy analysis: -

3.11.1. Polishing of sintered specimen:

Prior to Microscopy analysis the samples were polished using rotating disk and Automatic Grinding & Polishing Unit (Buehler, Ecomet 3-Automet 3). The specimen surface was ground on a rotating disk using SiC powder. This process was followed up by grinding the surface on the above-mentioned grinding and polishing unit using 240 grit and 600 grit emery paper disks. The speed of the rotating disk and load at which grinding was carried, was varied according to desired status. After this the samples were polished using 6-μm diamond paste on a texmet cloth. Special oil was used as lubrication agent. Final polishing was done using 1 μm diamond paste on a texmet cloth to create a mirror finish.

3.11.2. Thermal Etching of Polished specimens:

The polished samples were cleaned up in a Ultrasonic bath with acetone as the medium. Prior to the SEM analysis, the polished and cleaned samples were thermally etched at a temperature of 150^0C less than the sintering temperature. The rate of heating here was maintained at 5^0C/ minute. The thermally etched samples were mounted on a metal stub with carbon paint. In a vacuum evaporator the samples were thin coated with palladium-gold under vacuum of 0.01 torr to make the surface conducting for viewing through SEM. The mounted specimens were studied by SEM (JEOL-JSM840) with an EDAX and EPMA attachment. The microstructure analysis has been discussed in Section 4.2.5 of Chapter 4.

3.12 SEM analysis: -

Microstructures of the sintered specimens were analyzed using a scanning electron microscope. The system set up is shown in the Fig.3.5. Scanning electron microscope was used to study the microstructural feature of samples as it has a much greater resolution power compared to the optical microscope.

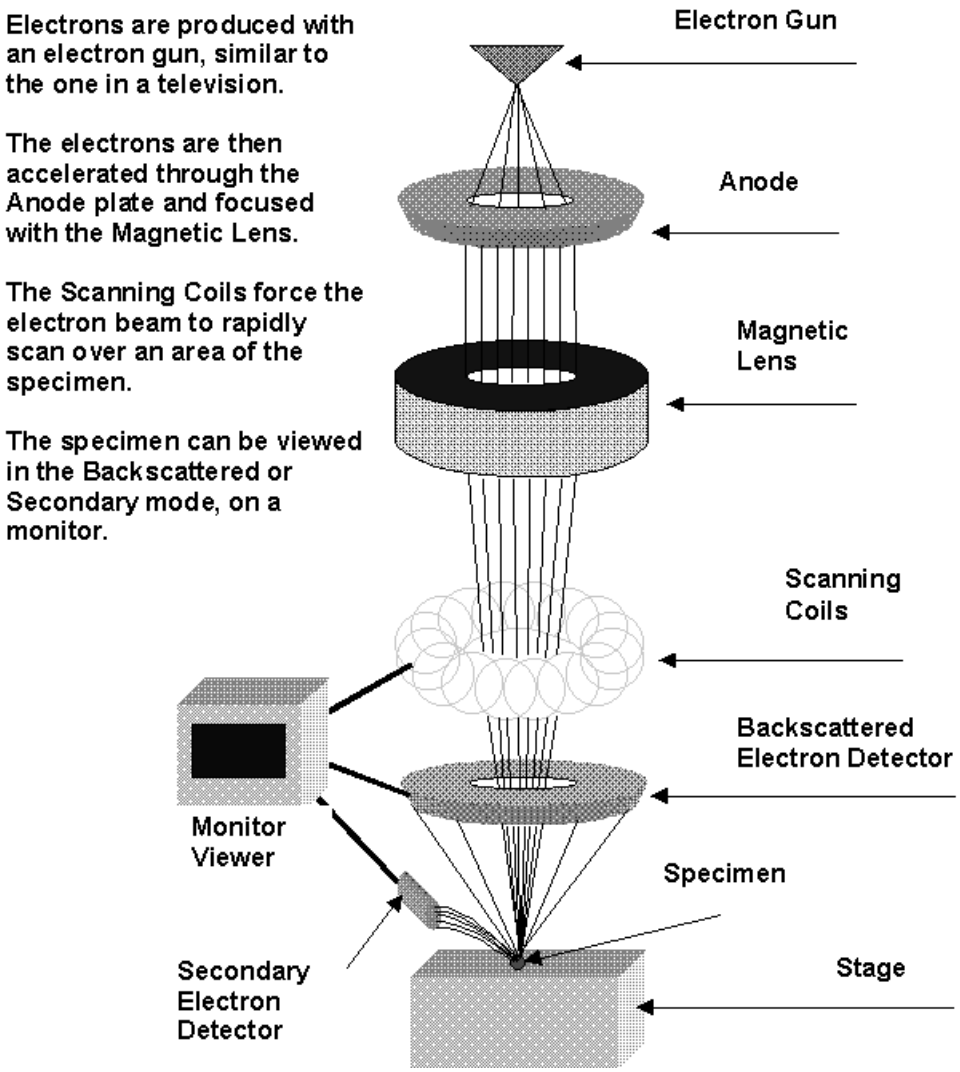

Fig.3.5: Layout of Scanning Electron Microscope

In SEM, a hot tungsten filament electron gun, under vacuum emits electrons; which pass through a series of electromagnetic lenses. The sample is then bombarded with a fine beam of electrons. The acceleration potential ranges from 1-30 KV. A part of the beam is reflected back as back-scattered electrons. The filament assembly has a cap cover called Wehnelt cap. This cap has a fine central hole (about 1-2mm diameter) through which electrons pass. The electron beam produced by tungsten filament is of 50μm in diameter. The condenser lenses help reduce the beam diameter to the desired size. Altering the focal length of the objective lens the focus is controlled. This also helps alter the position of focus of electron beam and gives a slight change in magnification. Images formed from the secondary electron beam were studied in the extrinsic mode of SEM. While the images obtained appear very real and as if they were photographed by ordinary means, the apparent illumination is a function of particle emission

rather than radiation we are familiar with. These particles emitted are termed secondary electrons, and their detection via detector is displayed on a scanning TV display. The detector consists of scintillator, which produces light when struck by electrons. The light is amplified in a photomultiplier and then converted back to an electrical signal, which drives the waveform monitor and the Cathode Ray Tube. A bright image will be the result of high secondary electron emission, while the primary influence on high emission is the surface structure of the specimen. The end result is therefore brightness associated with surface characteristics and an image that looks very much like a normally illuminated subject.

3.13 Mechanical Properties analysis

The mechanical properties of ceramics are a complex function of the microstructure. Almost all properties of ceramics are dependent on composition and porosity; strength and fracture behavior apart from these depend on the grain size. Generally, the tensile strength is low and compressive strength is high. This behavior arises because the flaws in the ceramics are effectively closed under compressive stress but rapidly enlarged under tensile stress (Fig.4.21). Ceramics tend to fail in tension; in a three-point bend (flexural) test failure usually occurs on the side under tensile stress commonly originating from a microstructural, strength-limiting flaw. Tensile strength is a significant mechanical property since the component's reliability and ultimate failure is governed by it. The sintered specimens were characterized for mechanical properties

3.13.1. Hardness measurement:

Hardness is usually defined as resistance to penetration. It is a measure of the yield stress of the ceramic. Usually the measured value of hardness is load-dependent. Especially at low loads the measured values of microhardness tend to increase. This reflects an effect of a ratio of the impression size to a characteristic microstructural dimension such as grain size, pore size and distribution, inclusions, and the range of residual stresses. The microhardness also depends on the relationship of surface properties vs. bulk properties and on environmental interactions. At high loads, such as several kilograms, the measured hardness of ceramics decrease due to the fracture of the material during indentation.

Hardness is a measure of a reaction of a material to the type of disturbing force imposed (different hardness test results for different techniques) and relates to:

-ease of dislocation movement e.g. to shear modulus *G* and yield stress

-the type of atomic bonding

-the presence of impurities in solid solution or at grain boundaries and/or as precipitates, or inclusions

-the microstructure (grain size and texture, porosity), phase composition and residual stresses

.

Fig.3.6 Vicker's Hardness tester

Effectively, hardness increases in an order similar to the increase in stiffness:

Metals < Oxides < Carbides/borides

The sintered pellets were polished in the same manner as done for SEM analysis (as discussed in section 3.12.). After cleaning the specimens with acetone in a Ultrasonic bath (TEKSONICS make) the specimen were taken for indentation at different loads using Vicker's Hardness Tester

The samples were indented by a diamond indenter with 49N, 98N and 147N load and 15seconds dwell time. The hardness of the materials was calculated from the size of the impression produced under load by a pyramid-shaped diamond indenter. The indenter employed in the test is a square based pyramid whose opposite sides met at the apex at an angle of 136°. The size of the impression (diagonals) was measured with the aid of a calibrated optical microscope (make ZEISS). The hardness of various samples was measured by using the following equation: -

$$H_v = 1.854\left(F \big/ D^2\right) \quad \text{.....}^{64}(15)$$

F being the applied load measured in kgf

D^2 is the area of the indentation (measured in mm^2)

3.13.2. Diametrical Compressive Strength/ Brazilian Disk test analysis:

Diametrical Compression test is a test to determine the limit of performance of a material to stress. This test is also known as Brazilian Disk Test. This mechanical testing technique is used in many technological fields from concrete to ceramics: to metal composites to materials in dentistry. In this method a local tensile stress is induced in the transverse direction of the applied compressive stress. Usually specimen in the form of disk (pellets) is used. This test helps us to measure the limit force required to cause failure, which is used in estimation of tensile strength. The diametrical compressive strength was measured using Hertz equation[65]: -

$$\sigma_{comp.} = \left(\frac{2P}{\pi DT}\right) \text{----------(16)}$$

where $\sigma_{comp.}$ is the compressive strength

P is the breaking load

D is the diameter of the sintered compact

T is the thickness of the sintered compact

$\pi = 3.14$

The arrangement of the diametrical compressive test is shown in Fig. 3.6

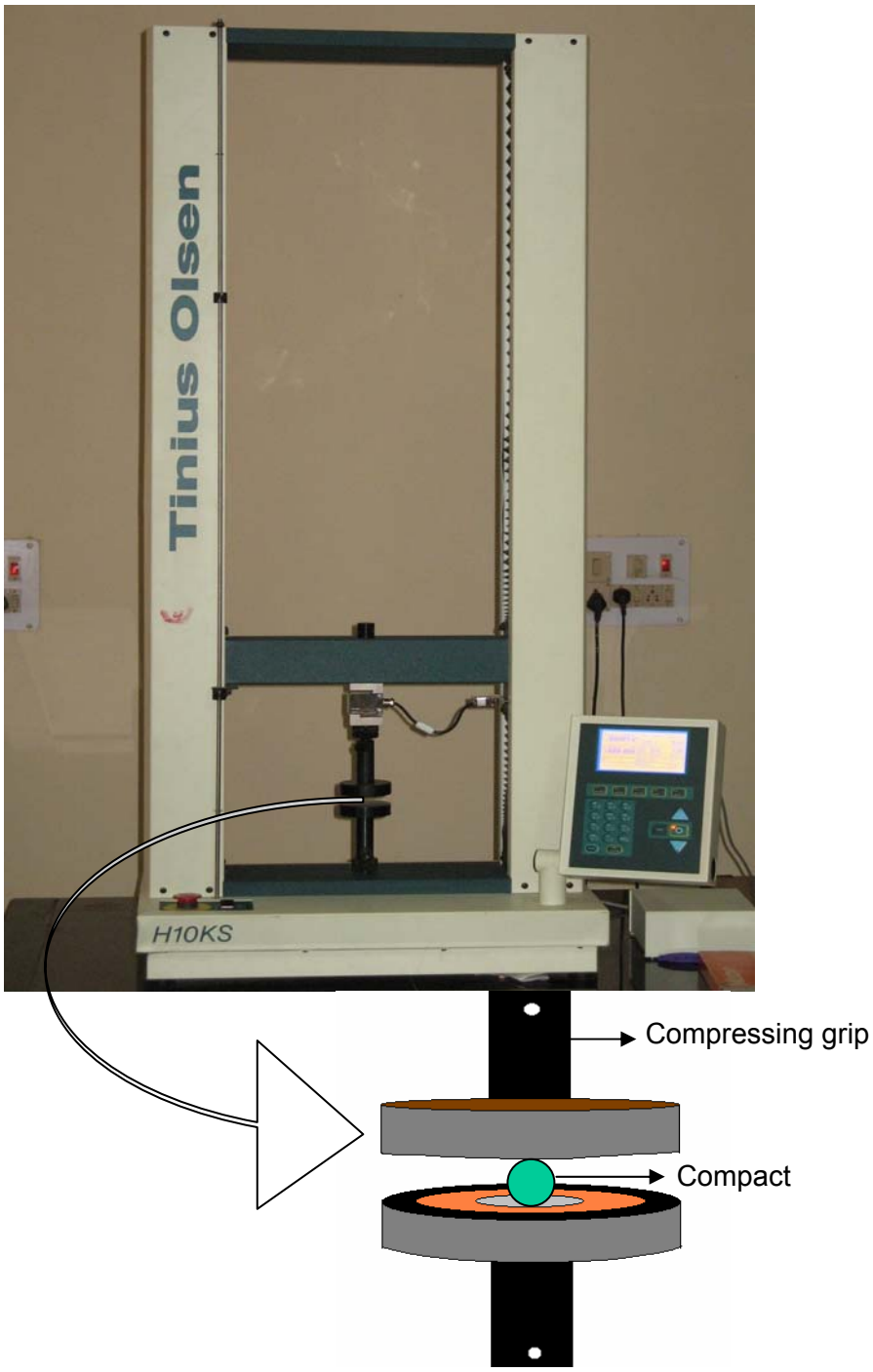

Fig. 3.7 Arrangement for Brazilian Disk Test

The advantages of Brazilian disk test are-

- its simple geometry,
- ease of specimen preparation and
- quickness of testing.

3.13.3. Flexural Strength at Ambient temperature:

A determination of the flexural strength is frequently necessary as a part of the design of structural ceramics to check compliance with established specifications or to provide information necessary to the design of an engineering structure. It is the ability of a bar or slab to resist failure in bending. The flexural strength is expressed as "Modulus of Rupture" (MR) in MPa. Flexural Strength is about 10 to 20% of compressive strength. However, the best correlation for specific materials is obtained by laboratory tests according to ASTM methods[66].

Five samples of each batch were taken to determine the flexural strength at each test and the average values have been reported here. Flexural strength was determined by standard three-point bending method in an instrument {Instron Universal Testing Machine (Hounsfield H10KS, U.K)}. The parameters for the three point bend test were- span length of 20mm with cross head speed of 0.2mm/min. The edges of the rectangular bars of 50 x 4 x 4 mm were ground on grinding discs of 600grit using polishing machine, Automet-3 and Ecomet-3(made Buehler) to give a parallel and smooth surface. Flexural strength was calculated from the following equation[66]:

$$\sigma_{flexural} = \left(\frac{3PL}{2WD^2} \right) \text{ ---------- (17)}$$

where P = fracture load; L = Span length/ distance between the rollers W = width of the sample; D = Thickness of the sample at the fracture plane**.**

3.13.4. Thermal Spalling:

Thermal shock can be defined as serious cracking in components subject to rapid changes in temperature. Rapid fluctuations of temperature generates stresses within a material. Resistance to initiation or propagation of crack under stresses generated due to thermal fluctuations is known as thermal shock resistance. Thermal shock resistance is measured as resistance to weakening or fracture under stresses generated due to thermal expansion mismatch at high temperature. Thermal shock resistance is usually evaluated by heating samples to various temperatures T_{max}. The samples are rapidly cooled by quenching them from T_{max} into medium, most commonly ambient temperature. The retained strengths are measured and plotted with respect to the composition.

Billets of 50mm X 4mm X 4mm dimension were heated in an electric furnace at 800^{o}C and soaked for 15 minutes. Subsequently, heated bars were quenched in air at room temperature, kept for 15 minutes followed by sudden reheating at corresponding tested temperatures for 15minutes. This cycle was repeated thrice and the retained flexural strength was measured by (Instron Universal Testing Machine (Hounsfield H10KS). The parameters for testing were same as that of flexural strength. The span length was maintained at 20 mm and the crosshead speed at 0.2mm/min. Specimens of different batches were done with the above spalling process and were tested to determine the retained flexural strength at each test and the average values have been reported here. The equation 17 was used to measure the strength of thermally spalled specimens.

CHAPTER 4

4.0. RESULTS AND DISCUSSIONS

Chemical analysis of as-received materials was done by acid dissolution method as mentioned in Section 3.2. The starting precursors were prepared according to the methodology illustrated in Fig. 3.1. Subsequently, the milled samples were characterized by particle size analyzer. The phase analysis in calcined as well as sintered samples was characterized by XRD. Sintered samples were characterized by XRD, density study and microstructure (SEM). Subsequently, compressive strength, flexural strength, hardness and thermal shock resistance were evaluated and analyzed with respect to microstructure.

4.1. Powder Preparation

4.1.1. Chemical Analysis:

Chemical properties of the starting oxides are listed in Table 4.1. It shows that both the raw materials are highly pure and contain little amount of SiO_2, Fe_2O_3, CaO and alkalis as impurities.

Table 4.1 Chemical analysis of Starting Materials

Constituents	Magnesia	Alumina
Al_2O_3	0.45	99.4
MgO	98.3	-
CaO	0.82	0.2
SiO_2	0.08	0.05
Fe_2O_3	0.09	-
LOI	-	-

4.1.2. Particle Size Analysis and XRD of milled powder:

Particle size distribution plays a significant role for green body formation through uniaxial cold pressing process. A mixture of different particle size is always beneficial to achieve better densification, where sufficient fine particles are present to fill in the interstices to reach high green density compact. Usually, the finer particle fraction leads to increased reactivity and reach higher sintered density. Fig. 4.1 shows the effect of milling time on the particle size.

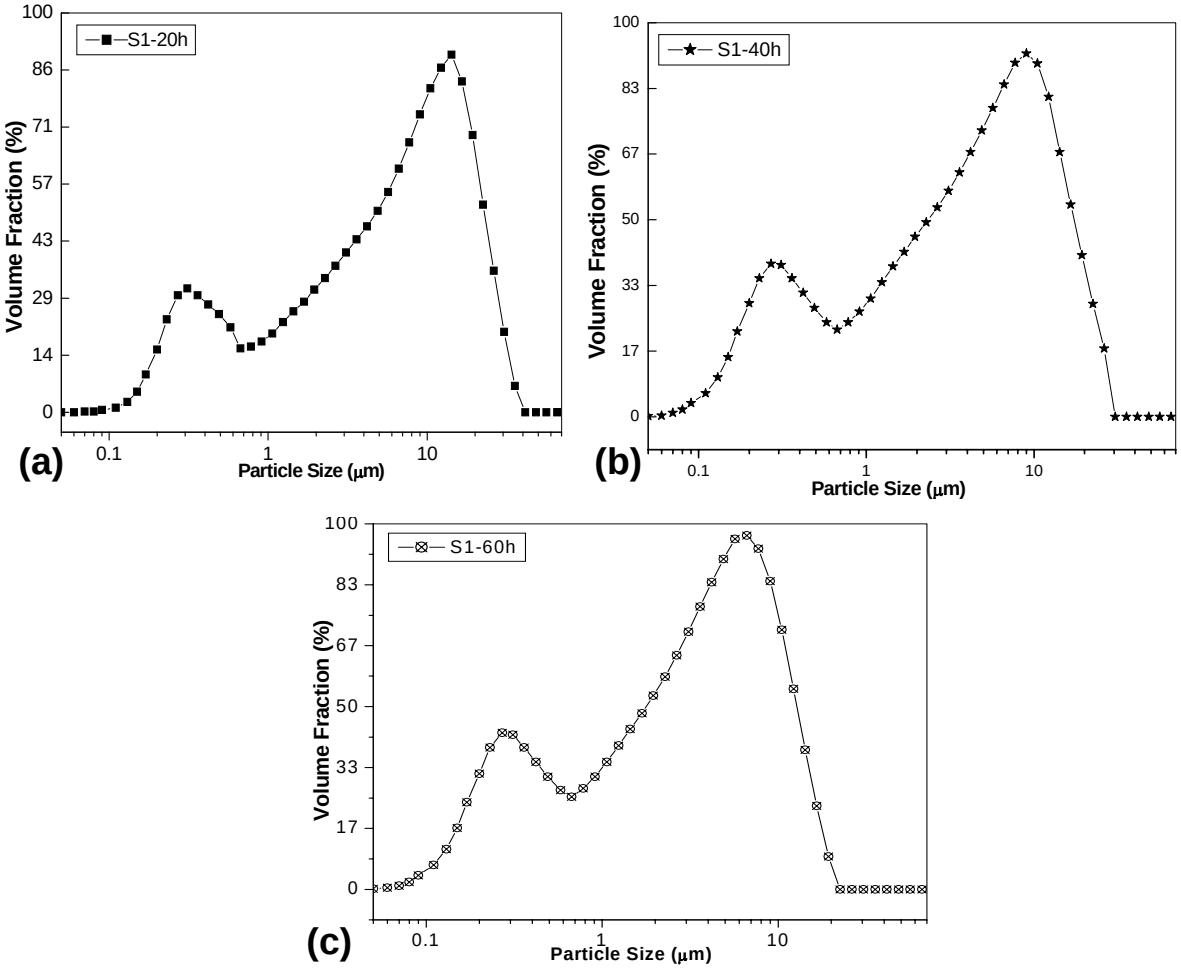

Fig.4.1 Particle Size Analysis after (a) 20h milling, (b) 40h milling and (c) 60h milling

The particle size distribution of the milled raw material mixture shows a bimodal distribution. The finer particle (1-10μm) represents the unagglomerated particles, while the agglomeration ranged from 10-100 μm. However, some particles may be in the range of more than 10μm. The volume mean diameter was observed to decrease with increasing milling time and the average particle size. Initially the fineness was observed to be around 28%, which is increased to 35% with time. But, beyond 60h no substantial increase in fineness was observed as

also reported in previous literature[67]. The particle (agglomerate) size distribution plot shows that as the milling time is increased from 20h to 60h a substantial decrease in average agglomerate size occurs (Fig. 4.2), with 3.48μm being the agglomerate size after 60h of ball milling. Limitation of the efficiency of this grinding is due to the frequency and one-dimensional nature of impacts. This is presumably due to the frequency of impacts in ball mill is limited by the tumbling velocity and the one-dimensional nature of impacts, and because the mill is partially filled. As well as during ball milling, collisions causing grinding occur primarily in the tumbling layers near the center[68].

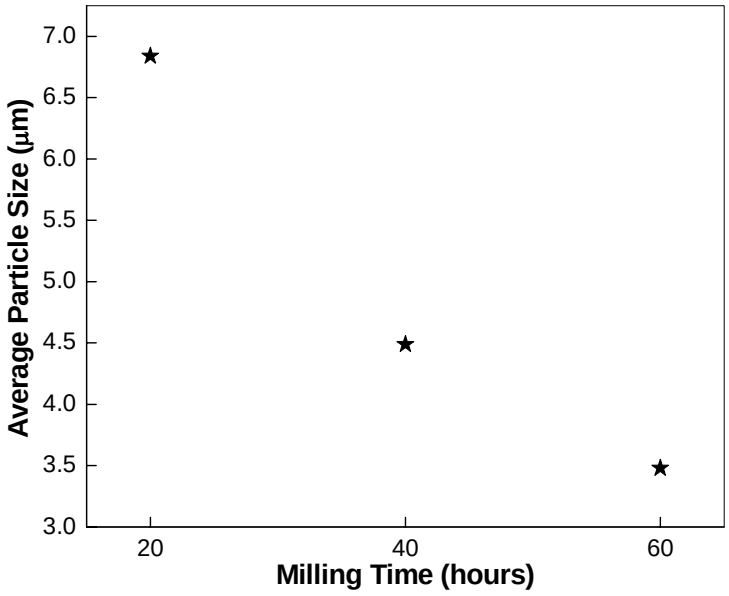

Fig. 4.2. Average Particle Size with respect to milling time

4.1.3. Phase Analysis of Calcined Powders:

The calcination process assists in spinel phase formation. Fig. 4.3(a-d) shows the effect of calcination on the spinel phase development from the constituent oxides i.e. MgO and Al_2O_3; in mixtures ground and calcined at various temperatures ranging from 1000°C to 1300°C with an interval of 100°C. The peaks corresponding to $MgAl_2O_4$ spinel start appearing in the powders calcined at 1000°C. The powder shows low crystallinity of the $MgAl_2O_4$ spinel phase to some extent even after calcination at 1000°C as exhibited by the broadened peaks. The phase evolution of calcined powders can be deliberated with reference to the diffraction pattern of a fully ordered spinel (ICDD File card no.05-0672). Calcination at higher temperatures did not change the peak position, but the intensity of the diffraction peaks of the $MgAl_2O_4$ spinel phase gradually

increased as the calcination temperature increased to 1300^{0}C. The diffraction peaks become stronger and sharper when calcined at 1300^{0}C. The sharper and higher intensity peaks confirmed the increase in crystallite size. From the Scherer's formula[62] (Equation 6 as mentioned in Section 3.7.1) the average crystallite size was calculated from peak broadening; with Silicon as internal standard. The crystallite size was found to range between 16nm for lowest calcination temperature to 33nm for highest calcination temperature. Fig. 4.4 shows a plot of crystallite size with respect to different weight ratios of Al_2O_3 : MgO at different calcination temperature. The measured crystal size for samples calcined at different temperatures is given in Table 4.2. The crystallite size was found to increase with increasing calcination temperature. Initially the powder surface area being high; leads to high reactivity. With rise in temperature, reactivity leads to particle agglomeration and crystallinity increases, due to spinel phase development, which is revealed in the XRD peaks of different compositions calcined at various temperature as shown in Fig. 4.3(a-d). The calculated average lattice parameter (a_o = 8.0792Å) of $MgAl_2O_4$ with highest MgO content has highest value. This may be due to the enlargement of spinel unit cell structure with the formation of oxygen vacant sites i.e. spinel structure becomes anion deficient due to excess MgO[52,67].

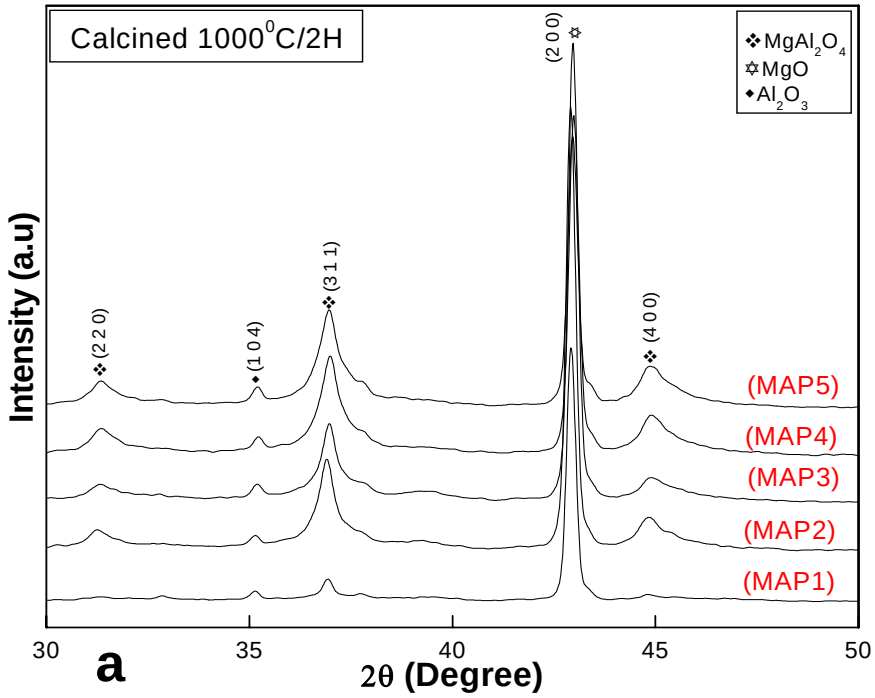

Fig.4.3 (a) XRD of Al_2O_3: *x*MgO powders calcined at 1000°C/2h; where *x*=1, 1.1, 1.2, 1.3, 1.4

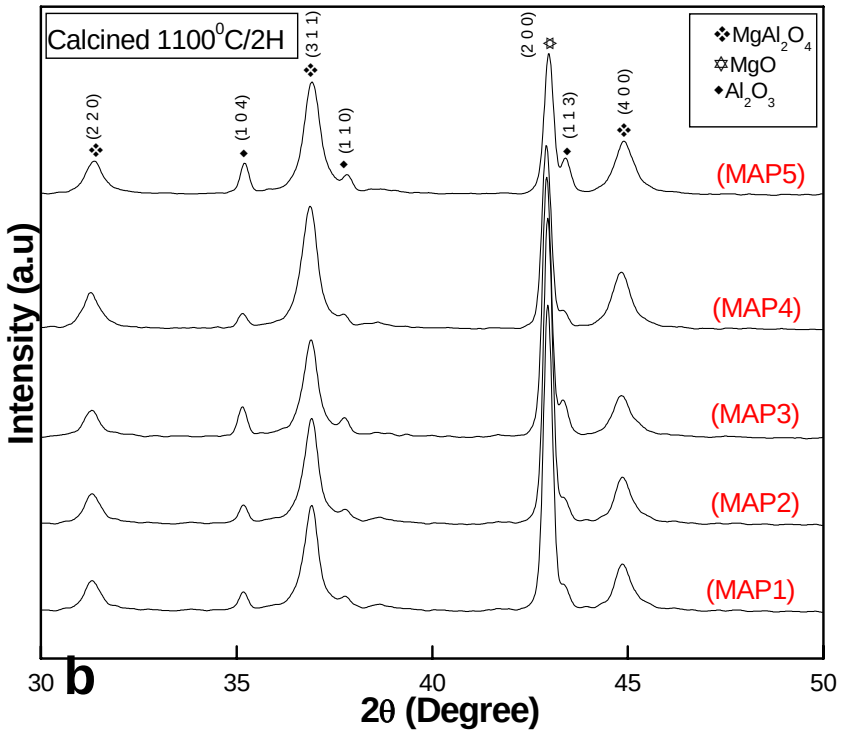

Fig.4.3 (b) XRD of Al_2O_3: *x*MgO powders calcined at 1100°C/2h; where *x*=1, 1.1, 1.2, 1.3, 1.4

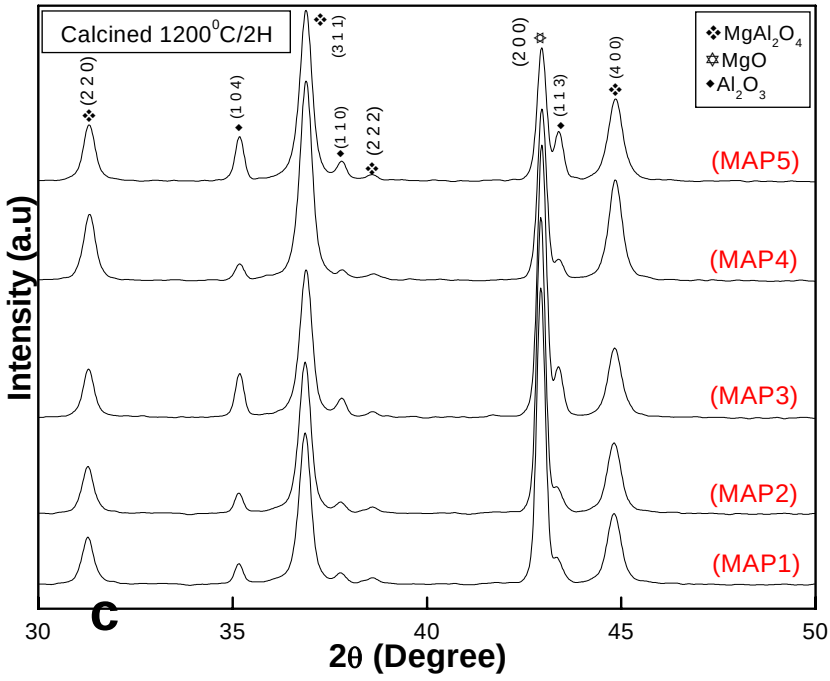

Fig.4.3 (c) XRD of Al_2O_3: *x*MgO powders calcined at 1200°C/2h; where *x*=1, 1.1, 1.2, 1.3, 1.4

The results also indicate that $MgAl_2O_4$ spinel phase develops with increasing calcination temperature. The major phases observed after calcination process in all the batches were that of $MgAl_2O_4$ (311), MgO (200), α-Al_2O_3 (104). Table 4.2 represents the crystallite size and the lattice constant as calculated from XRD analysis.

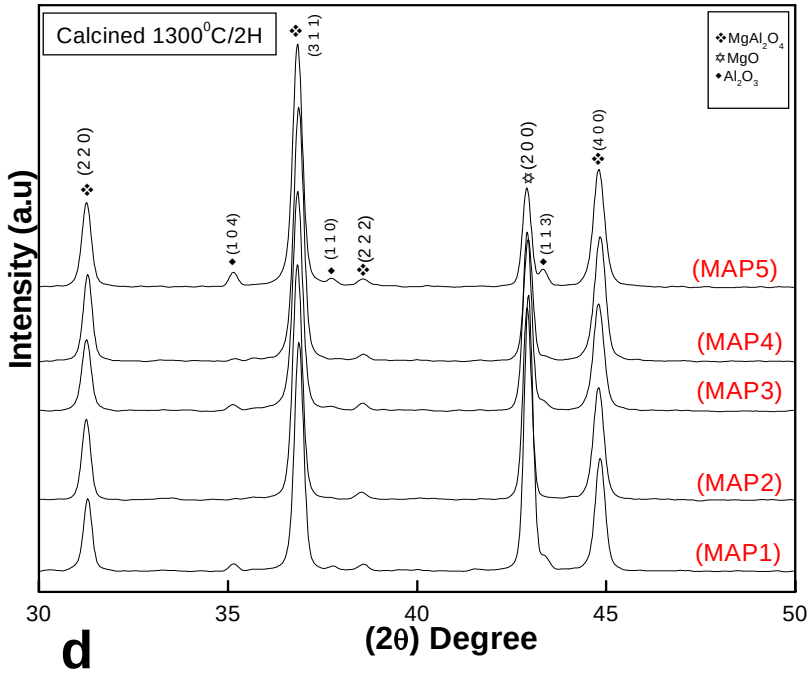

Fig.4.3 (d) XRD of Al_2O_3: *x*MgO powders calcined at 1300°C/2h; where *x*=1, 1.1, 1.2, 1.3, 1.4

Table 4.2: Average Crystallite size and Lattice parameter of spinel phase after calcination of mixed powders at different temperatures

Identity Al_2O_3 : MgO	Calcination Temperature (°C)							
	1000		1100		1200		1300	
	Crystal Size (nm)	a_o (Å)	Crystal Size (nm)	a_o (Å)	Crystal Size (nm)	a_o (Å)	Crystal Size (nm)	a_o (Å)
1:1	19.87	8.071	24.39	8.071	26.66	8.079	29.87	8.081
1:1.1	22.80	8.075	25.15	8.072	27.96	8.085	31.91	8.090
1:1.2	25.96	8.064	27.01	8.075	28.99	8.078	32.18	8.089
1:1.3	26.80	8.059	28.78	8.081	30.63	8.078	32.32	8.084
1:1.4	27.11	8.065	29.75	8.072	31.17	8.078	33.01	8.089

From equation 12 in Section 3.7.3 the extent of spinellisation in calcined samples were calculated from the XRD analysis of the calcined powders. The spinel producing reaction between Al_2O_3 and MgO is diffusion controlled process and mainly depends on the temperature apart from particle size of initial powders[2]. The increase in temperature led to increase in extent of spinellisation as revelaed from XRD diffractograms. Table 4.3 shows the calculated volume percent of $MgAl_2O_4$ formation after calcination at different temperatures. The corresponding data

for various calcination temperature confirms that spinellisation increases with increasing temperature.

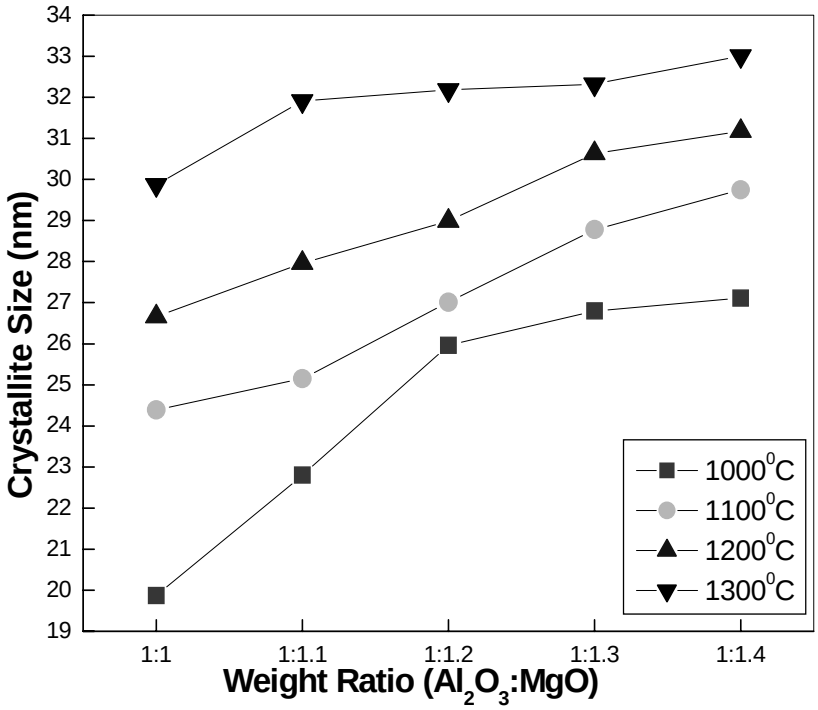

Fig. 4.4: Crystallite Size with respect to Al_2O_3: *x*MgO (weight ratio; where *x*=1, 1.1, 1.2, 1.3, 1.4) at different calcination temperatures

Table 4.3: The calculated volume % of spinel content of calcined powders obtained from mixture of Al_2O_3 : *x*MgO (where, *x* = 1:1, 1:1.1, 1:1.2,1:1.3, 1:1.4 in wt%)

Identification	Al_2O_3 : MgO	Vol% of $MgAl_2O_4$ formation after calcination at;			
		1000(^{0}C)	1100(^{0}C)	1200(^{0}C)	1300(^{0}C)
MAP1	1:1.0	5.59	7.79	26.20	27.58
MAP2	1:1.1	12.23	24.17	33.20	43.97
MAP3	1:1.2	14.33	26.09	34.86	46.52
MAP4	1:1.3	18.59	38.38	46.30	48.37
MAP5	1:1.4	30.32	40.65	48.27	48.26

Considering the two extreme calcination temperatures; in Table 4.3 at 1000^{o}C, ~5vol.% spinel phase could be observed, whereas ~30vol% spinel content is noted for highest MgO content composition. The detailed phase analysis of calcined powder illustrates a gradual trend of increasing spinel formation with increasing calcination temperature as well as increasing MgO content. The phase analysis of XRD peak demonstrates ~28 and ~48vol% spinel phase develops at 1300^{o}C for the lowest and highest MgO content respectively. It has been observed that the crystallite size is 19nm for lowest calcination temperature and lowest content of MgO. However,

the crystallite size gradually increases with increasing temperature and maximum 33nm has been detected for MAP5 powder at 1300°C for 2h. The calculated average lattice parameter (a_o = 8.0792Å) of $MgAl_2O_4$ with highest MgO content has also highest value. This may be due to the enlargement of spinel unit cell structure with the formation of oxygen vacant sites i.e. spinel structure becomes anion deficient due to excess MgO[67] and helps to increase the crystallite size. However, an optimum amount of MgO content in the calcined powder is expected to control the reaction kinetics during sintering[37].

4.1.4. Surface Area Analysis:

The surface area measurements of the processed as well as the calcined powders were performed using the BET Surface area analyzer. Table 4.4 shows surface area and particle size form BET analysis. The particle size has been calculated using equation 12. Only milled sample and calcined samples of two extreme compositions has been taken into consideration. A decrease in surface area with calcination temperature and increase in magnesia content has been observed. Particle size is seen to increase with increasing magnesia content. The increase in particle size can be attributed to the spinel phase development with calcination temperature.

Table 4.4 Surface area and particle size analysis of milled samples from BET surface area analyzer.

Identity Al_2O_3 : MgO	Surface Area (m^2/gm)	d_{BET} (nm)
Milled sample (1:1)	44.47	75.9
MAP1(1:1)	41.15	81.45
MAP5(1:1.4)	23.83	140.66

4.1.5. Compaction Behavior:

Compaction behavior of the powder basically determines the compressibility of the powder with compaction pressure. Free flowing powders will compact easily and will show a lower value of yield point. For studying the compaction behavior of the prepared different spinel compositions, a small amount of each type of powder was taken in a cylindrical die and slowly compacted in a universal testing machine under constant cross head speed and density of the green compact was measured as a function of compaction pressure. Fig.4.5 shows the

compaction behavior curve of powders with extreme compositions ie. MAP1 and MAP5 with lowest and highest MgO content respectively calcined at 1000°C. During compaction, the loose powder are first arranged in a close packed position due to particle rearrangement and sliding followed by fragmentation and compaction at higher load. The compaction behavior was determined from the intersection of the two segments of the density vs. compaction pressure curve. Table 4.5 shows the agglomeration strength of the powders with extreme compositions.

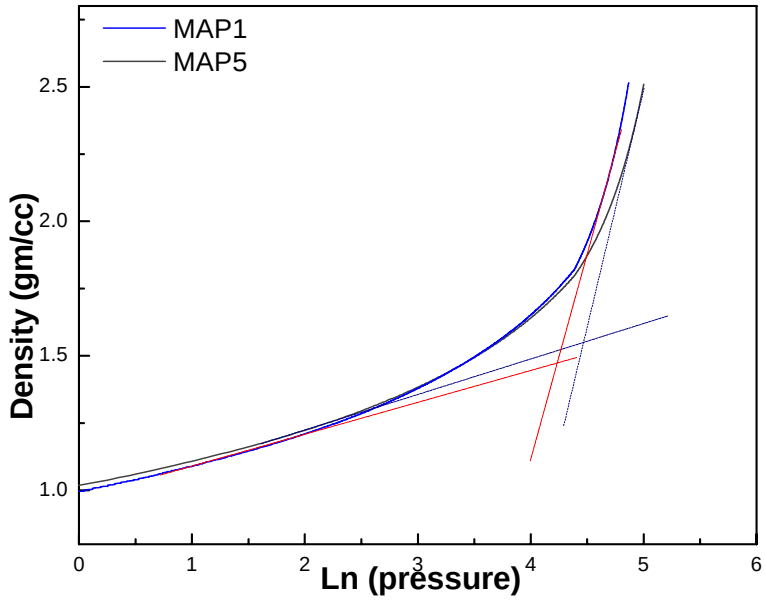

Fig.4.5: Compaction behavior of powders MAP1 and MAP5 with Al_2O_3 : MgO = 1:1 and 1:1.4; calcined at 1000°C/2h

However, in high pressure range densification continues- the density increases due to compression of internal agglomerates. It has been observed that beyond a certain pressure the density increases rapidly. This pressure is known as critical pressure. This is also known as the strength of agglomerates and is denoted by P_j. It has been listed in Table 4.4 that with calcination temperature the particle size increases. Increase in particle size leads to higher agglomeration strength (Pj) as listed in Table 4.5.

Table 4.5 Surface area and particle size analysis of calcined samples from BET surface area analyzer

Identity Al_2O_3 : MgO	Pj (MPa)
MAP1 (1:1)	69.4
MAP5	87.35

(1:1.4)

Low agglomerate strength (~69MPa) has been noted in the powders with low MgO content while it increased to ~87MPa for powders with high MgO content.

4.2. Densification and Microstructure

The powder preparation and its characterization have been discussed in section 4.1. The calcined powders of each batch were thoroughly mixed with 2wt.% PVA as binder and processed according to methodology mentioned in Fig. 3.2. The calcined powders and compacts after sintering were designated separately, as listed in the Table 4.6.

Table 4.6 Nomenclature given to calcined and sintered batches

Al_2O_3 : MgO (weight proportion)	Identification	
	After calcination	After Sintering
1:1	MAP1	MAS1
1:1.1	MAP2	MAS2
1:1.2	MAP3	MAS3
1:1.3	MAP4	MAS4
1:1.4	MAP5	MAS5

4.2.1. Densification Study without Isothermal Treatment:

Prior to sintering, dilatometer measurements were made on pressed compacts (5 x 5 x 15mm) prepared through uniaxial pressing to understand the densification behavior. In this experiment, a green density of 1.79gm/cc could be observed during uniaxial pressing (at 275MPa), which is because of high specific surface area of processed powders. Fig. 4.6 exhibits the dilatometric study of the compacted specimens up to 1250^{o}C without any isothermal treatment. The bar specimens were prepared after calcination of mixtures of MgO and Al_2O_3 oxides at 1000^{o}C for 2h. An increase in linear expansion was observed purely due to the thermal expansion at the initial stage, whereas expansion due to spinel formation may be the reason for the later stage densification above 1000^{o}C [Fig 4.3(a)]. The percentage linear change beyond 1000^{0}C is the combined effect of spinel formation (expansion) and densification (shrinkage)[46,48]. In Fig.4.6, MAP5 depicts sharp fall in slope; reason being the shrinkage rate from sintering of

MAP5 overtakes the expansion rate from spinel formation at about 100-150^{0}C lower than other batches. This shows greater sinterability of the batch with Al_2O_3 **:** MgO weight proportion 1:1.4(MAP5). The presence of inherent oxygen vacancy in magnesia rich spinel composition helps the transport of oxygen ion (the rate controlling factor), resulting in greater extent of amphoteric diffusion, greater mass transport and densification[45,68,69]. The slope of MAP5 falls beyond 1000^{o}C is due to the exceeding densification rate over the rate of spinel formation.

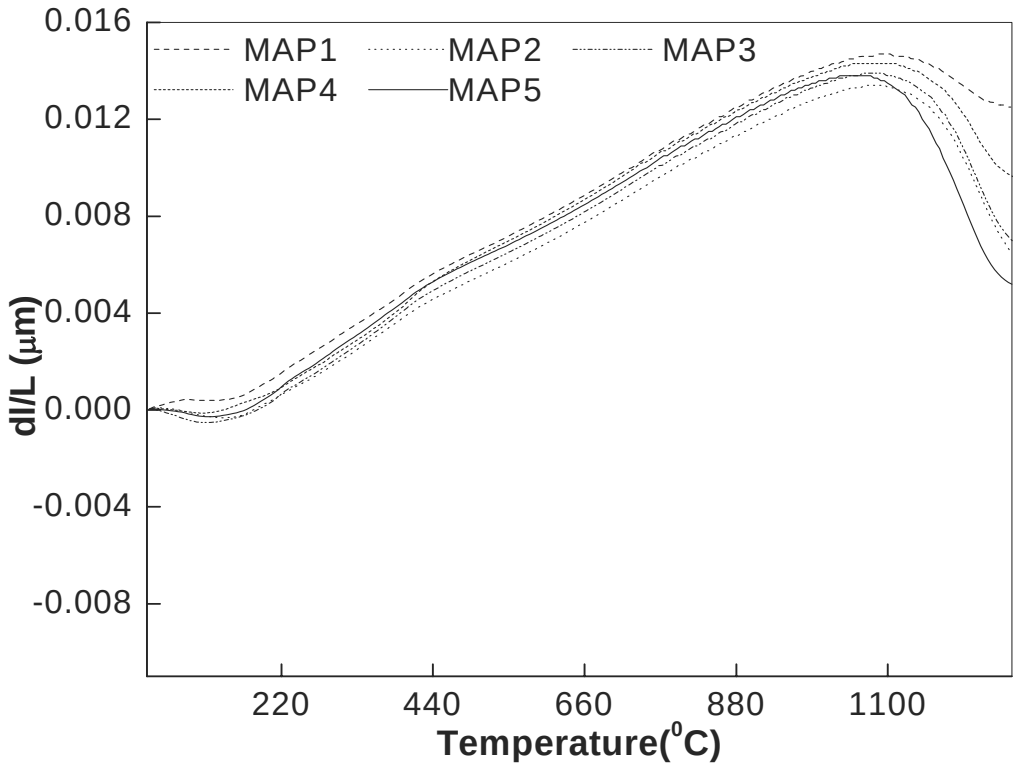

Fig.4.6: Dilatometric study of green bar specimen obtained from 1000^{o}C/2h calcined powders for all compositions

4.2.2. Sintering:

A powder compact before firing is composed of individual grains separated by 25 and 60 vol.% porosity, depending on the particular material used and the processing method. For maximizing properties such as strength, translucency, and thermal conductivity, it is desirable to eliminate as much of this porosity as possible. For some other applications it may be desirable to increase this strength without decreasing the gas permeability. These results are obtained during firing by the transfer of material from one part of the structure to the other. The pores initially present can change shape, becoming channels or isolated spheres, without necessarily changing in size. The size and shape of the pores present change during the firing process, becoming more

spherical in shape and smaller in size as firing continues. The free energy change that gives rise to densification is the decrease in surface area and lowering of the surface free energy by the elimination of solid-vapor interfaces[70]. This process is called sintering.

The process of complete spinelization requires higher calcination temperature as compared to partial spinelization, moreover, higher calcination temperatures always leads to the formation of hard agglomerates, which in turn results into poor sintering of the spinel body. Previous literature reports state that partially spinelized (70–80%) powders can be sintered into a high dense spinel body as compared to fully spinelized or uncalcined powder at elevated temperatures[70-72]. The methodology mentioned in Fig.2 was implemented for sintering of green compacts. A green density of nearly 50% was observed for the uniaxially pressed compacts. The sintering was carried out at 1600^{o}C for 4h dwell time at peak temperature. The sintering profile mentioned in Fig.3.4 was followed for the purpose of sintering. The bulk density was measured through Archimedes' principle. The details of the bulk density and apparent porosity for sintered specimens are represented in Fig 4.9 and Fig 4.10. The material follows solid-state sintering; so according to the ternary diagram in Fig.4.6 is represented by right hand edge of the figure, involving only solid and pores[73]. As the reaction progresses, with increase in temperature the individual molecules coalesce to form dense spinel by elimination of pores. Solid-state reaction between MgO and Al_2O_3 to form spinel is a counter diffusion process and occurs at the Al_2O_3-$MgAl_2O_4$ and the MgO-$MgAl_2O_4$ interfaces.

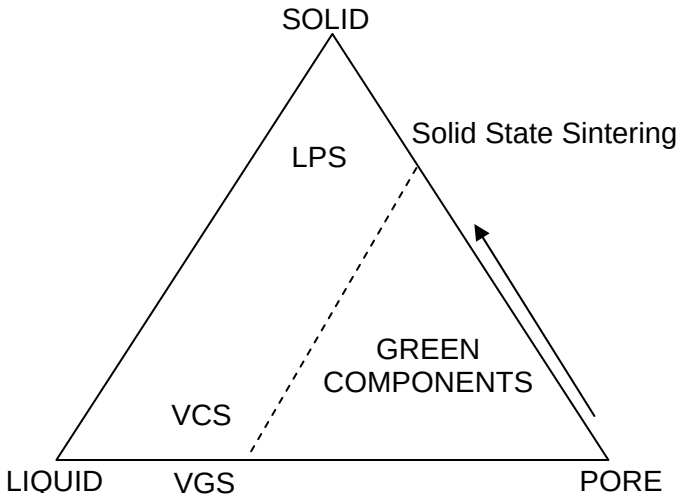

Fig.4.7: Ternary diagram illustrating the types of sintering.

The reaction between the MgO and Al_2O_3 phases is governed by counter diffusion of the Al^{3+} and Mg^{2+} ions through the rigid oxygen lattice or the spinel phase. Three Mg^{2+} ions diffuse

for every two Al^{3+} ions, which diffuse in the opposite direction. Three moles of spinel are formed at the Al_2O_3-$MgAl_2O_4$ interface for every mole formed at the MgO-$MgAl_2O_4$ interface because of ionic charges and stoichiometry[31,32,74]. The excess MgO produce solid solution through consumption of free Al_2O_3, with formation of residual MgO. This is illustrated by the following schematic section through a growing $MgAl_2O_4$ layer, which is called as Jander solid-state reaction geometry.

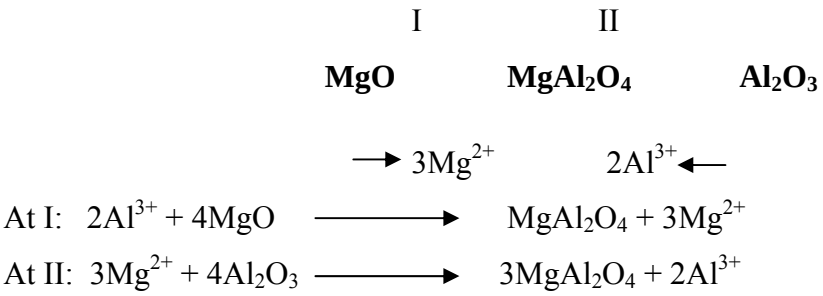

4.2.3. Phase Analysis of sintered specimens:

Fig.4.8 shows the XRD patterns of sintered samples. There is no evidence of corundum phase in all the different batches, which confirms the consumption of Al_2O_3 in formation of spinel phase, and excess MgO remained as free periclase phase. This observation is well matched with the previous reported sintering mechanism[40,75]. The major phases observed after sintering process in all the batches were that of $MgAl_2O_4$ (311) (220) (400) and MgO (200). The extent of spinel formation has been calculated from the XRD analysis and tabulated in Table 4.7.

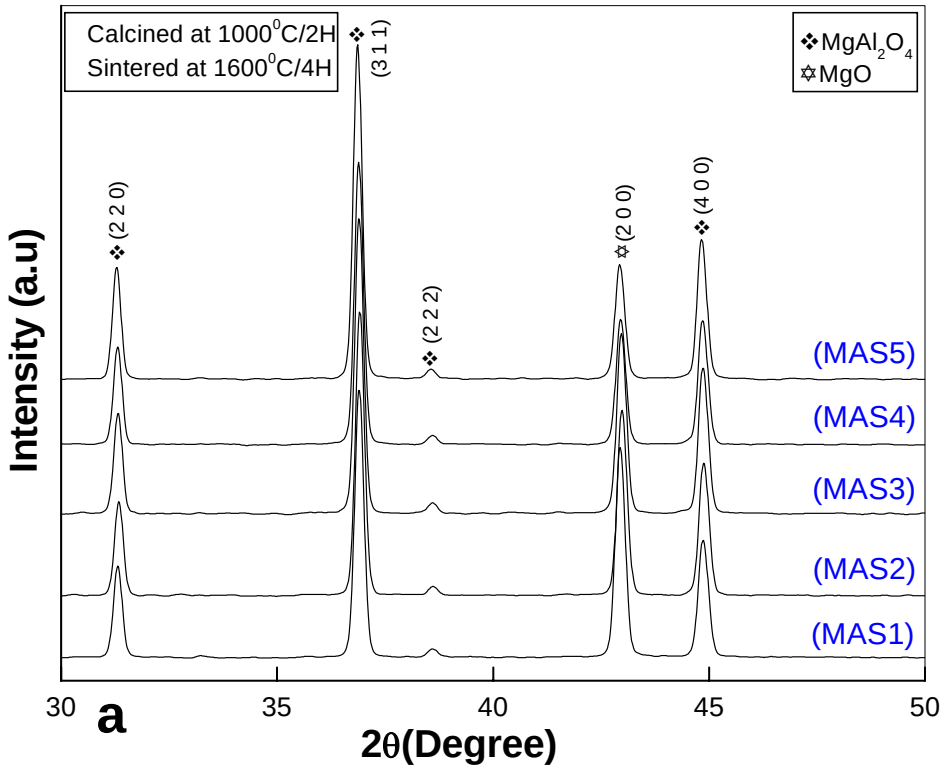

Fig.4.8 (a): XRD of samples calcined at 1000°C/2h and sintered at 1600°C/4h

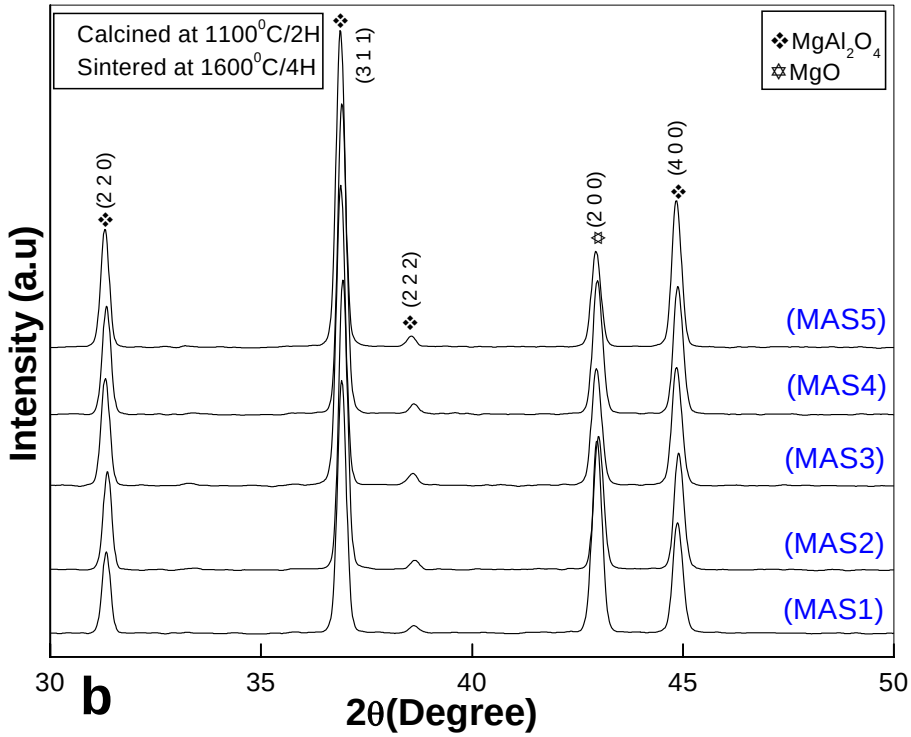

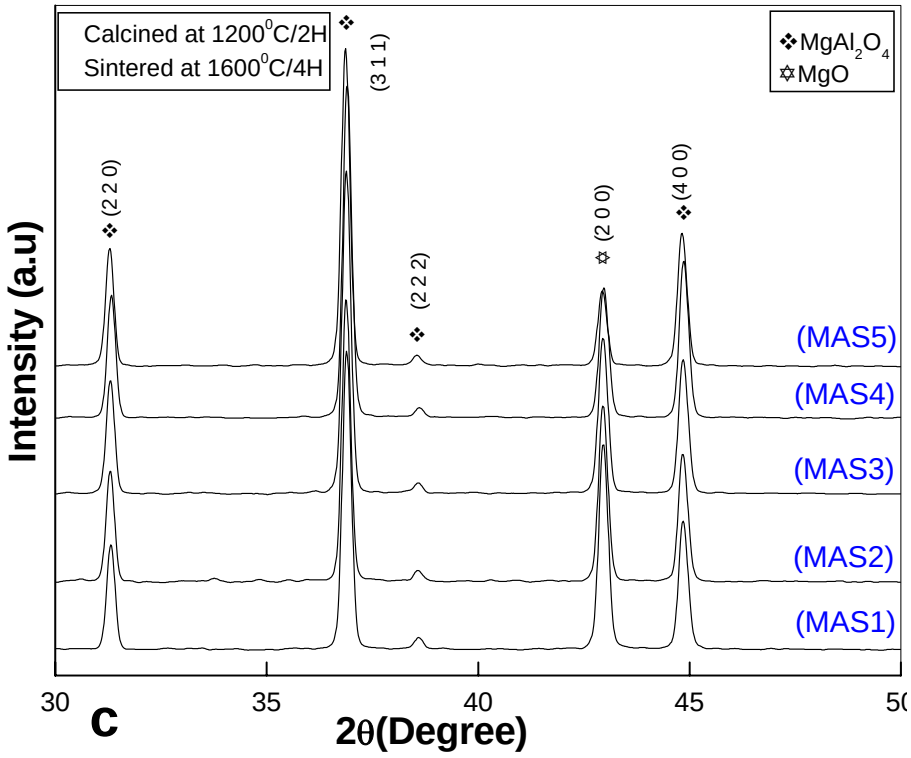

Fig.4.8: (b) XRD of samples calcined at 1100°C/2h (c) 1200°C/2h and sintered at 1600°C/4h

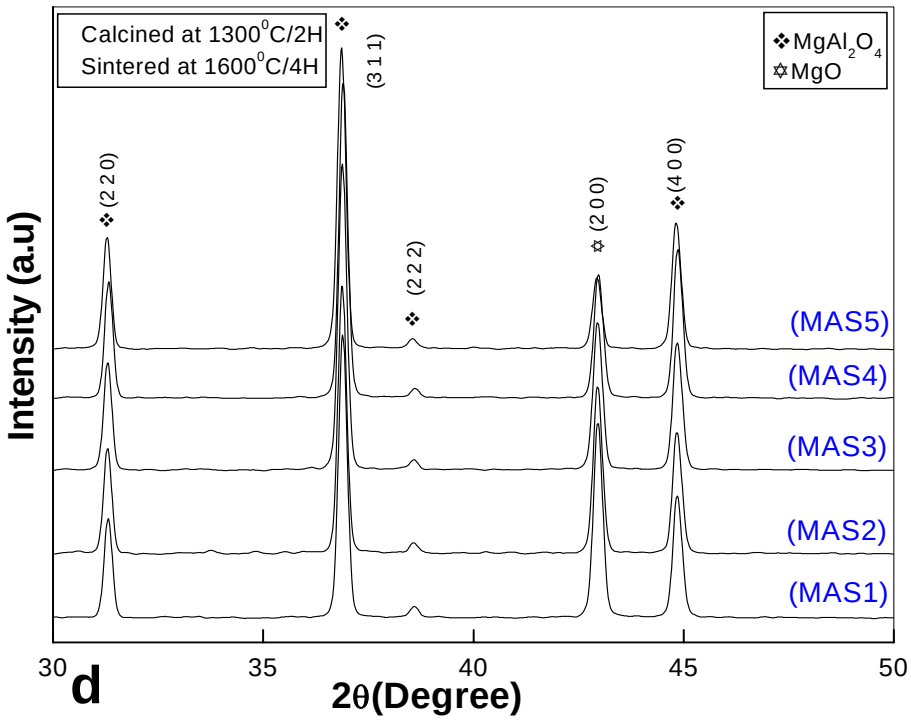

Fig.4.8 (d) XRD of samples calcined at 1300°C/2h and sintered at 1600°C/4h

The total amount of spinel content of sintered specimen is low for MAS5 composition with ~50vol.% of spinelization. Calcination of the milled powders causes inertness and this reduces the spinel content (Table 4.6) in the sintered bodies. Again calcination has also got a great influence on the densification behavior. The higher the calcination temperature, the greater is the agglomeration of the starting oxides, leading to inertness (lesser reactivity) and hence lesser shrinkage. This leads to reduced densification with increasing calcination temperature.

Table 4.7: Spinel and MgO phase after sintering (1600^{o}C/4h) of compacts obtained from calcined powders.

Identification	Al_2O_3:MgO	vol% $MgAl_2O_4$ content sintered at 1600^{o}C calcined at ;		vol % MgO Content sintered at 1600^{o}C calcined at ;	
		1000(^{0}C)	1300(^{0}C)	1000(^{0}C)	1300(^{0}C)
MAS1	1.1.0	70.54	62.36	28.12	37.64
MAS2	1:1.1	67.92	60.81	32.07	38.45
MAS3	1:1.2	65.16	58.74	34.14	40.25
MAS4	1:1.3	59.25	52.29	38.80	47.10
MAS5	1:1.4	55.49	49.56	40.74	50.03

Highest spinel phase formation in sintered specimen is observed in presence of ~5vol% seed content in green pellets, and a gradual decreasing trend could be observed with increasing initial seed content. In presence of in-situ 5vol% spinel seed spinellisation reaches ~70vol% for MAS1 at 1600^{o}C for 4h through nucleation and growth process, whereas this content reduces to ~62vol% with increasing temperature when initial seed content was ~28vol%. However, with increasing MgO content, the extent of spinel phase formation decreases and reaches upto ~50vol%. Hence, an optimum amount of seed has significant effect on formation of MgO-rich spinel composite. This may be attributed to the effect of the content of spinel crystal seeds, which act as the substrate for heterogeneous nucleation. The rate of nucleation in a unit area of substrate is temperature dependent, which can be expressed as[37,76]:

$$I^{h} = k^{h} \exp\left(-\frac{\Delta G_{k}^{h}}{kT}\right)$$

where, I^h is the rate of nucleation in a unit area of substrate, K^h a constant irrespective of the substrate, k is the Boltzman's constant, T temperature and ΔG^h_k is the potential barrier for heterogeneous nucleation, which can be expressed as:

$$\Delta G_k^h = \Delta G_k \left[\frac{1}{4} \left((2+\cos\theta)(1-\cos\theta)^2 \right) \right] \quad \ldots\ldots (4)$$

where, ΔG_k is the potential barrier for homogeneous nucleation, and θ is the contact angle between the crystal nuclei and the substrate. When the substrate is identical to the nucleating crystal, θ = 0 and consequently $\Delta G^h_k = 0$, i.e., the potential barrier to nucleation does not exist. However, when significant differences exist between the substrate and the nucleating crystal, i.e., θ = 180, $\Delta G^h_k = \Delta G_k$, hence, they cannot interact and therefore no acceleration of the nucleation can occur. Assuming this theory, it can be suggested that optimum amount of $MgAl_2O_4$ crystal seeds could decrease the potential barrier for nucleation and therefore accelerate nucleation and growth of the final product ($MgAl_2O_4$) with low seed content. On the other side, the presence of excess seed accelerates the grain growth at high temperature rather than any nucleation effect. Hence, higher percentages of seed have not any advantages on the further spinel formation.

4.2.4. Bulk Density and Apparent Porosity:

Dense magnesium aluminate spinel bodies with superior properties have good prospects as refractory component. The relative density of different samples was measured after sintering of green pellets obtained from calcined powders and PVA binder. From Fig.4.9 the specimens show an increasing trend with temperature till a calcination temperature of 1200°C and subsequent sintering, but beyond that the density decreases. This can be attributed to the increased in-situ spinel content and subsequent coarsening of grains during sintering. Fig.4.10 reveals the relative density of specimens with extreme compositions.

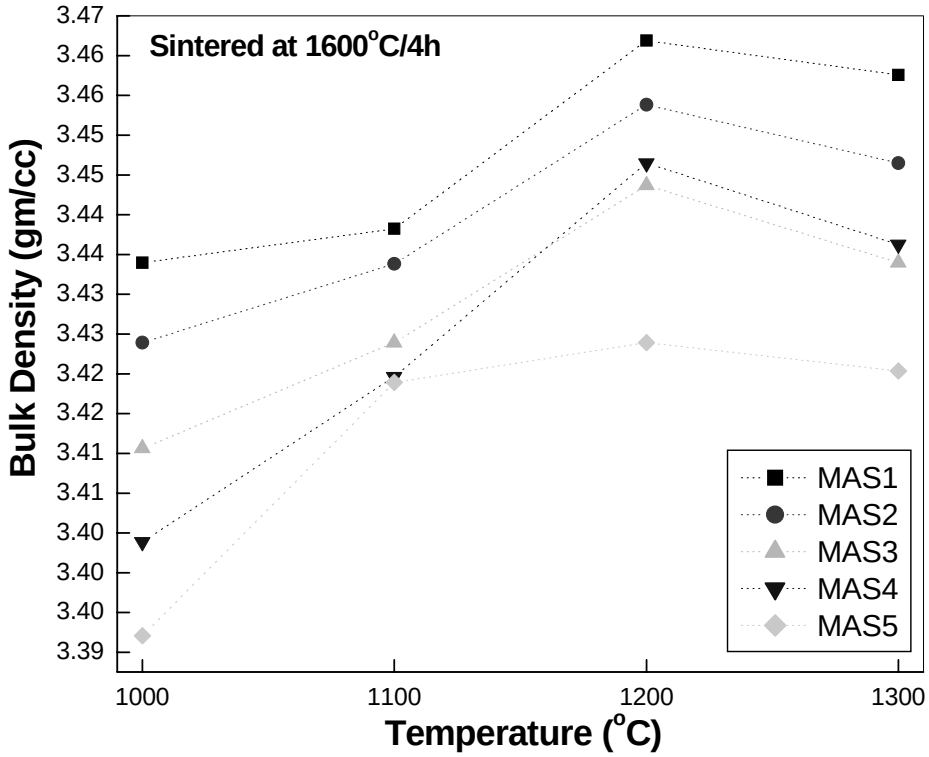

Fig.4.9: Bulk Density of 1600°C/4h sintered compacts with respect to temperature

Table 4.8: Bulk Density of sintered compacts calcined at various temperature and sintered at 1600°C

Calcination (°C)	MAS1	MAS2	MAS3	MAS4	MAS5
1000	3.43	3.42	3.41	3.40	3.39
1100	3.44	3.43	3.42	3.42	3.42
1200	3.46	3.45	3.44	3.45	3.42
1300	3.46	3.45	3.43	3.44	3.42

Fig. 4.10 illustrates that the maximum density of MAS1 could be achieved after calcination at 1300°C/2h and subsequent sintering at 1600°C for 4h. However, the relative density may be affected in presence of seed content in precursor and calcination temperature. Table 4.3 and Table 4.7 reveals that the spinel content of the sintered specimen can be controlled by the initial calcination temperature of the mixture of starting materials. The characteristic curve of both the specimen (MAS1 and MAS5) illustrates the higher content of spinel seed has deleterious effect on densification behavior. An increase in trend of density may be associated with better sintering of the body due to the presence of reactive spinel phase with average crystallite size of 19-30nm and proper densification of the body in between MgO grains by finer

spinel phase as observed in micrographs in Sec 4.2.5. High temperature calcined (1300°C) materials exhibit a low value of relative density due to the coarsening effect and this is presumably higher content of spinel favors more diffusion and favors grain growth.

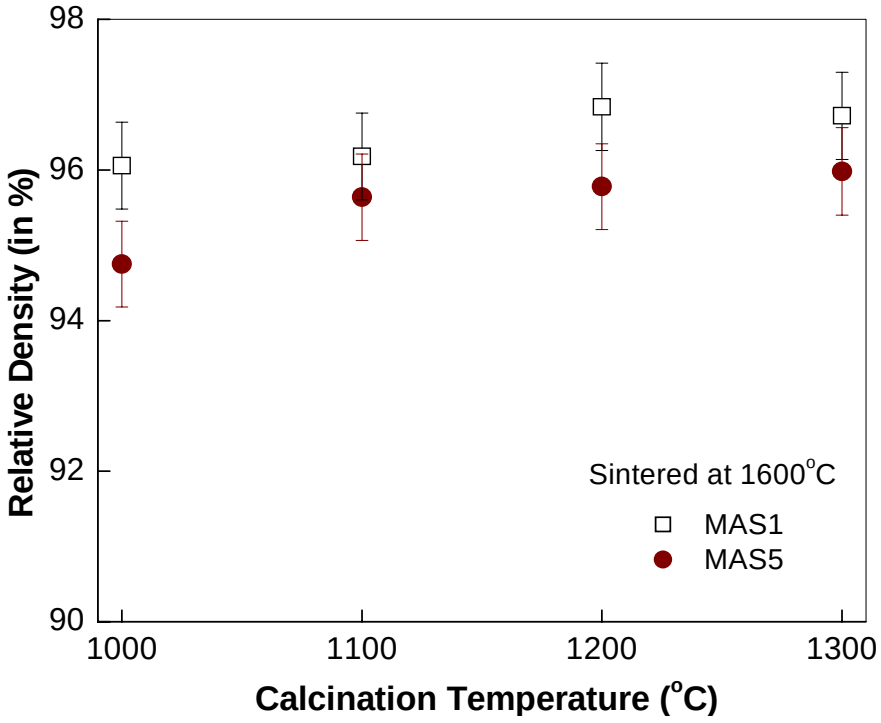

Fig.4.10: Relative density of 1600°C/4h sintered samples calcined at various temperatures and sintered at 1600°C. The other samples showed the same trend as shown by MAS1 and MAS5.

The comparatively coarser particles densify intensely, but, particle size much finer to a certain critical value is of no benefit for densification[77]. Very coarse materials reveal the poor density, which follows the general conditions of sintering. In case of MAS1 and MAS5, the coarsening is predominant rather than diffusion due to presence of more than 26vol% spinel content. When the seed content is 30vol% the volume expansion is predominant and hence the reduced relative density. The relative density varies between 96-98% for MAS1, whereas MAS5 exhibits this variation within the range of 95-97%. However, the densification study does not show any significant difference among the batches, which may be due to the similar true density values for both spinel and periclase phases.

Nearly 96% relative densification is exhibited for highest MgO containing (MAS5) specimen when constituent powder was calcined at 1300°C for 2h and followed by sintering at 1600°C for 4h. The densification process is greatly influenced by calcination process, and the presence of free periclase (as revealed in Fig.4.8) hinders the grain boundary migration. MgO rich composition is itself very active for higher densification, due to creation of vacancies as

suggested by Hing[78]. The bulk density and relative density of samples varied between the two (MAS1 and MAS5) extreme compositions. The density was seen to decrease with samples calcined at 1300°C may be due to increased inertness at higher calcinations temperature. The linear diametrical shrinkage of the samples was quite high and it varied between 16 and 20%.

The Apparent porosity of the sintered samples have been listed in Table 4.9 and shown in Fig.4.11. The micrographs in Sec.4.2.5 reveal good grain size distribution with presence of pores in between the grains in sintered samples. Microstructures shows the presence of big grains in samples calcined at higher temperature and sintered at 1600°C/4h in comparison to the grain size[79] depicted by the powders calcined at lower temperatures followed by sintering.

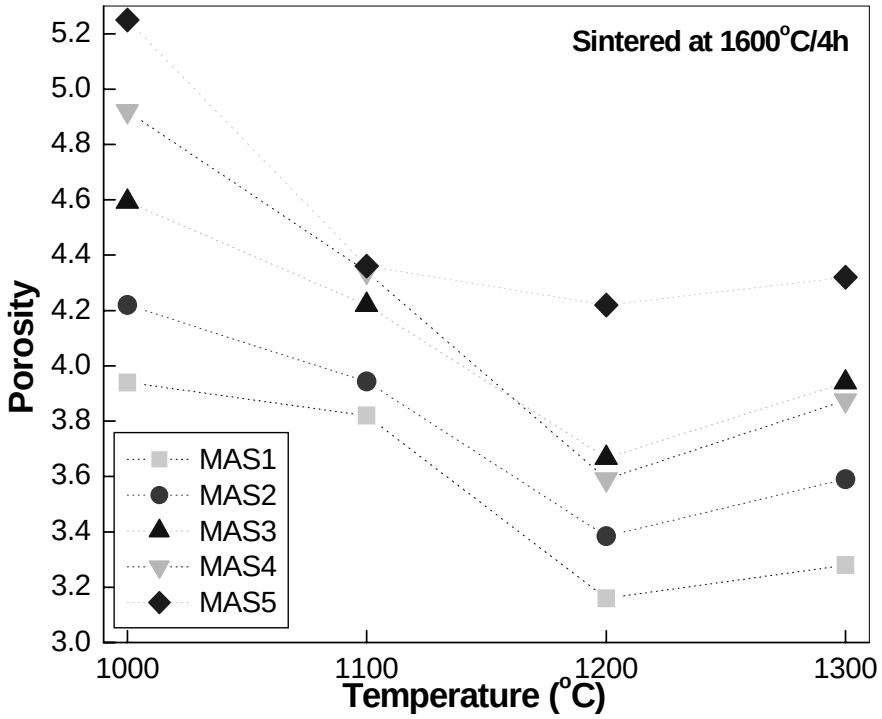

Fig.4.11: Apparent Porosity of 1600°C/4h sintered compacts with respect to temperature

Table 4.9: Apparent Porosity of sintered compacts calcined at various temperature and sintered at 1600°C

Calcination (°C)	MAS1	MAS2	MAS3	MAS4	MAS5
1000	3.93	4.22	4.59	4.92	5.25
1100	3.82	3.94	4.22	4.34	4.36
1200	3.16	3.38	3.66	3.58	4.22
1300	3.27	3.58	3.93	3.87	4.32

The low content of in-situ spinel seeds and low crystallite size in powders calcined at lower temperature bring about better densification due to high reactivity. On the contrary, the high calcination temperature increases inertness of the system, which due to coarsening effect leads to lower densification. This leads to slight increase in porosity and decrease in density as revealed from Fig.4.9 and 4.10. Usually a trend similar to that of density can be observed for porosity, with a value of 5.25% for MAS5 and a low value of 3.16% for MAS1. The high value may be due to the coarsening effect due to large grain size as revealed in the microstructure.

4.2.5. Microstructure:

Fig. 4.12 - 4.15 shows the scanning electron microscopic images of the sintered, polished and thermally etched $MgAl_2O_4$ pellets. The precursor powders were calcined at various temperatures for 2h, uniaxially pressed at 275MPa and sintered at 1600^oC for 4h at the peak temperature. The difference in grain morphology is due to the difference of contrast of MgO and spinel phases. This is because the theoretical density of MgO (3.6g/cc) is higher than that of spinel (3.58g/cc). The micrographs also exhibit white streaks which is MgO. The grains of the magnesia rich spinel are non-uniform and pores are present in between the grains. The micrographs reveals the presence of excess MgO (non-solid soluble in spinel) present in between the spinel grains, which suppress grain growth and helps in densification. This observation is supported by the X-ray diffractograms of sintered specimens.

Fig. 4.12 and 4.13 represents the microstructure of MAS1 specimen, which are calcined at 1000 and 1300^oC and sintered at 1600^oC/4h. Micrograph reveals that average grain size of MAP1 calcined at 1300^oC is ~8μm in comparison to average grain size of ~5μm of MAP1 calcined at 1000^oC. Similarly, Fig. 4.14 and 4.15 exhibits the microstructure of MAS5 with relatively larger and elongated grain at around ~9 and 16μm, when specimens have been sintered after calcination at 1000^oC and 1300^oC temperature respectively. Direct-bonded and rounded spinel–spinel grains with relatively few edges are also observed. Fig 4.12 reveals that grains of MAS1 are non-uniform and pores (intergranular) are present in between the grains. However, some abnormal grains could be noticed in Fig 4.13 where content of in-situ crystal seed is ~30vol%. This can be due to the coarsening effect at higher calcination temperature.

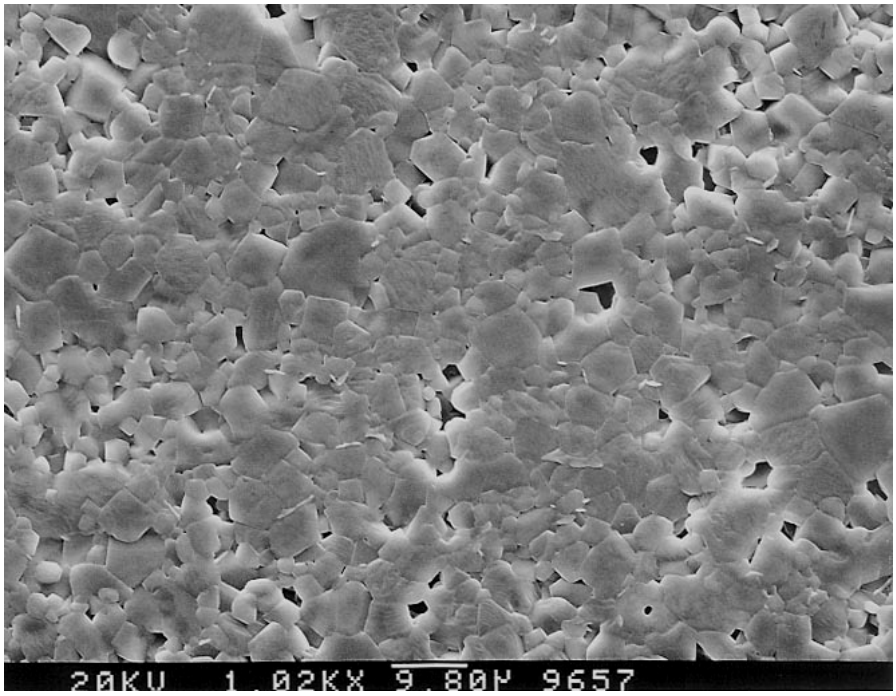

Fig.4.12: Microstructure of MAP1 powder calcined at 1000^{o}C & sintered at 1600^{o}C/4h

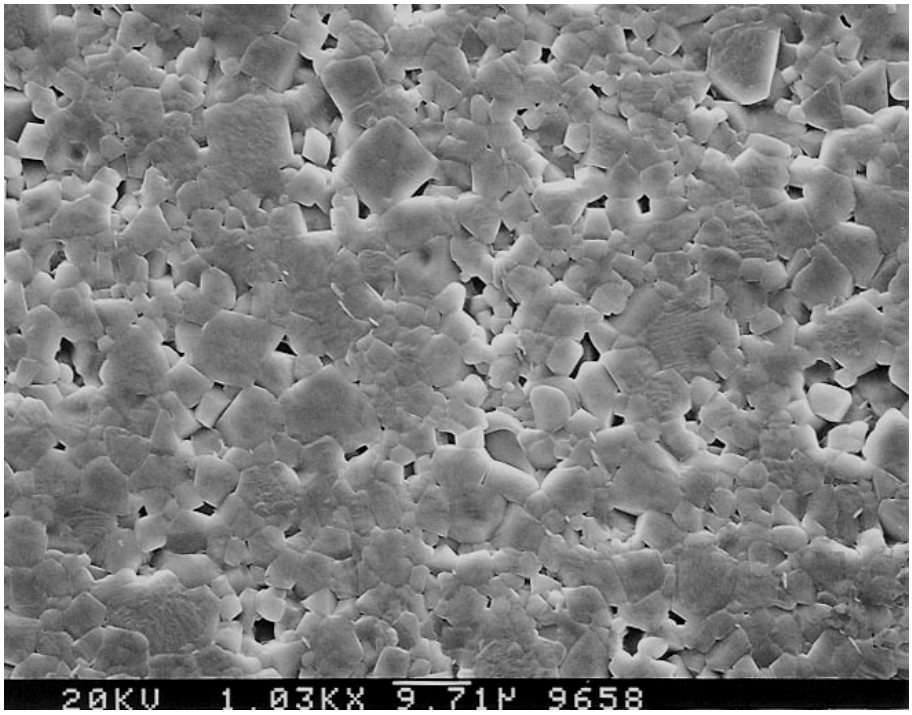

Fig.4.13: Microstructure of MAP1 powder calcined at 1300^{o}C & sintered at 1600^{o}C/4h

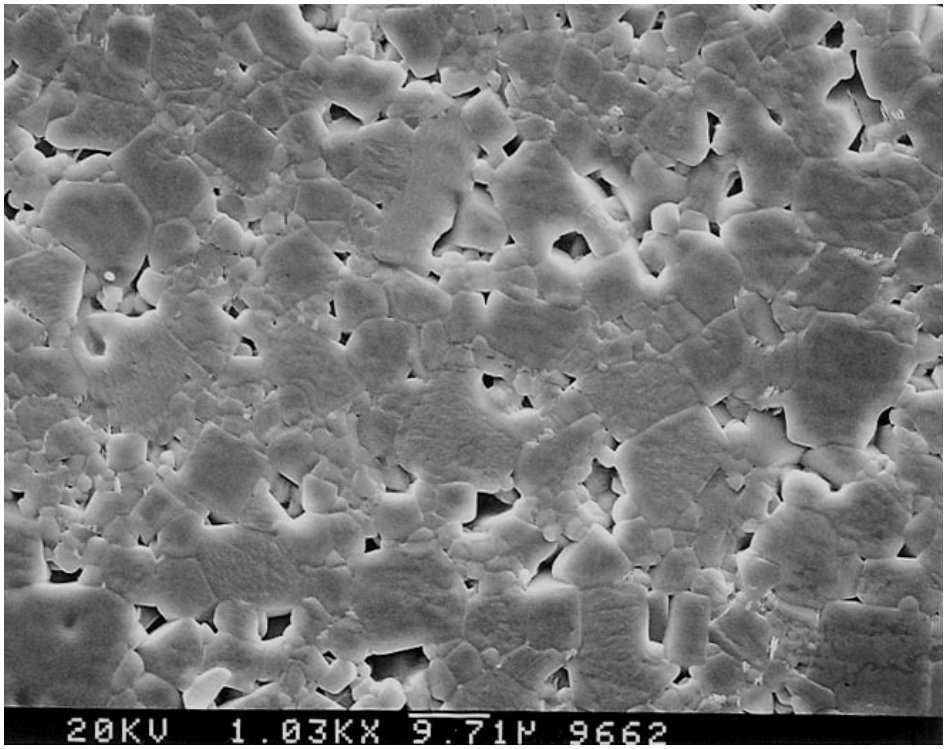

Fig.4.14: Microstructure of MAP5 powder calcined at 1000^{o}C & sintered at 1600^{o}C/4h

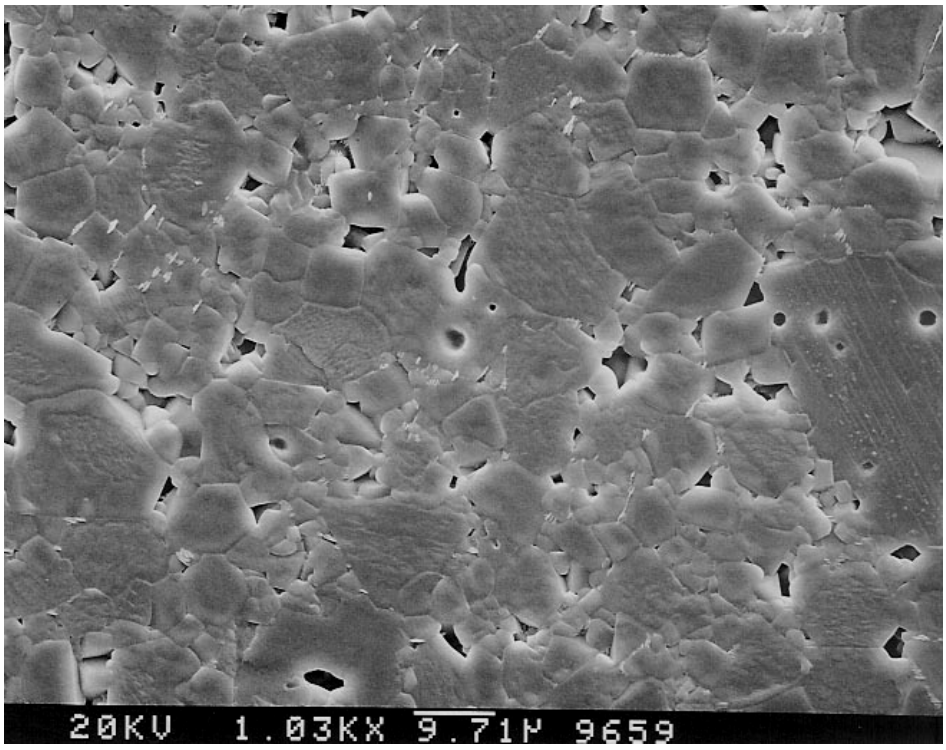

Fig 4.15: Microstructure of MAP5 powder calcined at1300^{o}C & sintered at 1600^{o}C/4h.

Fig 4.15 illustrates the microstructure of sample MAS5 which has large grain structure and direct bonded spinel grains which confirm the results of densification parameter. The grains in samples MAS5 seem to appear as layered grains. Abnormal grain growth was identified when the powders calcined at 1300^{o}C and sintered at 1600^{o}C for 4h.

Random grain orientation and increased intergranular porosity is responsible to deteriorate the density of MAS5 specimen. From the microstructure, the average grain size ~5μm of MAS1 calcined at 1000^{o}C and sintered at 1600^{o}C/4h may exhibit improved room temperature mechanical properties, whereas MAS5, calcined at 1300^{o}C and sintered at 1600^{o}C/4h is expected to provide better high temperature mechanical properties because of elongated and larger grain size.

4.3 Mechanical and Thermal Properties

Generally, the oxide ceramics by themselves do not exhibit high fracture toughness or strength from room temperature to elevated temperature. However through composite ceramic materials have there is possibility of developing microstructures, where the mechanical properties can be tailor-made to suit the service requirements. Magnesia-spinel composites have possibilities of exhibiting good strength properties. Mechanical strength of ceramic composites depends mainly on two parameters. One is the intrinsic property of the phases present and the microstructure of the material. In multiphase material, microstructure of the materials, i.e. the amount and distribution of the phases play a crucial role in determining the mechanical strength. The test methodologies also play significant role on the strength values. According to the application, the material can experience fully compressive strength, tensile strength and/or intermediate of these. Actually, bend or MOR strengths are intermediate between tensile and compressive strengths. In this chapter the hardness, compressive strength and flexural strength tests have been carried out. Attempts have been made to correlate the compressive strength with the bending strength values. Finally, the thermal shock resistance has been evaluated for specimens spalled at 800^{o}C for three cycles at room temperature.

4.3.1. Hardness:

The hardness of a material is a parameter describing its ability to withstand penetration by a surface contact, through a combination of plastic flow and brittle fracture. Hardness of the studied materials may be explained on the basis of the grain size and morphology. Vickers Hardness of sintered samples with different content of spinel is shown in Fig. 4.16. Usually the measured value of hardness is load-dependent. Especially at low loads the measured values of microhardness tend to increase. This reflects an effect of a ratio of the impression size to a characteristic microstructural dimension such as grain size, pore size and distribution, inclusions, and the range of residual stresses. The microhardness also depends on the relationship of surface properties vs. bulk properties and on environmental interactions. At high loads, such as several kilograms, the measured hardness of ceramics decrease due to the fracture of the material during indentation.

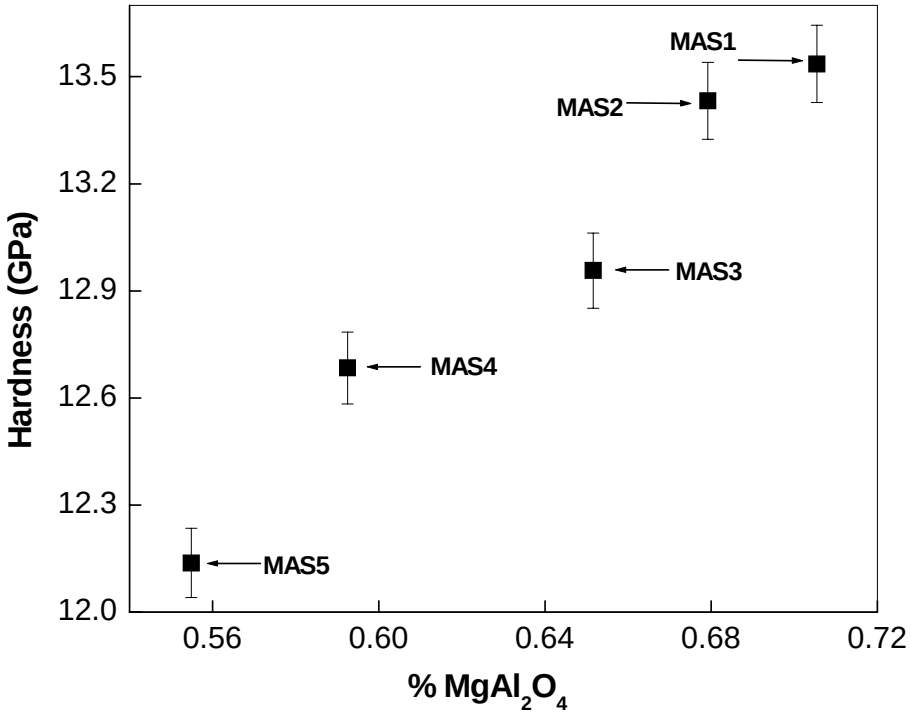

Fig. 4.16: Hardness of various sintered specimen w.r.t increasing spinel content

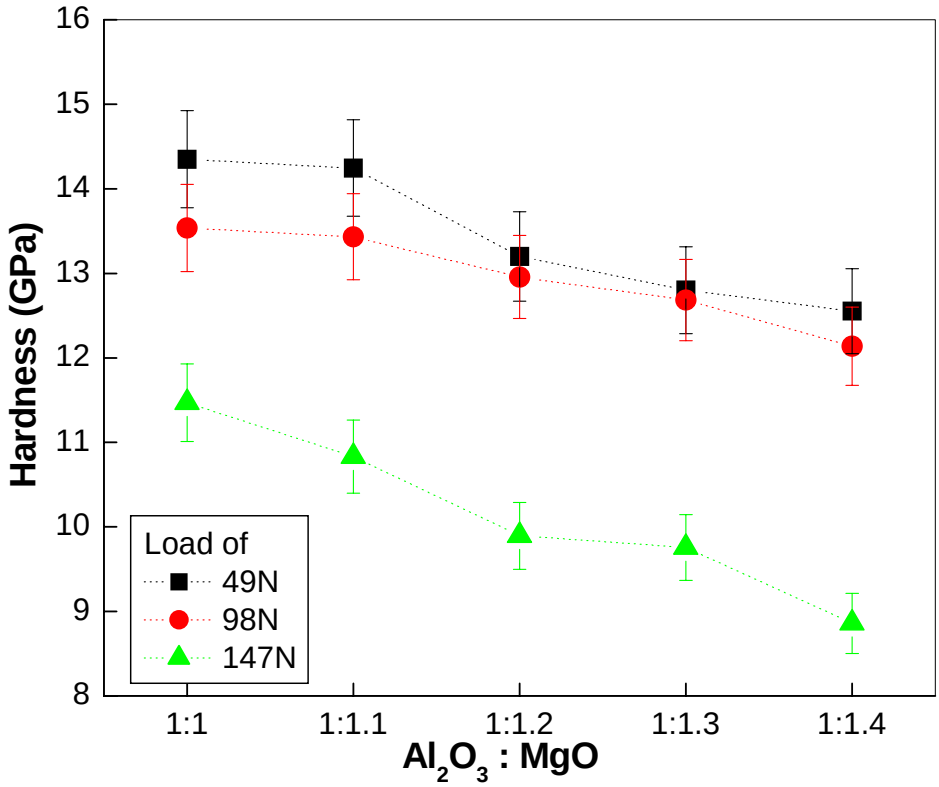

Fig.4.17: Composite Hardness of specimens at different loadings with respect to Al_2O_3 : MgO

From Fig.4.16 it can be observed that the hardness of the composites had an increasing linear relationship with increasing spinel content. The hardness of MgO-Spinel composite (MAS1) is ~13.5GPa, which continuously decreases (13.7–12.1GPa) with the content of spinel phase at sintered specimen. From Fig. 4.17, higher amount of seed addition has an adverse affect on the hardness of the composites due to coarsening of the spinel grains and formation of subsequent porosity. It has also been noticed that these composite materials also obey Hall–Petch relationship[80,81]. The present study shows that the average particle size has significant impact on mechanical properties, which is controlled by spinel seed content and initial calcination temperature.

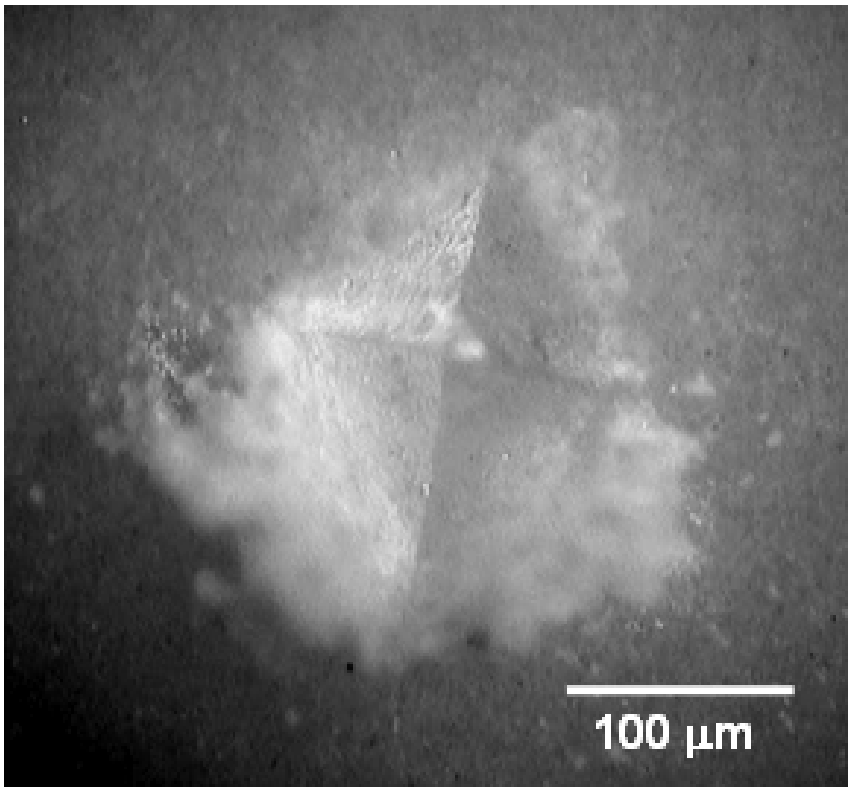

Fig.4.18: Optical Image of indentation shape of MAS1 (Al_2O_3 : MgO =1:1) at load of 98N

Fig.4.18 shows an optical image of the sintered specimen, MAS1 (Al_2O_3 : MgO =1:1) at a load of 98N.

4.3.2. Diametrical Compression Test / Brazilian Disk Test:

Strength tests such as the tension test, the diametrical compression test/Brazilian disk test[65], and the simple compression test determine the limit of performance of a material to stress.

As such, strength criteria can be built using a combination of the local principal stresses. Compressive strength, in general is high because the flaws in ceramics in this case are close[73].

The mechanical properties of MgO-spinel composites containing preformed spinel are more strongly influenced than the in-situ formed spinel composites by sintering temperature, volume fraction and particle size of spinel[55]. The evaluation of compressive strength of spinel based refractory has significant effect under loading[57]. Fig.4.19 illustrates that the compressive strength of both of the MAS1 and MAS5 specimens does not have significant change with respect to preformed spinel addition and/or calcination temperature.

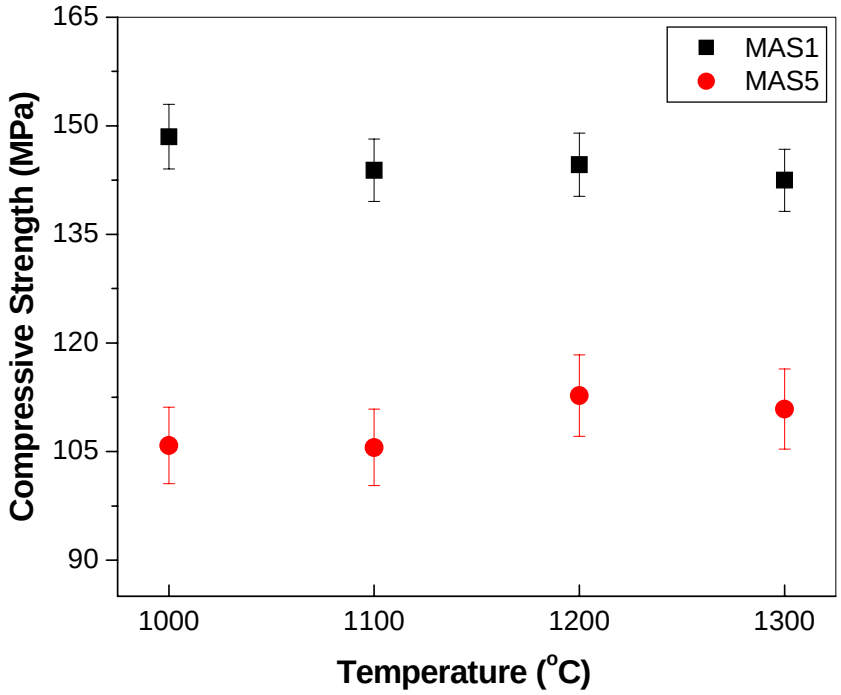

Fig.4.19: Compressive Strength (σ_{comp}) of MAS1 and MAS5 as a function of temperature. The sintering was carried out at 1600°C/4h

Around 20% fall in strength could be noticed for MAS5, this is presumably due to: a) the excessive grain growth of spinel phase during sintering and b) the partial bonding within preformed spinel grain and magnesia. MgO-Spinel composites with α_{spinel} ($7.6MK^{-1}$) < α_{MgO} ($13.5MK^{-1}$) show low strength in comparison with pure MgO, because the thermal expansion mismatch leads to large tensile hoop stresses and microcrack development around the spinel grains, and the radial cracks produced readily link together[55]. These cracks are the critical defects causing failure on loading.

4.3.3. Flexural Strength:

The flexural strength of sintered specimens (50x4x4mm) has been measured using three-point loading system. The strength at room temperature with respect to MgO addition and/or spinel content in sintered samples is shown in Fig.4.20. Strength values in general decreased markedly with increasing MgO content in sintered specimens. The maximum value for flexural strength was ~137MPa, observed for MAS1 with a spinel content of ~70vol.%. The tests revealed low strength values for high spinel content specimens, ~92MPa for MAS5 with ~56vol% spinel. The strength gradually decreases with increasing grain size as well as the content of MgO. A similar trend could also be noticed for different calcination temperature.

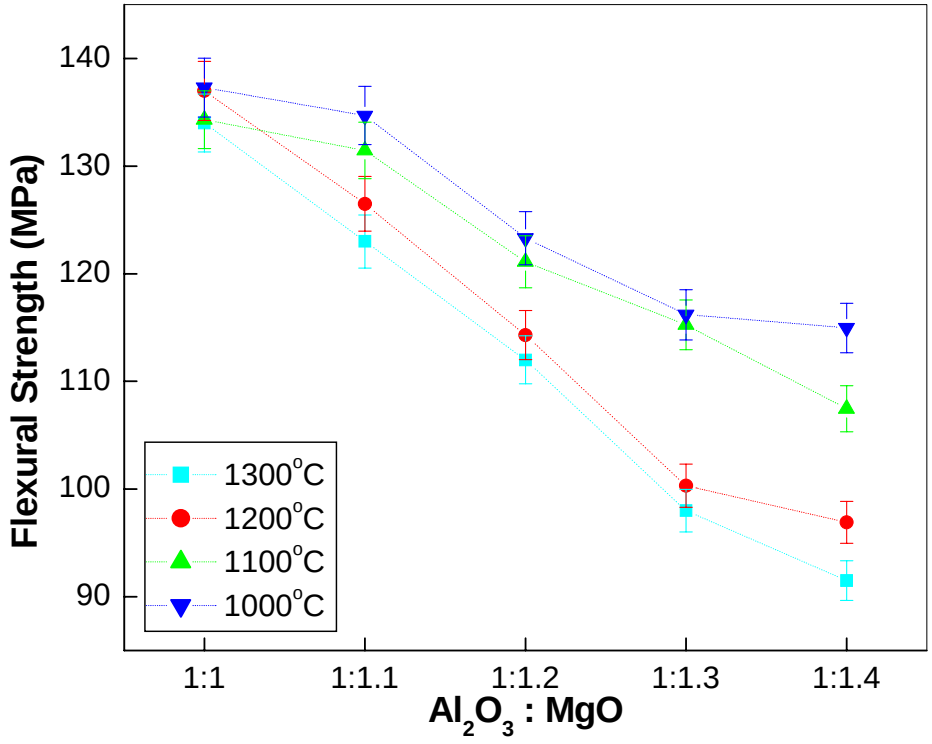

Fig 4.20: Flexural Strength of sintered specimens from 3pt. bend test with respect to Al_2O_3: *x*MgO (where x= 1, 1.1, 1.2, 1.3, 1.4)

The decrease in bending strength with increasing MgO content is followed with the generation of microcracks (originates at the MgO-spinel grain boundary interface). The microcracks are the result of the large thermal expansion mismatch between the magnesia and spinel grains. Here the increase in microcrack population and their extension is predominant, which is major factor behind reduction of strength. As MgO content increases, more extensive microcracks occur and hence decrease in strength values. Nearly 15% strength loss is observed

in samples of two extreme compositions, calcined at 1000°C and subsequent sintering. These cracks are the critical defects which causes failure on loading. However, a substantial decrease (~35%) could be noticed when the starting powders were calcined at 1300°C. This is an additional effect of increase in grain size with calcination temperature and MgO content. From "rule of mixtures", the calculated Young's modulus is seen to vary within the range of 260±5GPa for any compositions, hence this effect has not been considered. Thus, the decrease in strength of the MgO-rich spinel composites is, therefore, prone to fracture, and in particular to the change in nature of the critical flaw size arises due to the thermal expansion mismatch within the residual MgO grain and spinel phase.

Generally, the compressive strength of ceramic material is high and tensile strength is low. This behavior arises because the flaws (e.g. porosity) in the ceramic are effectively closed under compressive stress but rapidly enlarged under tensile stress (Fig. 4.21). Ceramics tend to fail in tension so, for example, even in a three-point bend (flexural) test failure usually occurs on the side under tensile stress commonly originating from a microstructural, strength limiting and flaws[73]. The earliest studies of ceramics also revealed the trend of decreasing strength with increased grain size or increased levels of porosity resulting in a maximum in strength as a function of sintering temperature.

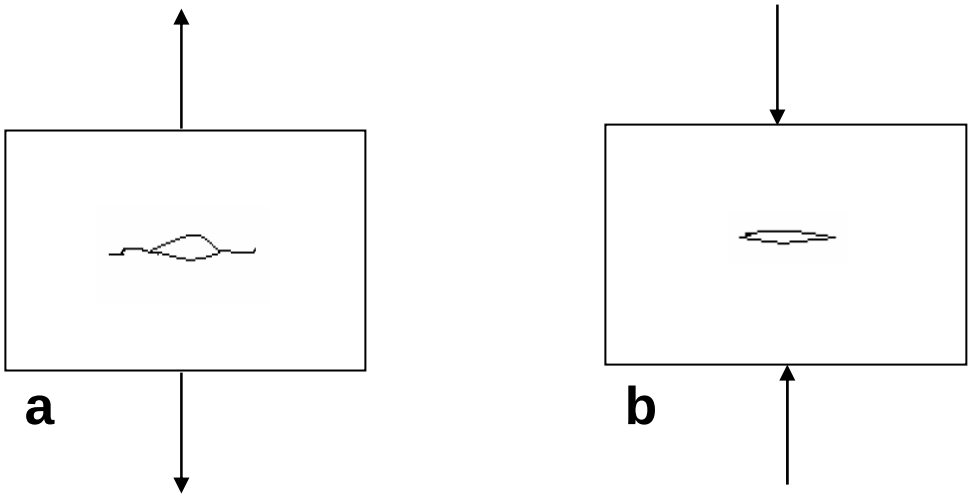

Fig. 4.21: Schematic of (a) crack opening in tension but (b) closing in compression[73].

From our research results it can be emphasized that the three point bending strength exhibit lower value in comparison to compressive mode of testing. Around 10% deviation for MAS1 could be noticed presumably due to pre-existing cracks. These cracks were generated because of thermal expansion mismatch in between MgO grains and spinel phase.

4.3.4: Thermal Shock Resistance:

Fig. 4.22 shows the variation of retained flexural strength of MgO-MgAl2O4 ceramics as a function of Al_2O_3: MgO ratio. The graph shows that the strength decreases with increasing Al_2O_3: MgO content. This may be due to the increasing amount of MgO which has lower thermal shock resistance. However, when retained flexural strength is plotted against calcination temperature for a particular composition (Fig.4.23), it shows increasing trend with calcination temperature for all the composition. This increase may be attributed to the presence of higher amount of $MgAl_2O_4$ spinel at higher calcination temperature.

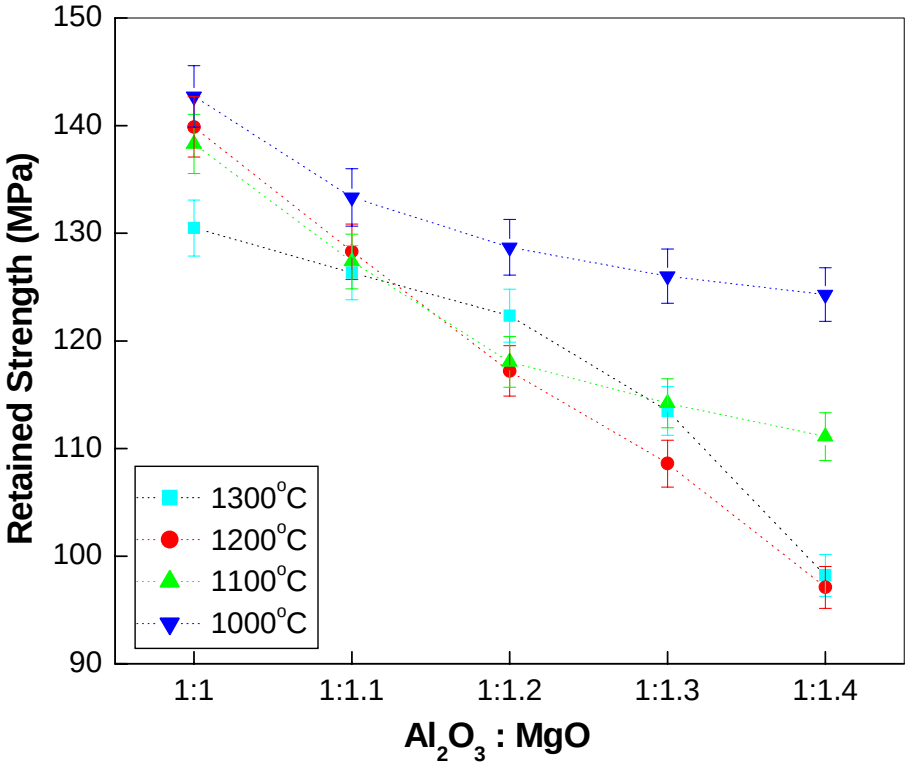

Fig.4.22: Retained Strength in samples after Thermal Spalling of 3 cycles (Spalling at 800°C)

Fig.4.22 shows the retained strength in sintered samples after performing 3 cycles of continuous air requenching at 25°C from 800°C. The improved resistance to thermal shock in the composites is attributed to the microcrack network interlinking as shown in Fig. 4.24. This interlinking of microcrack network leads to a decrease in fracture surface energy; because the amount of energy required, to initiate the crack propagation decreases with increasing concentration of pre-existing connecting cracks.

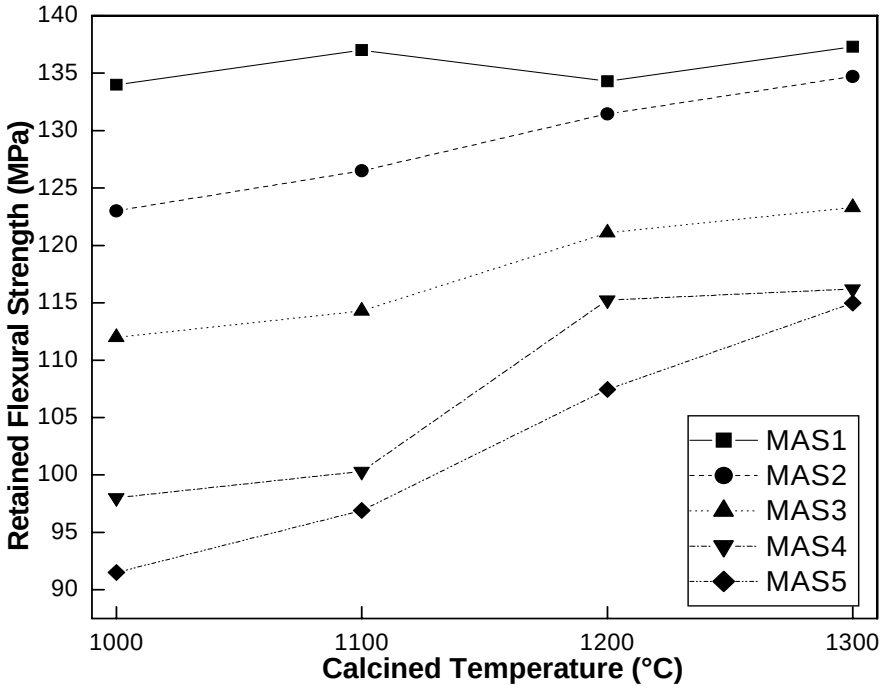

Fig.4.23: Retained Strength in samples calcined at various temperature, after Thermal Spalling of 3 cycles

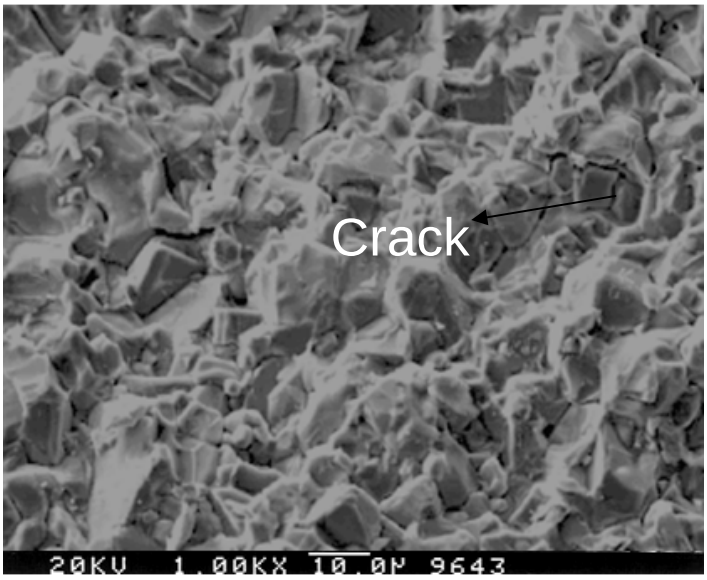

Fig.4.24: SEM micrograph of fractured surface showing intergranular fracture MAS5 (1:1.4)

The large thermal expansion coefficient difference between MgO and spinel, leads to extensive microcracking in composite materials with loss in strength values. Lower the residual MgO content, the lesser the concentration of pre-existing connecting cracks due to the thermal expansion mismatch. With high content of MgO, coarser grains as revealed from microstructure the longer cracks are generated and leading to lower fracture strength values.

CHAPTER 5

5.0. CONCLUSIONS

The MgO-$MgAl_2O_4$ powders were processed using solid-state reaction route. The processed powder was characterized by XRD. The particle characteristics of the processed powders were determined through particle size analyzer and BET surface area analyzer. The densification study was carried out using high temperature dilatometer. The densification of calcined powders was carried out for the corresponding batches. The effects of in-situ spinel seeds (after calcination stage) on densification of corresponding batches were studied. The sintered microstructures were analyzed through SEM studies. Subsequently, the mechanical properties as well as the thermal shock resistance of the specimens were characterized systematically and analyzed with respect to composition and spinel content in sintered specimens. The overall experimental results and their analysis are represented as follows:

5.1. Powder Processing and Characterization

a) The fineness of the powders was increased with milling time. Beyond 60h, no further reduction in fineness was observed.

b) Particle size analysis indicated a bimodal size distribution with both unagglomerated and agglomerated particles. The average agglomerate size varied between 3.48 to 6.84μm. The surface area of the milled powders was observed to be ~45m^2/gm for powders with lowest MgO content. The particle size of the milled powders measured from BET surface area analyzer was found to be ~76nm and was observed to increase with increasing MgO content.

5.2. XRD Analysis of Calcined powders

(a) Calcination led to spinel phase development around 1000^oC. The crystallinity as well as the spinel content increased with increasing calcination temperature and magnesia content. The crystallite size was 19nm and 33nm for composition with lowest and highest MgO content respectively. The increase in crystallite size with temperature is attributed to spinel phase development and increase with magnesia content is due to enlargement in spinel unit cell structure due to the formation of oxygen vacant sites i.e. spinel structure becomes anion

deficient due to excess MgO. The average lattice parameter calculated was around 8.0792Å for composition with highest MgO content.

(b) At calcination temperature of 1000^{o}C; ~5vol.% spinel phase could be observed, whereas ~30vol% spinel content was observed for highest MgO content composition. The detailed phase analysis of calcined powder illustrates a gradual trend of increasing spinel formation with increasing calcination temperature as well as increasing MgO content. The phase analysis of XRD revealed ~28 and ~48vol% spinel phase development at 1300^{o}C for the lowest and highest MgO content respectively.

(c) The surface area of the calcined powders was observed to decrease with increasing calcination temperature and increasing MgO content. At 1000^{o}C the surface area of the powders was ~41m^{2}/gm and ~24m^{2}/gm for composition with lowest and highest MgO content respectively. The particle size of the calcined powders measured from BET surface area analyzer was found to increase with calcination temperature. After calcination at 1000^{o}C, the powders revealed a particle size of 81nm and 140nm for powders with lowest and highest MgO content respectively.

5.3. Densification Study

(a) The dilatometry study of the powders of all the composition showed a similar expansion pattern. A sharp fall in slope was observed for MAP5; reason being the shrinkage rate from sintering of MAP5 was higher than the expansion rate from spinel formation at about 100-150^{o}C lower than other batches. The presence of inherent oxygen vacancy in magnesia rich spinel composition helps the transport of oxygen ion (the rate controlling factor), resulting in greater extent of amphoteric diffusion, greater mass transport and densification.

(b) A green density of nearly 50% was observed for the uniaxially pressed compacts. Calcination and subsequent spinel content has got a great influence on the sintering behavior. The higher the calcination, the greater is the agglomeration of the starting oxides, leading to inertness (lesser reactivity) and hence lesser shrinkage. Nearly 96-98% densification is observed for composition with equal proportion of starting materials while it was 95-97% for highest MgO content.

(c) The initial spinel seed content after calcination stage was observed to have a great influence on the sintering/densification. Lower in-situ spinel seeding had beneficial effect on densification while higher in-situ spinel seeding had a detrimental effect on density.

5.4. Phase and Microstructure Analysis

(a) In sintered specimens, $MgAl_2O_4$ was the major phase with a residual MgO content.

(b) An optimum amount of seed had significant effect on spinelization in MgO-rich spinel composite. Highest spinel phase (~70%) formation in sintered specimen was observed in presence of ~5vol% seed content in green pellets, and a gradual decreasing trend could be noticed with increasing initial seed content. At 1300^{o}C, spinel content of ~62vol% was observed in sintered specimens, when initial seed content was ~28vol%. However, with increasing MgO content, the extent of spinel phase formation decreased and reached upto ~50vol%.

(c) The microstructure revealed non-uniform grains with intergranular pores present in between the grains. The average grain size of MAP1 calcined at 1300^{o}C was observed to be ~8μm in comparison to average grain size of ~5μm of MAP1 calcined at 1000^{o}C. MAS5 exhibited relatively larger and elongated grain at around ~9 and 16μm, upon sintering after calcination at 1000^{o}C and 1300^{o}C temperature respectively. Direct-bonded and rounded spinel–spinel grains with relatively few edges were also observed.

5.5. Characterization of Mechanical Properties

a) Higher amount of seed addition had an adverse affect on the hardness of the composites due to coarsening of the spinel grains and formation of subsequent porosity. Hardness of the material revealed an increasing linear relationship with increasing spinel content. Hardness of MgO-Spinel ceramic (MAS1), calcined at 1000^{o}C and sintered at 1600^{o}C/4h was ~13.5GPa. The hardness value was observed to decrease continuously (13.7–12.1GPa) with the content of spinel phase in sintered specimen.

b) Around 20% fall in compressive strength could be noticed for MAS5, which can be attributed to: (i) the excessive grain growth of spinel phase during sintering and (ii) the low bond strength within preformed spinel grain and magnesia. In MgO-Spinel ceramics, due to the thermal expansion mismatch between spinel grains and magnesia, microcrack is developed around the spinel grains. These cracks are the critical defects causing failure on loading.

(c) Flexural strength values was observed to decreased markedly with increasing MgO content in

sintered specimens. A decrease of ~35% could be noticed when the starting powders were calcined at 1300^{o}C, which is due to the increase in grain size.

(d) Nearly 15% flexural strength loss was observed in samples of two extreme compositions, calcined at 1000^{o}C and subsequent sintering. The decrease in strength was due to change in nature of the critical flaw size that arises due to the thermal expansion mismatch within the residual MgO and spinel phase.

(e) Compressive strength of MgO-spinel ceramics was observed to be higher than 3-point flexural strength. This behavior arises because the flaws (e.g. porosity) in the ceramic are effectively closed under compressive stress but rapidly enlarged under (tensile stress) flexural testing arrangement.

(f) Improved resistance to thermal shock in the MgO-$MgAl_2O_4$ ceramics is attributed to the microcrack network interlinking. A significant decrease in strength was observed with increasing residual content of MgO in sintered samples. Lower the residual MgO content, the lesser the concentration of pre-existing connecting cracks due to the thermal expansion mismatch and hence better resistance to thermal shock.

(g) With increasing MgO content, the resultant spinel grains were found to be coarser. These coarser grains led to longer cracks at MgO-spinel interface thereby leading to lower fracture values in flexural test.

Initial calcination temperature and in-situ formation of spinel phase have significant contribution on the composition and microstructure of sintered specimens. Around 5vol% spinel seed is effective for the synthesis of MgO-70vol% $MgAl_2O_4$, whereas MgO-50vol% $MgAl_2O_4$ ceramic can be synthesized in presence of ~50vol% initial seed content. Higher content of seed has no contribution to nucleation rather it accelerates the grain growth at high temperature. This growth of grain size is detrimental for mechanical properties. By adjusting the level of spinel phase in the green pellets and the sintering conditions, the physical properties can be synchronized.

CHAPTER 6

SCOPES FOR FUTURE WORKS

The densification behavior of MgO-$MgAl_2O_4$ ceramics and subsequently the mechanical properties may be enhanced by using different sintering aids and mineralizers. In the present work, several mechanical properties have been evaluated; however, the real modes of applications of this material are neglected. Hence, the scopes of future works are proposed as:

1. Densification study of these compositions with sintering additives like Fe_2O_3, TiO_2, $AlCl_3$ etc.
2. Synthesis of low cement castables from respective developed spinel from various compositions and their property evaluation for refractory applications
3. Evaluation of slag erosion and penetration resistance of the developed spinel compacts of varying compositions.

REFERENCES

1. R. D. Maschio, B. Fabbri, and C. Fiori, Industrial applications of refractories containing magnesium aluminate spinel, Industrial Ceramics 8 (2) (1988) 121–126.

2. A. Sainz, A. Mazzoni, E. Aglietti and A. Caballero, In Proc. UNITESR'97, 1995, pp. 387-392.

3. A. D. Karisheff, Refractory products and method of fabrication, France patent no. 350016, 24 August 1905.

4. E. Ryshkewitch, Oxide Ceramics, Academic Press, New York, 1960, pp. 257-274.

5. J. T. Bailey, R. Russel, Sintered spinel ceramics, American Ceramic Society Bulletin 47 (11) (1968) 1025-1029.

6. V. K. Singh and R. K. Sinha, Low temperature synthesis of spinel (MgAl2O4), Mater. Lett., 1997, 31, 281-285.

7. S. K. Behera, P. Barpanda, S. K. Pratihar and S. Bhattacharyya, Synthesis of magnesium-aluminate spinel from autoignition of citrate-nitrate gel, Mater. Lett., 2004, 58, 1451-1455.

8. G. I. Antonov, A. V. Kushchenko, O. M. Semenenko and G. N. Shcherbenko, Synthesis of magnesia-alumina spinel using periclase and bauxite, Ogneupory, no. 10, pp. 2-4, October, 1991.

9. G. I. Antonov, A. P. Yan'shina, S. M. Zubakov, and F. M. Menzhulina, Periclase- spinel refractories from seawater magnesia and beneficiated chromite, Ogneupory, [9], 35-40, September, 1971.

10. E. Kostic and I. Momcilovic, Reaction sintered $MgAl_2O_4$ bodies from different batch compositions, Ceramurgia International, [3] n. 2, 1977.

11. W. H. Gitzen, Alumina as a ceramic material, Columbus: The American Ceramic Society, (1970).

12. H. Winchell, Navigation in Crystallography. Bull. Geol. Soc. Am. 57 295-308, (1946)

13. F. F. Lange, B. I. Davies and D. O. Raleigh, Transformation strengthening of β"-Al_2O_3 with tetragonal ZrO_2, J. Am. Ceram. Soc. 66, C125-127, (1983).

14. M. L. Kronberg, Plastic deformation of single crystals of sapphire: basal slip and twining. Acta Met. 5 , 507-524, (1957).

15. J. H. Chesters, Refractories Production and its Properties, Inst of Materials (1983).

16. H. H. Chesney, Steetley Company, 1938.

17. Stephen C. Carnlglia and Gordon L. Barna, Handbook of Industrial Refractories Technology: Principles, types, properties, and applications, Noyes Publications, Fairview Avenue, Westwood, New Jersey, U.S.A, 1992.

18. A. Rashid Chesti, In: Refractories – Manufacture properties and applications, Prentice Hall of India, New Delhi (1991), p. 96.

19. S. C. Cooper and P. T. A. Hodson, Magnesia-magnesium aluminate spinel as a refractory, Trans. J. Brit. Ceram. Soc., 81 (1982) 121-128.

20. W. H. Bragg, Philos. Mag., 1915, 176(30), 305.

21. E. H. Wallker Jr., J. W. Owens, M. Etinne and Don Walker, Mater. Res. Bull. 37 (2002) 1041–1050.

22. G.D. Price, S.L. Price, J.K. Burdett, Phys. Chem. Miner. 8 (1982) 69.

23. R. Dekkers and C.F. Woensdregt, Crystal structural control on surface topology and crystal morphology of normal spinel ($MgAl_2O_4$), J. Crystal Growth 236 (2002) 441–454

24. M.A. Serry, S.M. Hammad, M. F. Zawrah, Br. Ceram. Trans. 97 (6) (1998) 175–178.

25. L. Schreyeck, A. Wlosik and H. Fuzellier, Infuence of the synthesis route on $MgAl_2O_4$ spinel properties, J. Mat. Chem.11 (2000) 483-486.

26. H. Cinn, S. K. Sharma, T. F. Cooney and M. Nicol, Phys. Rev. B, 1992, 45(1), 500.

27. R. L. Millard, R. C. Peterson and B. K. Hunter, Am. Mineral., 1992, 77, 44.

28. G. Baudin, R. Martinez, and P. Pena, High-temperature mechanical behavior of stoichiometric magnesium spinel, J. Am. Ceram. Soc., 1995, 8(7), 1857-1862.

29. L. Vollweiller, H. Jost and H. Housner, Key Engineering Materials, 132-136 (1997) 1814-1817.

30. R.E. Carter, Mechanism of solid state reaction between $MgO–Al_2O_3$ and $MgO–Fe_2O_3$, J. Am. Ceram. Soc. 44 (3) (1961) 116–120.

31. R. E. Carter, J. Am. Ceram. Soc., 44 [3] (1961), 116.

32. J. Beretka and T. Brown, J. Am. Ceram. Soc. 66 [5] (1983), 383.

33. P. Bartha, Magnesia spinel bricks-properties, production and use. In Proc. Int. Symp. Refractories, Refractory Raw Materials and High Performance Refractory Products, ed. X. Zhong et.al. Pergamon, Hangzhou, 1989, pp. 661-674.

34. T. Yamamura, T. Hamazaki and H. Kato, Alumina spinel castable refractories in steel teeming ladles, Taikabutsu Overseas 12 (1992) 21-27.

35. I. S. Kainarskii, N. V. Gul'ko, E. V. Degtyareva and S. V. Totsenko, Reaction of sintered spinel and corundum refractories with some compounds, Ogneupory, [1] 37-42, Jan., 1968.

36. G. I. Antonov, A. P. Yan'shina, S. M. Zubakov and F. M. Menzhulina, Periclase-Spinel refractories from sweater magnesia and beneficiated chromite, Ogneupory [9] 35-40, Sept., 1971.
37. J.F. Pasquier, S. Komarneni, R. Roy, Synthesis of $MgAl_2O_4$ spinel: seeding effects on formation temperature J. Mat. Sc. 26 (1991) 3797-3802.
38. G. Gusmano, P. Nunziante, E. Traversa and G. Chiozzini, The mechanism of $MgAl_2O_4$ spinel formation from thermal decomposition of coprecipitated hydroxides, J. Eu. Ceram. Soc., 7(1991) 31-39.
39. Y. C. Ko and C. F. Chan, Effect of spinel content on hot strength of alumina-spinel castables in the temperature range 1000-1500^oC, J. Eu. Ceram. Soc. 19 (1999) 2633-2639.
40. R. Sarkar and G. Banerjee, Effect of compositional variation and fineness on the densification of MgO-Al_2O_3 compacts, J. Eu. Ceram. Soc. 19 (1999) 2893-2899.
41. W. Kim and F. Saito, Effect of grinding on synthesis of $MgAl_2O_4$ spinel from a powder mixture of $Mg(OH)_2$ and $Al(OH)_3$, Powder technology 113 (2000) 109-113.
42. R. Sarkar and G. Banerjee, Effect of addition of TiO_2 on reaction sintered MgO-Al_2O_3 spinels, J. Eu. Ceram. Soc. 20 (2000) 2133-2141.
43. I. Ganesh, S. Bhattacharjee, B. P. Saha, R. Johnson, K. Rajeshwari, R. Sengupta, M. V. Ramana Rao and Y. R. Mahajan, An efficient $MgAl_2O_4$ spinel additive for improved slag erosion and penetration resistance of high Al_2O_3 and MgO-C refractories, Ceram. Int. 28 (2002) 245-253.
44. L. B. Kong, J. Ma and H. Huang, $MgAl_2O_4$ spinel phase derived from oxide mixture activated by a high energy ball milling process, Materials Letters 56 (2002) 238-243.
45. R. Sarkar, S. Chatterjee, B. Mukherjee, H. S. Tripathi, M. K. Haldar, S. K. Das and A. Ghosh, Effect of alumina reactivity on the densification of reaction sintered non- stoichometric spinels, Ceram. Int. 29 (2003) 195-198.
46. R. Sarkar, A. Ghosh and S. K. Das, Reaction sintered magnesia rich magnesium aluminate spinel: effect of alumina reactivity, Ceram. Int. 29 (2003) 407-411.
47. R. Sarkar, S. K. Das and G. Banerjee, Effect of additives on the densification of reaction sintered and presynthesised spinels, Ceram. Int. 29 (2003) 55-59.
48. H. S. Tripathi, B. Mukherjee, S. Das, M. K. Haldar, S. K. Das and A. Ghosh, Synthesis and densification of magnesium aluminate spinel: effect of MgO reactivity, Ceram Int. 29 (2003) 915-918.
49. P. Barpanda, S. K. Behera, P. K. Gupta, S. K. Pratihar and S. Bhattacharyya, Chemically induced disorder order transition in magnesium aluminium spinel, 26, 13 (2006) 2603-2609.

50. Z. Haijun, J. Xiaolin, L. Zhanjie and L. Zhenzhen, The low temperature preparation of nanocrystalline MgAl2O4 spinel by citrate sol-gel process, Materials Letters 58 (2004) 1625-1628.

51. J. Xiaolin, Z. Haijun, Y. Yongjie and L. Zhanjie, effect of the citrate sol-gel synthesis on the formation of $MgAl_2O_4$ ultrafine powder, Mat. Sci. Engg. A 379 (2004) 112-118.

52. M. F. Zawrah, Investigation of lattice constant, sintering and properties of nano Mg-Al spinels, Mat. Sci. Engg. A 382 (2004) 362-370.

53. A. Ghosh, R. Sarkar, B. Mukherjee and S. K. Das, Effect of spinel content on the properties of magnesia-spinel composite refractory, J. Eu. Ceram. Soc., 24 (2004) 2079-2085.

54. C. Aksel and F. L. Riley, Effect of the particle size distribution of spinel on the mechanical properties and thermal shock performance of MgO-spinel composites, J. Eu. Ceram. Soc. 23 (2003) 3079-3087.

55. C. Aksel, B. Rand, F. L. Riley and P. D. Warren, Mechanical properties of magnesia-spinel composites, J. Eu. Ceram. Soc., 22 (2002) 745-754.

56. C. Aksel and P. D. Warren, Work of fracture and fracture surface energy of magnesia-spinel composites, Composites Science and Technology 63 (2003) 1433-1440.

57. K. V. Simonov, V. D. Koksharov, A. I. Zabotka and L. A. Reinov, Thermo-mechanical and deformation properties of periclase and magnesia-spinel refractories, Ogneupory, no.1, pp. 7-14, January, 1983.

58. C. Haung, T. Lu, L. Lin, M. Lei and C. Huang, A study on toughening and strengthening of Mg-Al spinel transparent ceramics, Key Engineering Materials Vols. (2006) pp. 1207-1210.

59. R. Sarkar, S. K. Das and G. Banerjee, Effect of attritor milling on the densification of magnesium aluminate spinel, Ceram. Int. 25 (1999) 485-489.

60. I. Ganesh, B. Srinivas, R. Johnson, B. P. Saha and Y. R. Mahajan, Microwave assisted solid state reaction synthesis of $MgAl_2O_4$ spinel powders, J. Eu. Ceram. Soc., 24 (2004) 201-207.

61. M.N.Rahaman, Ceramic Processing and Sintering, Marcel Dekker, Inc, New York 1995 edition pp -115.

62. B. D. Cullity, Elements of X-Ray Diffraction, Second Edition, 1978, p- 351.

63. D. Domanski, G. Urettavizcaya, F. J. Castro and F. C. Gennari, Mechanochemical Synthesis of Magnesium Aluminate Spinel Powder at Room temperature, J. Am. Ceram. Soc., 87 (11) (2004) 2020-2024.

64. G.R. Anstis, P. Chantikul, B.R. Lawn, D. B. Marshall, A critical evaluation of indentation techniques for measuring fracture toughness: I. Direct crack measurements, J. Am. Cer. Soc. 64 (1981) 533.

65. A.T. Procopio, A. Zavaliangos, J. C. Cunningham, Analysis of the diametrical compression test and the applicability to plastically deforming materials, J. Mat. Sc. 38 (2003) 3629-3639.

66. ASTM C1161-90, Standard test method for flexural strength of advanced ceramics at ambient temperature, Annual Book of ASTM Standards, Vol. 15.01. ASTM, 1991, pp. 327-333.

67. M. Matsui, T. Takashi, I.Oda, Effects of starting materials and calcining temperature on sintering of spinel ceramics. In Advances in Ceramics, ed. W. D. Kingery, The American Ceramic Society, Columbus, OH, Vol 10, 1984, pp. 562-573.

68. R. Sarkar, H. S. Tripathi and A. Ghosh, Reaction sintering of different spinel compositions in the presence of Y_2O_3, Mat. Lett. 58 (2004) 2186-2191.

69. H. Kenya, O. Tadashi, N. Zenbee, Effects of starting materials and calcining temperature on sintering of spinel ceramics. Rep. Res. Lab. Eng. Mater., Tokyo Institute of Technology, No. 2,1977, pp. 85-94.

70. (a) J.T. Baitley, R. Russel Jr., Sintered spinel ceramics, Presented at the 69th Annual Meeting of the American Ceramic Society, New York, 3 May, 1967. (b). J.T. Baitley, Preparation and properties of dense spinel ceramics in the $MgAl_2O_4$–Al_2O_3 system, Ph.D. Thesis, Department of Ceramic Engineering, The Ohio State University, 1966.

71. W. T. Bakker, J. T. Lindsay, Reactive magnesia spinel, preparation and properties, Am. Ceram. Soc. Bull. 46 (11) (1967) 1094–1097.

72. I. Ganesh, S. Bhattacharjee, B.P. Saha, R. Johnson, Y.R. Mahajan, A new sintering aid for magnesium aluminate spinel, Ceram. Int. 27 (7) (2001) 773–779.

73. W. E. Lee and W. M. Rainforth, Ceramic Microstructures: Property control by processing, 1st edition, p-34, Chapman and Hall, 1994.

74. C. Aksel, Densification properties of magnesia-spinel composites, Key Engg. Mat. 264-268 (2004) 1071-1074.

75. J. T. Bailey and R. Russel, Preparation and properties of dense spinel ceramics. American Ceramic Society Bulletin, 1971, 50, 493-496.

76. W. D. Kingery, H. K. Bowen, D. R. Uhlmann, Introduction of Ceramics, 2nd Edition, P-335, John Wiley & Sons, 1991.

77. J. Petkovic and M. M. Ristic, The influence of specific surface area on sintering of alumina powders, Ceramurgia 3 (1) (1973) 12-14.

78. P. Hing, Fabrication of translucent magnesium aluminate spinel and its compatibility in sodium vapours, J. Mat. Sci. 11 (1976) 1919-1926.
79. Wurst, J. C. and Nelson, J. A., Lineal intercept technique for measuring grain size in two phase polycrystalline ceramics, J. Am. Ceram. Soc., 55 (1972) 109.
80. E.O. Hall, Proc. Phys. Soc. (Lond.) B64 (1951) 747–753.
81. N.J. Petch, J. Iron Steel Inst. 174 (1953) 25–28.
82. M. W. Barsoum, Fundamentals of Ceramics, McGRAW-HILL International Editions, 1997.